AD-A041 499 IIT RESEARCH INST CHICAGO ILL F/G 21/5
TURBINE ENGINE PARTICULATE EMISSION CHARACTERIZATION.(U)
SEP 76 D L FENTON DOT-FA75-WA-3722
UNCLASSIFIED IITRI-C6352-10 FAA/RD-76-141 NL

1 OF 2
ADA
041499

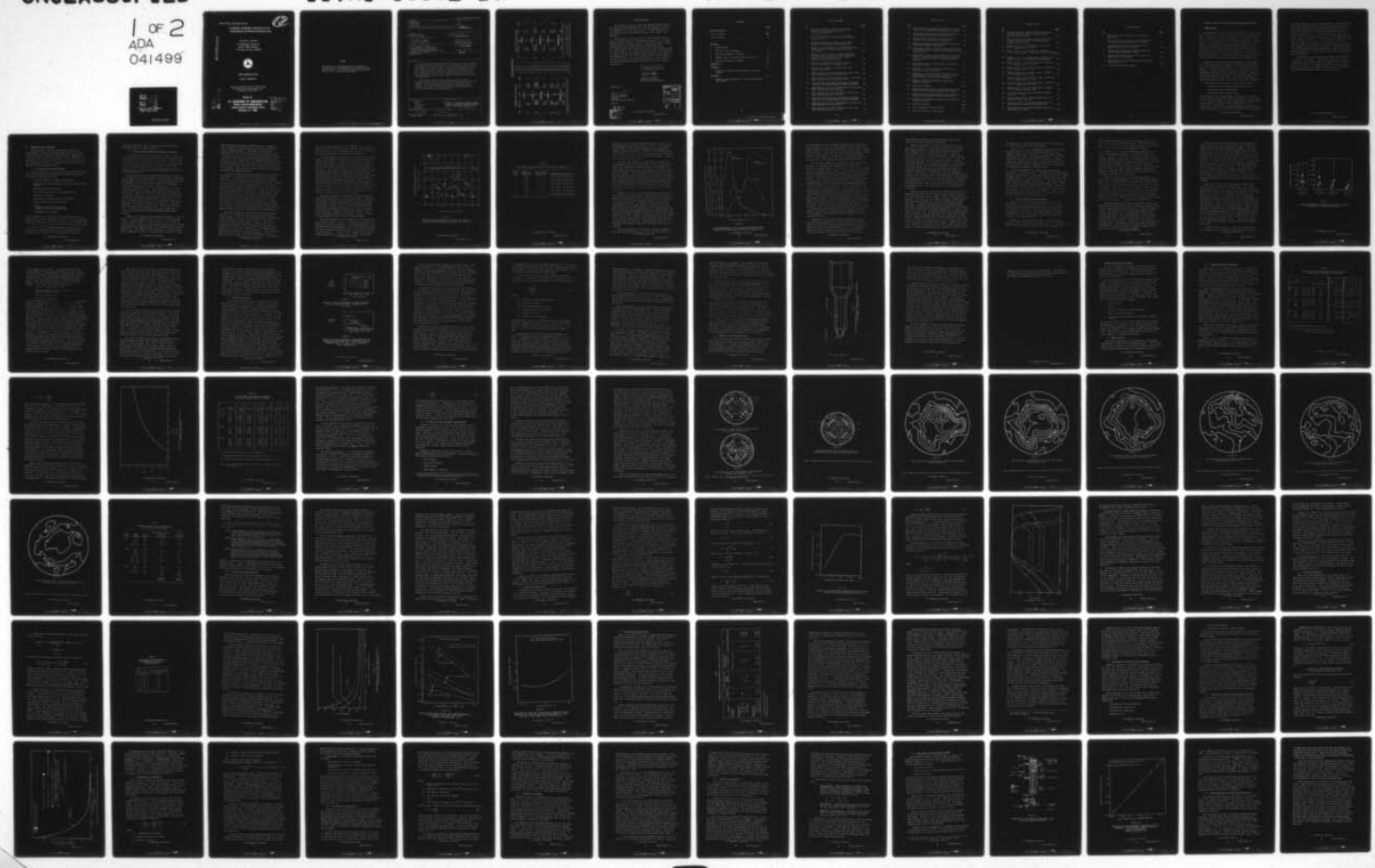

Report No. FAA-RD-76-141

TURBINE ENGINE PARTICULATE EMISSION CHARACTERIZATION

AD A041499

Donald L. Fenton

IIT Research Institute
10 W. 35th Street
Chicago, Illinois 60616

SEPTEMBER 1976

FINAL REPORT

Document is available to the U.S. public through the National Technical Information Service, Springfield, Virginia 22161.

AD No.
DDC FILE COPY

Prepared for

U.S. DEPARTMENT OF TRANSPORTATION
FEDERAL AVIATION ADMINISTRATION
Systems Research & Development Service
Washington, D.C. 20590

DDC
JUL 11 1977
D

NOTICE

This document is disseminated under the sponsorship of the Department of Transportation in the interest of information exchange. The United States Government assumes no liability for its contents or use thereof.

Technical Report Documentation Page

1. Report No.	2. Government Accession No.	3. Recipient's Catalog No.
FAA-RD-76-141		

4. Title and Subtitle	5. Report Date
Turbine Engine Particulate Emission Characterization,	September 1976
	6. Performing Organization Code

7. Author(s)	8. Performing Organization Report No.
Donald L. Fenton	IITRI-C6352-10

9. Performing Organization Name and Address	10. Work Unit No. (TRAIS)
IIT Research Institute 10 West 35th Street Chicago, Illinois 60616	11. Contract or Grant No. DOT-FA75-WA-3722
	13. Type of Report and Period Covered Final Report
12. Sponsoring Agency Name and Address U.S. Department of Transportation Federal Aviation Administration Systems Research and Development Service Washington, D.C. 20590	14. Sponsoring Agency Code ARD-550

15. Supplementary Notes

16. Abstract

A particulate material sampler was designed to be used in conjunction with commercial aircraft turbine engines. The engines of interest include a low-bypass ratio turbofan (JT3D), a mixed-flow turbofan (JT8D), and a high by-pass ratio turbofan (JT9D). The samples and information provided by the sampler include: particle size distribution (minimum particle size = 0.001 μm), particle size shape characteristics, and particulate mass concentration. The influence of engine operating variables such as power setting and compressor inlet conditions on particle characteristics can be determined.

The sampler designed utilizes a mixing-type probe assembly, a specialized aerosol transport system which also provides conditioning, and a sample collection system near the engine to minimize particle-loss problems. The extracted sample is bifurcated -- the larger stream yielding a bulk sample and the smaller stream undergoing further dilution for detailed particle characterization.

17. Key Words	18. Distribution Statement
Pollution Smoke Gas Turbines Emissions Aerosols	Document is available to the U.S. public through the National Technical Information Service, Springfield, Virginia 22161.

19. Security Classif. (of this report)	20. Security Classif. (of this page)	21. No. of Pages	22. Price
Unclassified	Unclassified		

Form DOT F 1700.7 (8-72) Reproduction of completed page authorized

METRIC CONVERSION FACTORS

Approximate Conversions to Metric Measures

Symbol	When You Know	Multiply by	To Find	Symbol
	LENGTH			
in	inches	*2.5	centimeters	cm
ft	feet	30	centimeters	cm
yd	yards	0.9	meters	m
mi	miles	1.6	kilometers	km
	AREA			
in^2	square inches	6.5	square centimeters	cm^2
ft^2	square feet	0.09	square meters	m^2
yd^2	square yards	0.8	square meters	m^2
mi^2	square miles	2.6	square kilometers	km^2
	acres	0.4	hectares	ha
	MASS (weight)			
oz	ounces	28	grams	g
lb	pounds	0.45	kilograms	kg
	short tons (2000 lb)	0.9	tonnes	t
	VOLUME			
tsp	teaspoons	5	milliliters	ml
Tbsp	tablespoons	15	milliliters	ml
fl oz	fluid ounces	30	milliliters	ml
c	cups	0.24	liters	l
pt	pints	0.47	liters	l
qt	quarts	0.95	liters	l
gal	gallons	3.8	liters	l
ft^3	cubic feet	0.03	cubic meters	m^3
yd^3	cubic yards	0.76	cubic meters	m^3
	TEMPERATURE (exact)			
°F	Fahrenheit temperature	5/9 (after subtracting 32)	Celsius temperature	°C

*1 in = 2.54 (exactly). For other exact conversions and more detailed tables, see NBS Misc. Publ. 286, Units of Weights and Measures, Price $2.25, SD Catalog No. C13.10:286.

Approximate Conversions from Metric Measures

Symbol	When You Know	Multiply by	To Find	Symbol
	LENGTH			
mm	millimeters	0.04	inches	in
cm	centimeters	0.4	inches	in
m	meters	3.3	feet	ft
m	meters	1.1	yards	yd
km	kilometers	0.6	miles	mi
	AREA			
cm^2	square centimeters	0.16	square inches	in^2
m^2	square meters	1.2	square yards	yd^2
km^2	square kilometers	0.4	square miles	mi^2
ha	hectares (10,000 m^2)	2.5	acres	
	MASS (weight)			
g	grams	0.035	ounces	oz
kg	kilograms	2.2	pounds	lb
t	tonnes (1000 kg)	1.1	short tons	
	VOLUME			
ml	milliliters	0.03	fluid ounces	fl oz
l	liters	2.1	pints	pt
l	liters	1.06	quarts	qt
l	liters	0.26	gallons	gal
m^3	cubic meters	35	cubic feet	ft^3
m^3	cubic meters	1.3	cubic yards	yd^3
	TEMPERATURE (exact)			
°C	Celsius temperature	9/5 (then add 32)	Fahrenheit temperature	°F

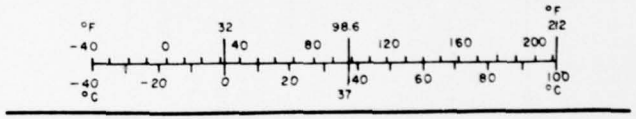

ACKNOWLEDGEMENT

This document presents the work completed under Phase I of Contract No. DOT-FA75WA-3722. The IIT Research Institute is indebted to Mr. John Tigue and Mr. William Westfield at the Federal Aviation Administration for their support and guidance.

The program was directed by Mr. John Stockham, Manager, Fine Particles Research, IIT Research Institute. Dr. Donald Fenton served as Project Leader. Other staff members making significant contributions were Mr. William Courtney, Mr. George Yamate, Mr. Ronald Draftz, Ms. Anne O'Donnell, and Dr. Jack O'Neill. Mr. Ronald Kaminecki and Ms. Mary Romberger of IITRI's Information Science Center performed the computer literature search. Mr. Ralph Johnson and Mr. Paul Campbell of the United Airlines maintenance facility in San Francisco provided technical assistance relating to aircraft engine operations.

Respectfully submitted,
IIT RESEARCH INSTITUTE

Donald L. Fenton

Donald L. Fenton
Research Scientist
Fine Particles Research

Approved by

John D. Stockham
Science Advisor
Manager
Fine Particles Research

DLF/cs

ACCESSION for
NTIS White Section
DDC Buff Section
UNANNOUNCED
JUSTIFICATION
BY
DISTRIBUTION/AVAILABILITY CODES
Dist. AVAIL. and/or SPECIAL
A

DDC
RECEIVED
JUL 11 1977
D

CONTENTS

		Page
Acknowledgements		v
List of Figures		viii
List of Tables		xi
Sections		
1	Introduction	1
2	Review of the Literature	3
3	Conceptual Design of Sampler	28
4	Sampler Data and Sample Handling Protocol	87
5	Mechanical Design of Sampler	89
REFERENCES		107
APPENDIX A		113
	Analysis by Electron Microscopy of J-93 Test Samples	
APPENDIX B		123
	Organic Chemical Analysis of Collelcted Engine Soot Sample	

PRECEDING PAGE BLANK-NOT FILMED

LIST OF FIGURES

No.		Page
1	Particulate Emission Rates for the JT8D Aircraft Trubine Engine Measured by Johansen and Kumm (5)	7
2	Size Distribution of Jet Aircraft Exhaust Particles Sampled at Runway Two Miles After Takeoff (10)	10
3	Aldehyde Emissions as a Function of Power Setting With Engine to Engine Variations	16
4	Effect of Inlet Temperature on Smoke Emissions (501-K Industrial Engine, Constant Speed JP-5 Fuel)	20
5	Effect of Inlet Pressure on Carbon Monoxide and Hydrocarbon Emissions (501-K Industrial Engine, Constant RPM, JP-5 Fuel, 37°C Compressor Inlet Temperature)	20
6	Nozzle Configuration for the U.S. Navy's Automated EPA Method 5 Sampler (12)	25
7	Variation of Normalized Displacement with Sampling Area Ratio	32
8	JT3D Isopleth for Carbon Monoxide at Idle with NAFEC Sampling Nozzle Locations (38)	38
9	JT3D Isopleth for Total Hydrocarbons at Idle with NAFEC Sampling Nozzle Locations (38)	38
10	JT3D Isopleth for Oxides of Nitrogen at Maximum Continous with NAFEC Sampling Nozzle Locations	38
11	JT8D Isopleth for Total Hydrocarbons at Idle with NAFEC Sampling Nozzle Locations	40
12	JT8D Isopleth for Carbon Monoxide at Idle with NAFEC Sampling Nozzle Locations	41
13	JT8D Isopleth for Oxides of Nitrogen at Maximum Continous with NAFEC Sampling Nozzle Locations	38
14	JT9D Isopleth for Total Hydrocarbons at Idle with NAFEC Sampling Nozzle Locations	43
15	JT9D Isopleth for Carbon Monoxide at Idle with NAFEC Sampling Nozzle Locations	44

Figures (cont.)

No.		Page
16	JT9D Isopleth for Oxides of Nitrogen at Maximum Continous with NAFEC Sampling Nozzle Locations	45
17	Variation of Dimensionless Deposition Velocity with Normalized Particle Relaxation Time	53
18	Penetration of an Aerosol as a Function of Particle Size for Typical Conditions	55
19	Temperature History in Main Sample Diluter as a Function of Engine Power Level	62
20	Deposition of Small, Medium, and Large Particles vs Transpiration Flow Rate with Varying Particle Concentration	63
21	Deposition of Particles in Relation to Particle Size at Intermediate Levels of Particle Concentration, Sample Flow Rate, and Transpiration Flow Rate	64
22	Particle Collection Efficiency as a Function of Particle Size	73
23	Schematic of the Thermo-System Model 3030 Electrical Aerosol Analyzer	83
24	Comparison of the Instrument Indication with the Response to Monodisperse Aerosols for the Model 3030 Electrical Aerosol Analyzer	84
25	Schematic Diagram of Exhaust Particulate Sampler Components	90
26	Probe Inlet Design	94
27	Sampling Nozzles, Lines, and Structural Support Details for the Upper Portion of the Probe	96
28	Sampling Nozzles, Lines and Structural Support Details for the Upper Portion of the Probe	97
29	Sampling Line Manifold Assembly for Transition to One Inch Tube	99
30	Flexible Connector	100
31	Inlet Assembly for Main Diluter	101
32	Outlet Assembly for Main Diluter	102

Figures (cont.)

No.		Page
33	Top View Sketch of United Airlines Test Cell #3 Where JT3D and JT8D are Operated with Exhaust Sampler Layout	104
34	Top View Sketch of United Airlines Test Cell #4 Where the JT9D Engine is Operated with Exhaust Sampler Layout	105
A1	Sample I-25; J-93: Afterburning, 65,000 ft. M = 2; Magnification = 1.6K	117
A2	Sample I-26; J-93: Afterburning, 65,000 ft. M = 2; Magnification = 20K (First Photomicrograph)	118
A3	Sample I-26; J-93: Afterburning, 65,000 ft. M = 2; Magnification = 20K (Second Photomicrograph)	118
A4	Sample II-68; J-93: Military Power, 55,000 ft. M = 2; Magnification = 1,000X	119
A5	Sample II-68; J-93: Military Power, 55,000 ft. M = 2; Magnification = 6.6K	119
A6	Sample II-68; J-93: Military Power, 55,000 ft. M = 2; Magnification = 20K	120
A7	Sample III-20; J-93: Military Power, 55,000 ft. M = 2.7; Magnification = 10K	
A8	Sample III-20; J-93: Military Power, 65,000 ft. M = 2.7; Magnification = 20K	121
A9	Sample III-5; J-93: Military Power, 35,000 ft. M = 1.4; Magnification = 90X	121
B1	Initial UV Scan of Extracted Carbon Residue (dilution = 1:500)	125
B2	High Pressure Liquid Chromatography Trace of Extracted Carbon Residue	127
B3	High Pressure Liquid Chromatography Trace of Extracted Carbon Residue (Concentrated)	128
B4	High Pressure Liquid Chromatography Trace of MeOH (Methanol) Blank	129

LIST OF TABLES

No.		Page
1	Exit Plane Plume Survey of a J79 Turbojet Engine (8)	8
2	Engine Exit Plane Conditions and Prediction* of Sampling Flow Parameters at Sea Level	30
3	Calculations for Inertial Parameter with Engines Operating at Sea Level	33
4	Performance Comparison of NAFEC Diamond and 4-Point Exhaust Sampling Probes	46
5	Temperature and Dew Point as a Function of Dilution Mass Flow Ratio	60
6	Instruments for Direct Measurement of Aerosol Mass Concentration	66
A1	J-93 Exhaust Particle Samples	116

TURBINE ENGINE PARTICULATE EMISSION CHARACTERIZATION

1. INTRODUCTION

Mass emission levels of particulate material from selected types of commercial aircraft turbojet engines have been measured. However, the physical and chemical characteristics of the emitted particles has not received comprehensive investigation. The particulate material sampler described in this report was designed in cooperation with the Unites States Federal Aviation Administration to generate data regarding the nature of the engine's exhaust particles. The dominant design feature of the sampler is the bifurcation of the extracted exhaust sample -- the larger portion for bulk analysis and the smaller for detailed particulate characterization.

Mandatory in the design of the sampler is the acquisition of a representative sample of the particulate material. Bias within the collected sample can alter the measurement results. To ensure that the sample is representative, consideration has been given to isokinetic sampling, sampling nozzle configuration, location of the sampling nozzle array at the exit plane of the engine, and particle deposition within the sampling line to the point of particle collection.

The information generated by the sampler includes:

- Particle size and shape ranging from 0.001 μm
- Particle chemical composition
- Particulate mass emission rate

The particle size and shape data are obtained from analysis of the smaller of the two sample flow streams. Direct analysis of the collected particulate samples by an electron microscope enables attainment of the required 0.001 μm size resolution. The resultant photomicrographs yields particle size distributions, the variation of particle shape parameters

with size, and general particle morphology. Elemental analysis through the X-ray probe (electron microscope) of the collected particulate sample provides chemical data on the particle's composition. An electrical aerosol analyzer is installed parallel to the electron microscope collection stage. This instrument provides real-time particle size data in the range of 0.01 to 0.7 μm size range and serves to indicate the "operating behavior" of the sampler. The main (larger) sample flow stream undergoes filtration collecting a bulk sample of the particulate material. The mass emission rate is determinable through gravimetric weighing, and bulk chemical analyses -- trace elements and organic constituents -- can be performed.

The following text discusses the design decisions made in regard to the sampler. The sample flow rates, probe geometries, sample tube diameters, location of the particle collection "stage", and sample conditioner are all given. The last section gives design drawings of the major components where complicated fabrication is required.

2. REVIEW OF THE LITERATURE

The literature review was conducted in two parts. A comprehensive search was performed with the aid of a computerized system. Results of this work were augmented with a separate but limited manual search. After completion of both parts, the literature was merged to form a single list. The significant literature is discussed as it relates to the design of the particulate sampler.

2.1 Computerized Literature Search

Several different data bases were selected for searching due to their extensive abstracting of the open literature. The sources investigated include:

- Chemical Abstracts (January 1969-present)
- National Technical Information Service (January 1969-present)
- Defense Documentation Center
- Air Pollution Technical Information Center
- Biological Abstracts
- Smithsonian Science Information Exchange
- Pollution Abstracts (1972-present)
- IEEE:
  INSPEC 1 Computer and Controls
  INSPEC 3 Electrical Engineering
- IFI-PLEMUM, U.S. Patents

In this review, over 9,000 citations were identified and approximately 300 were examined. Exploratory searches through Biological Abstracts, IEEE, and U.S. Patents (IFI-PLEMUM) data bases yielded little information and were consequently dropped.

The goal of the computer literature search is the construction of a working bibliography. The bibliography generated here resulted in the systematic collection of

pertinent articles. Over 150 articles and reports were secured during the conduct of Phase I.

2.2 Aircraft Engine Exhaust Particulate Sampling

Particulate emissions from aircraft turbine engines has only received partial investigation to date. Limited exhaust particle size data is available, some chemical analysis data is available on the particulate material, and incomplete mass emission data for each engine is available. A thorough review of the particulate sampling and measurement work performed to date is necessary to gain experience and avoid the common difficulties.

Particulate extraction procedures from the exit plane of the engine have been specified for the purpose of obtaining smoke number data in ARP 1179 (1). All operating conditions are defined, and all construction details are specified. A single sampling nozzle is used to extract the 1.7 m^3/hr (1.0 scfm) sample flow rate. The determination of a smoke number requires only a small amount of material and no precautions for sample preservation. Problems with preservation include both transport of the "aerosol" itself and chemical stability of the particulate material once collected. To date, the EPA has not specified any standards for particulate emissions from aircraft engines and, therefore, a standard method for collection does not exist. This being the situation, a comprehensive literature search was undertaken to study all the gas turbine exhaust sampling methods used recently.

Nelson (2) investigated two commercial engines -- JT3D and JT8D. A 12-point sampling probe was used -- three sampling nozzles located radially at the centroid of four quadrants equally spaced. Only total particulate emissions were obtained employing the Los Angeles County Air Pollution Control District Method (3). This sampling train consists of three Greenberg-Smith impingers in series, a Whatman thimble filter, a vacuum

pump, and flow measurement instrumentation. Klarman (4) has investigated the applicability of common stationary source sampling methods -- EPA Method 5 Particulate Sampling Train for the determination of the concentration of particulate material. In the tests performed by Klarman, a J57-P8B engine was used where the mean particulate concentration of the exhaust gas was 0.08064 gm/m^3 (measured by EPA (Environmental Protection Agency) particulate sampling train) and the mean deviation was 28.5 percent between duplicate samples. These results indicate the precision presently available with standard methods.

Use of the stationary source sampling methods are not appropriate for detailed characterization of the exhaust particles. First, particle size and shape are important, thus, at least requiring modifications in the method. Second, the actual mass collected (or sampling flow rate) is not great enough for detailed chemical analysis. And third, the question of obtaining a representative sample is unresolved as the sampling probe is essentially a single point. The EPA method and numerous others employ single-point methods and are generally successful because they can be easily designed to accomodate a specific application. A single-point probe is not appropriate for turbine engine sampling as the location and/or positioning mechanism present enormous problems. The time required to obtain a representative sample through single-point sampling is also prohibitive.

Johansen and Kumm (5) have reported experimental data relating to the sampling of particulate material behind turbine engines. The test data reported was concentrated on a TPE 331 turboprop engine (single shaft). Some data is given concerning the JT8D engine. Separate exit plane mapping was performed for particulate mass using 21 points located at the centroid of equal areas. The mapping was performed over four power levels (TPE 331): idle, 30% rated power, 90% rated power, and 100% rated power. The probe configuration used was the 12-point cruciform. The reported

particulate mass emission rate was approximately 1.5 to 2.0 times the results obtained through mapping. No explanation for mass emission rate discrepancy was offered by Johansen (6) but probably resulted through sampling difficulties.

The JT8D engine was sampled at 30 and 85 percent rated power. The 12-point cruciform probe was also used here by Johansen and Kumm (5). Rotation of the probe through 90° was performed where variation of the particulate material emitted with rotation was masked by overall experimental variation. The results obtained are given in Figure 1 where the ambient dust levels are indicated. Observed is the apparent small difference between the 30% rated power level and the ambient dust level. This result seems unlikely in comparison to the reported mass emission factors, but is conceivable due to the high ambient dust levels known to exist in Phoenix, Arizona area (68). Detailed mapping of the particulate emissions at the JT8D exit plane were not performed. Therefore, in this instance, performance of the 12-point cruciform probe was not evaluated.

Davidson and Domal (7) performed limited particulate emission measurements on a J93 turbojet engine. High altitude flight conditions were simulated over a full range of engine power settings including the afterburning regime. Observed was a slight change in total emissions with combustor inlet pressure and temperature. This may indicate that atmospheric conditions alone could affect the particulate material in quantity or quality, or both. Results of this program will have input to this question.

Particle size data is less plentiful in the literature. The results obtained, however, do indicate the general size range of the exhaust particles. Hall and Shaffermocker (8) performed emission measurements on a J79 to determine particle size and approximate composition. The maximum sampling Mach number was 0.7. Table 1 gives results for the plume survey conducted at the exit plane. Teller (9) reports

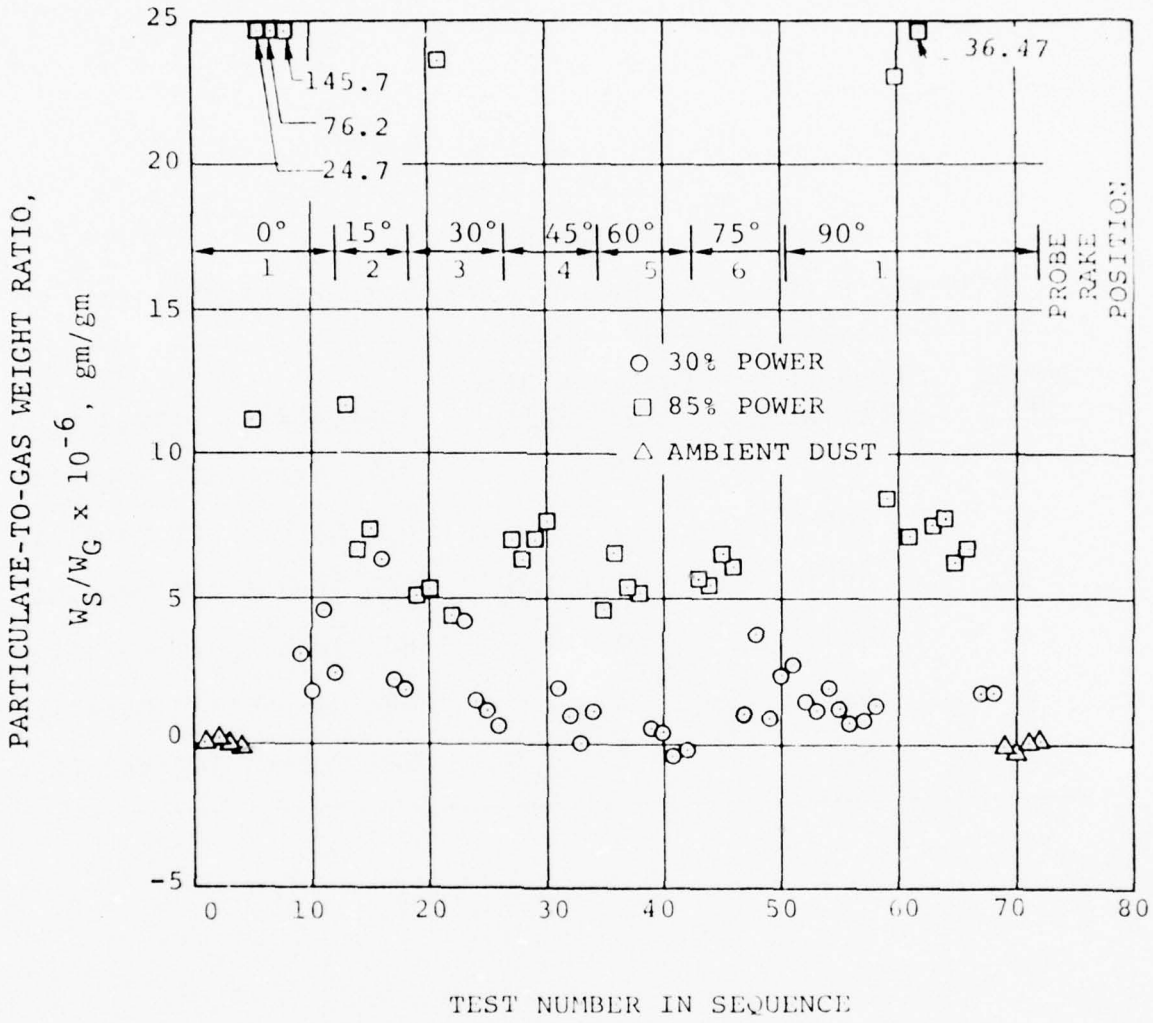

Figure 1

PARTICULATE EMISSION RATES FOR THE JT8D AIRCRAFT TURBINE ENGINE MEASURED BY JOHANSEN AND KUMM (5)

Table 1

EXIT PLANE PLUME SURVEY OF A J79 TURBOJET ENGINE (8)

Sample No.	Exhaust Temp. (°C)	Particle Size Range (μm)	Approximate Composition
1	639	0.5 - 1	88% Carbon 10% Metallic
2	660	1 - 2	45% Carbon 50% Metallic
3	595	1 - 1.5	80% Carbon 10% Metallic
4	654	1 - 2	80% Carbon 12% Metallic
5	616	1 - 2	60% Carbon 30% Metallic
6	604	1 - 1.5	50% Carbon 50% Metallic

results of other studies indicating particle size to be in the approximate size range 0.05 μm to 0.12 μm. Photomicrographs taken of the collected particles show agglomerate chains of carbon particles -- as many as 20 submicron particles may form a chain. Also, probe washings yielded anywhere from 35 to 95% of the total collected particulate. Sampling system details were not given.

Sem (10) also reports that jet exhaust contains high concentrations of submicron particles. A bag sample of the exhaust was obtained on take-off with an instrumented aircraft about two minutes after the runway was used by a commercial jetliner. The resulting distribution was obtained with an electrical aerosol analyzer and is shown in Figure 2. The particle size distribution may not represent the exhaust from a specific engine type because previous airport traffic and surrounding sources of particulate emissions may have interfered. Subsequent dilution and aging of the aerosol may also have changed its size distribution from the initial condition.

Boderick (11) has also collected and measured the size distribution of aircraft engine exhaust particles using a scanning electron microscope. An electrostatic precipitator was used to collect the particles directly onto electron microscope (EM) grids. Calibration of the electrostatic precipitator was performed against a thermal precipitator where the collection efficiencies can be reliably calculated. The calibration was necessary because the electrostatic precipitator is known to exhibit collection efficiencies varying with particle size. Results from the calibration indicated a very low but uniform collection efficiency over the particle size range of interest -- approximately 0.005 to 0.1 μm. Therefore, corrections resulting from sample bias were not required.

Results of Boderick's microscopic analysis indicates that the count mean size was 0.02 μm. He also points out

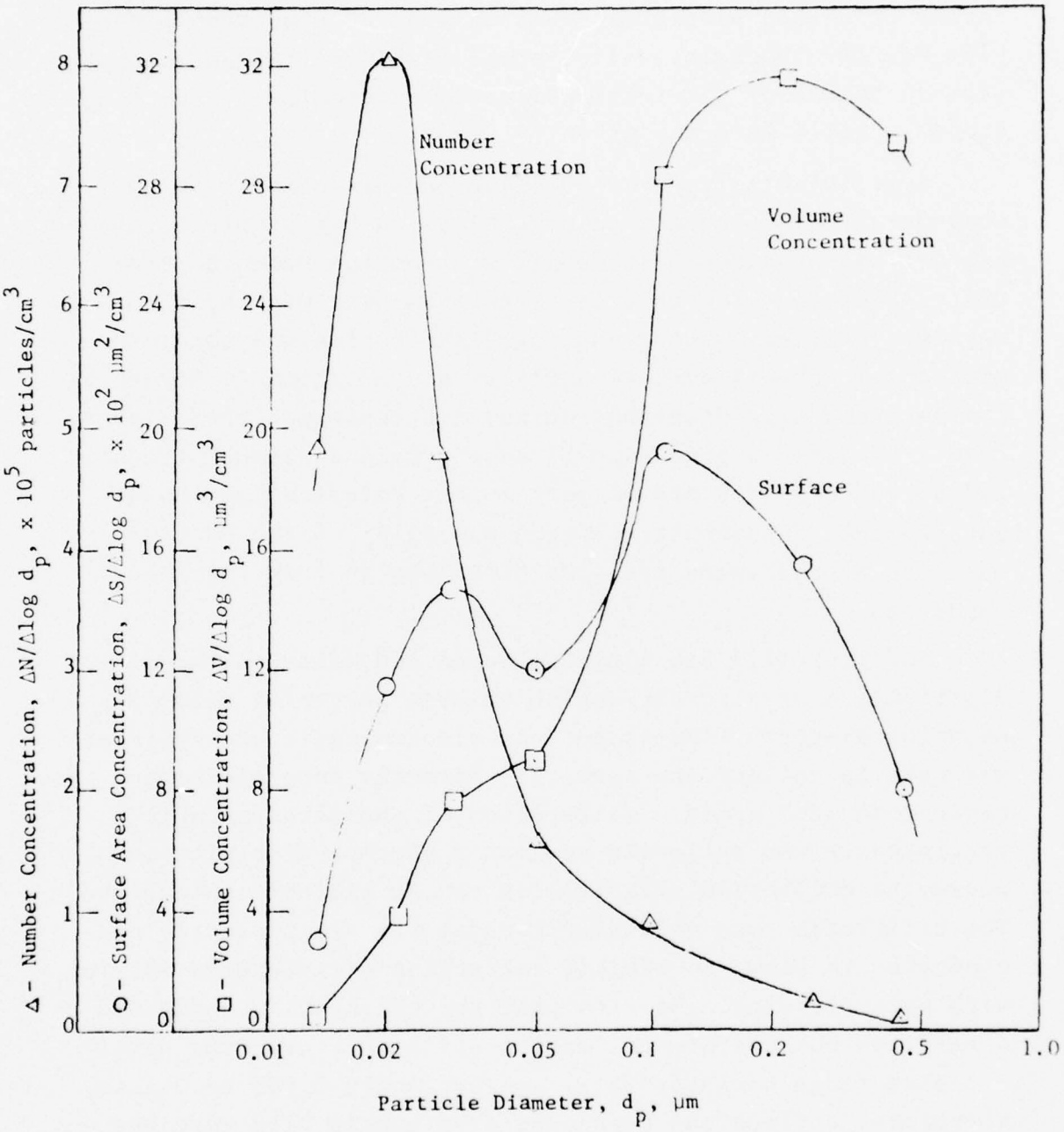

Figure 2

SIZE DISTRIBUTION OF JET AIRCRAFT EXHAUST PARTICLES SAMPLED AT RUNWAY TWO MINUTES AFTER TAKEOFF (10)

the importance of the instrument's resolution and how results can be biased as a result. Microscopes of lesser resolution tend to shift the mean count size toward larger sizes. Looking back to Figure 2, note that the count mean size (number concentration) is about 0.023 μm which is very near Boderick's 0.02 μm. This suggests that the electrical aerosol analyzer is applicable to size analysis of the exhaust particles.

The U.S. Navy, under the direction of Longley-Cook and Michalec, is directing an ongoing program conducted by Aerotherm in Mountain View, California, to construct an exhaust particulate sampler (12). The U.S. Air Force is also involved through supplemental funding. The sampler is directed toward meeting the EPA Method 5 criteria for sampling stationary sources. This approach is necessitated by the classification of engine test cells as stationary sources. Although the original design of the sampler meets the sampling criteria, funding difficulties to date have required compromises that fail to meet the sampling criteria. The sampling probe is a single nozzle, thus mandating a traversing mechanism to obtain a representative sample from the tailpipe exit plane of an engine. At present, the traversing mechanism is deleted from the sampler package. For the determination of mass emission rates, a four filter turret was considered necessary to avoid the manual changing of filter paper after each sample is obtained. Also, the moisture content of the exhaust gas was to be measured automatically and real-time, but was deleted. However, an electrical aerosol analyzer (EAA) is included in the sampler to determine the size distribution of the submicron particles.

Operation of the Navy's exhaust particulate sampler was observed during December 1975 at Alameda, California. Although formal data was not obtained, the mean size of the exhaust particles was approximately 0.3 μm. A long sample tube was used to transport the particles to the EAA and, therefore, probably introduced a bias in the size data.

Mass emission rates were not determined and the complex sample flow control system malfunctioned.

Shabod and Smirnov (13) have recently collected samples from a turbojet (TU-104) aircraft engine to determine PNA compound content -- specifically benzo(a)pyrene (BaP). Soot obtained from the exhaust nozzle walls contained 350 $\mu g\ kg^{-1}$ of BaP for the turbojet engine. Higher concentrations of BaP were measured -- 27,000 $\mu g\ kg^{-1}$ -- when the engine was operated in a test stand and special sampling procedures applied. The collection method is not described in detail, but the use of benzol adsorbents is indicated. The total BaP emission rate of the engine operating at 10,500 rpm (engine air flow and fuel flow not given) was 2,000 to 4,000 μg/min. Additional tests were conducted to determine how fuel might effect emission of BaP. The emission rate of BaP was reduced with a kerosene-type fuel containing a magnesium additive by 32% and was also reduced by 59% with dearomatized fuel. While the total BaP mass emission rate increased uniformly with engine speed, the reductions were consistent.

A design study has recently been completed by Fenton (14) regarding the design of an aircraft engine sampler specific for the polynuclear aromatic (PNA) content of the particulate material. In the study, the chemical analysis method specified required approximately 1 gram of exhaust particulate material. A sampling configuration was recommended which collected a representative particulate sample of the required mass and met the time constraints imposed by the engine's operation in a test cell. An important factor was the degradation and volatility of certain PNA species as a function of temperature. These materials must first be condensed to the particulate form and then maintained at as low a temperature as practical for overall stability of the sample. Results from this work, therefore, have implication to the present sampler under design -- samples undergoing organic chemical analysis should

be collected at a minimum temperature and stored properly to reduce the species stability problem.

Conkle, et al. (15) constructed a multistage cyrogenic trapping system to collect the organic portion of the engine's exhaust gas. Actually, a single combustor from a T-56 engine was used to generate the exhaust. A very comprehensive analysis of the organic portion of the particulates was achieved utilizing a coupled gas chromatograph-mass spectrometer system. However, more collected material was necessary for adequate quantification.

Gearhart and Benek (16) applied ARP 1179 sampling methods to a J85-GE-5 turbojet. The power range investigated included afterburning. A small diameter (0.94 cm I.D.) sample transport pipe 15.3 m long was used. Deposition losses were probably large but were not determined. The engine was operated outdoors and downstream measurements were made. From the results obtained, turbulent mixing dominated spreading of the plume. Increasing the power from idle increased the smoke number until rated power was achieved. Ambient temperature and relative humidity changes (-2 to 27°C, 20 to 50%) did not influence the smoke number data.

2.3 Aircraft Engine Exhaust Sampling

Because sampling exhaust particles behind aircraft engines has only received casual interest to date, methods and results obtained through gaseous pollutant sampling are considered important. Sampling probe design has been investigated to some extent for gaseous sampling and this information will be used in determining the final configuration of the probe used here.

Sampling at the engine exit plant with mulitple-inlet probes has been investigated by Vaught, et. al. (17), Nelson (2), Klueg and Slusher (13), and Souza (19, 20). The sampling

probe geometry varied in each of the studies, but the goal was to obtain a representative sample. Substantial improvement over any one single-point measurement was achieved with each of these probes for gaseous emission sampling.

Vaught, et al. (17) used a 28-hole sampling probe to give a representative sample of the exhaust from a T-56 engine. The probe is claimed to correct for radial distributions within the exhaust jet. The probe clamped directly onto the engine's tailpipe flange and sampled at the centroid of four equal quadrants. All but 5% of the carbon was accounted for in an overall carbon balance. Sample flow rate was 1.7 m^3/hr (1.0 scfm), and the sampling system corresponded to ARP 1256 (21), which is only concerned with the continuous sampling of exhaust gases.

Nelson (2) used a 12-point cruciform applied to the JT3D, JT8D, and JT9D engines. The probe was located approximately 25 cm downstream from the exit plane of each engine (exit mixing tube for JT9D) to insure no impairment of engine performance. Distances of 5 and 15 cm were evaluated in a preliminary manner and observed to influence engine performance. The magnitude of the influence is not given but does depend on the projected cross-sectional area of the probe normal to the flow. Reduction of the cross-sectional area permits closer placement of the probe to the exit plane.

Nelson evaluated the 12-point cruciform by separately measuring and analyzing the flow through each sampling nozzle. This was achieved by the addition of 12 solenoid-activated valves. The summation of the individual sampling nozzle average fell within 3% of the measurement obtained from the complete probe. The emissions used in this evaluation included NO_x, CO, and total hydrocarbons. Particulate material was not evaluated. However, for the objectives of this FAA study, the evaluation procedure used by Nelson is considered to be biased because a separate mapping of the exit plane conditions was not performed.

Klueg and Slusher (18) made detailed measurements of exhaust emissions from a JT8D turbofan engine using both single and multiple-point sampling procedures. Results obtained for NO_x, CO, and total hydrocarbons indicate that stratification effects within the exhaust jet can only be overcome with mixing-type sampling probes. Stratification problems are even more pronounced with mixed-flow turbofan engines. Also noted during the study was the influence that the bearing support struts and the segregated combustion zones had on the emission patterns. The recommended shape for the sampling probe is a diamond with sampling ports located at 62% of the nozzle radius. Diameter of the sampling ports was approximately 0.0762 cm (0.030 in.). This diamond shaped probe gave results to within 10% of the detailed mapping for each of the three gaseous emissions measured.

Souza (19) conducted a program where emissions of military aircraft engines were determined. The engines tested were the J52, J57, and TF30, and the gases measured were CO, NO_x, total hydrocarbons, and aldehydes. The equipment used to collect the aldehydes included two glass bubblers in series, wet test meter, and a vacuum pump. A predetermined volume of exhaust gas was passed through the bubblers using 0.06% sulfamic acid solution which retained the aldehydes. Subsequent chemical analysis (MBTH method) was used to determine the aldehyde content. Figure 3 shows the results obtained for the aldehyde measurements. Note that the aldehyde generation rate is significantly greater at idle compared to the other three power settings tested. It is likely that the JT3D, JT8D, and JT9D will exhibit similar behavior regarding organics. The sampling probe used, though not discussed, was apparently of the single-point type.

Souza (20) has completed a study that investigated the variability in gas turbine engine sampling due solely

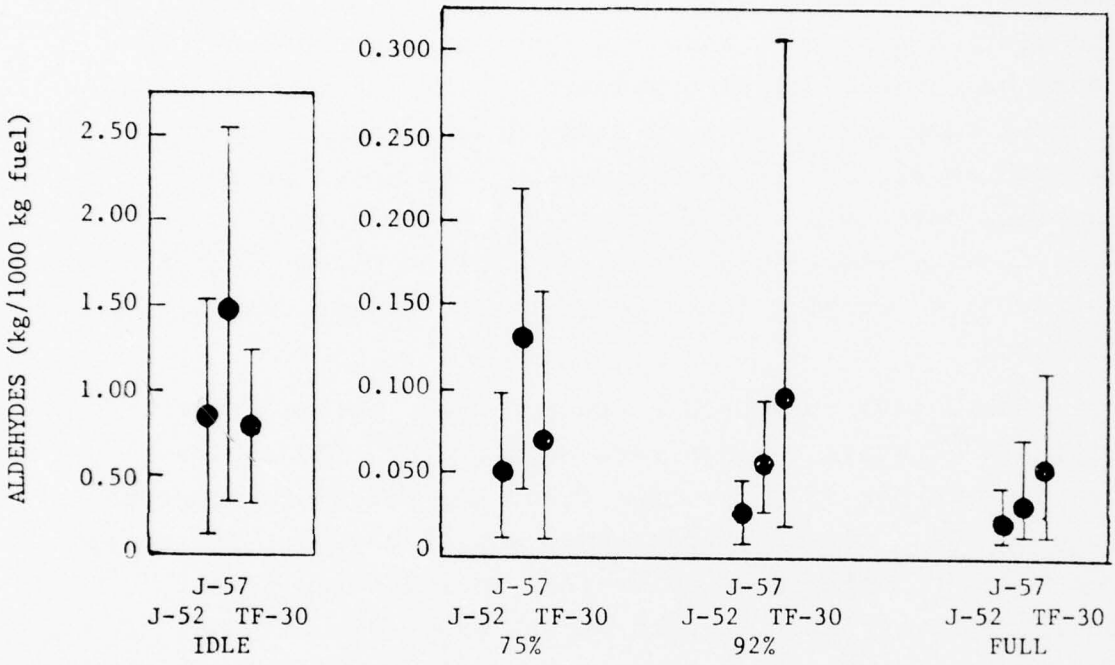

Figure 3

ALDEHYDE EMISSIONS AS A FUNCTION OF POWER SETTING WITH ENGINE TO ENGINE VARIATIONS (19)

to the sampling probe itself. Separately measured exit plane profiles of gaseous exhaust pollutants were obtained by detailed mapping incorporating a single-point traversing sampling probe. Then mixing-type sampling probes were subjected to the same conditions and the results obtained compared to the area weighted average result of the detailed mapping. Four mixing-type probes were tested:

- 12-point cruciform probe (EPA)
- 12-point diamond pattern (National Aviation Facility Engineering Center, NAFEC)
- 12-point cruciform probe, spiral hole pattern
- 24-point cruciform probe

A probe manipulator positioned the the three 12-point probes behind the engine (modified TF-30) automatically, thus avoiding problems with variability from duplicating engine power settings and changing atmospheric conditions. In the evaluation of the results, variations occurred in emission rates between the time of the detailed mapping and the mixing probe tests, from day to day, and even with individual test runs. These variations were found to be of approximately the same magnitude as the differences between the mixing probe types and the angular position of any one mixing probe. Performance of the three 12-point mixing probes were found to be within 10% of each other for a significant majority of the data. This means, in a practical sense, that probe geometry of either of the three types can be used with good assurance of obtaining a representative sample of gaseous exhaust pollutants generated by a TF-30. The 24-point probe was evaluated separately and performed in a similar fashion to the three 12-point probes -- no observable improvement. Careful analysis of the exit plane pollutant profiles is required also for the JT3D, JT8D, and JT9D before similar assurance can be given.

The effect of probe rotation on overall performance was also evaluated by Souza (20). When the 12-point cruciform and 12-point spiral was positioned between 15° and 45°, the sampled emissions increased by 15 to 20 percent. This fact can be explained by the non-symmetrical distribution of the chemical species at the exit plane. The NAFEC diamond demonstrated approximately the same variation upon rotation. However, with the NAFEC diamond, the sampling nozzle locations were selected directly from exit plane emission maps and the application of statistical methods. The result of the analysis placed the 12 assigned sampling nozzles in groups of three located 62 percent of the distance outward on four radial arms 45° from the vertical centerline. Therefore, rotation experiments with the NAFEC diamond are probably not appropriate although performance is typical of the two other probe configurations.

Lyon (22) has recently developed procedures for gaseous emissions measurement of afterburning engines. Because the chemical composition of the exhaust was important, an immediate quench was employed to freeze the reactions. The gas analysis system measured the concentrations of CO, CO_2, NO, NO_x, and unburned hydrocarbons. The pump used to transport the sample was placed directly downstream from the probe inlet. In this way, the pressure within the probe (less than 4,200 kg/m^2) provided the "aerodynamic" quench. Smoke number measurements were attempted but proved impossible because of pump location and long sampling lines.

The effect of ambient conditions of the emissions from turbine engines has been investigated experimentally by Souza (20,23) and Vaught (24). Souza's work utilized a military aircraft engine (TF-30) while Vaught's was concerned with a stationary gas turbine used for industrial applications (Allison model AG9102-2). The results obtained by both only pertain to gaseous pollutants, and as yet, no work has been done with the effects on exhaust particles.

In the work by Souza, additional sources of variation clouded the emission changes attributed to atmospheric conditions, but distinct trends were observed amounting to over 15 percent at rated power for total hydrocarbon content. Vaught's work, however, indicates detailed trends as shown in Figures 4 and 5. Figure 4 shows the variation in smoke number with output horsepower and compressor inlet temperature. The effect of inlet pressure on both CO and total hydrocarbon content is shown in Figure 5. How the exhaust particles themselves are influenced by changing atmospheric conditions remains unanswered.

2.4 Isokinetic Sampling

To insure the acquisition of a representative sample -- one which is correct with respect to both particle size distribution and concentration -- isokinetic sampling is usually required. Isokinetic sampling is defined as the situation where the gaseous sample is withdrawn at the same velocity as the gas stream at the point of sampling. If the velocity at the nozzle inlet does not match that of the gas stream, an erroneous sample is collected as a result of the inertia of the particles. When the sampling velocity is less than the gas stream velocity, part of the approaching stream is deflected. The light particles tend to follow the streamlines and do not enter the probe, but the heavier particles, due to their inertia, continue along their previous path and enter the nozzle. As a result, a high proportion of the heavier particles are sampled and the total particulate mass is therefore greater than expected. On the other hand, if the sampling velocity is greater than the main stream velocity, the gas stream will converge towards the nozzle inlet carrying the lighter particles. The heavier particles will tend to continue along their original path because of their greater inertia and thus miss the nozzle. The collected sample will contain a relative excess of the lighter particles and the particulate mass will be in error on the low side.

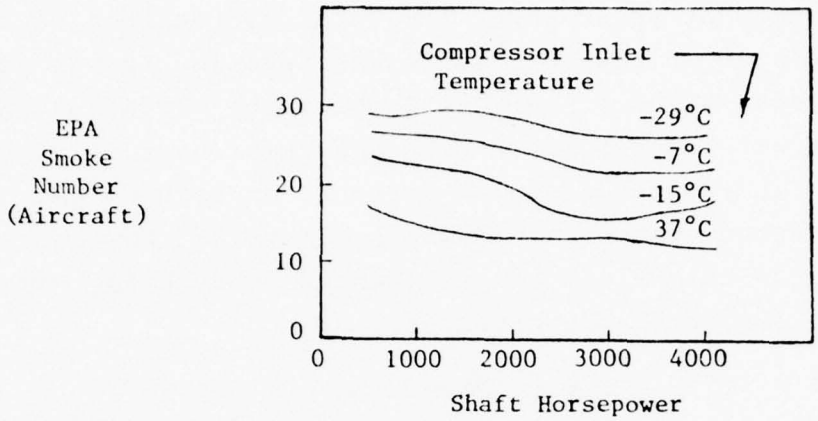

Figure 4

EFFECT OF INLET TEMPERATURE ON SMOKE EMISSIONS
(501-K INDUSTRIAL ENGINE, CONSTANT SPEED
JP-5 FUEL)

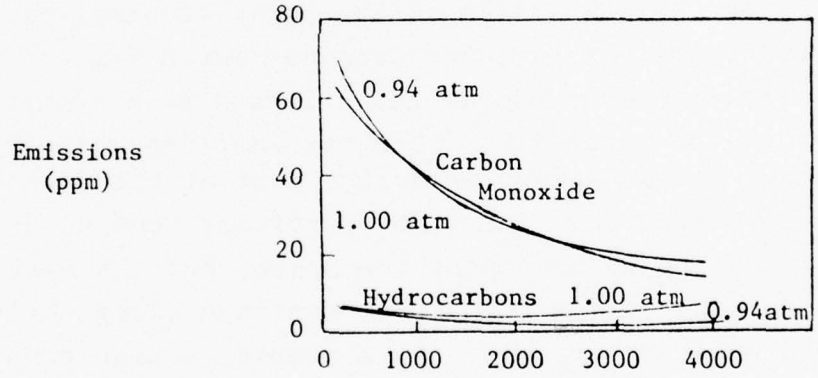

Figure 5

EFFECT OF INLET PRESSURE ON CARBON MONOXIDE AND
HYDROCARBON EMISSIONS (501-K INDUSTRIAL ENGINE,
CONSTANT RPM, JP-5 FUEL, 37°C COMPRESSOR
INLET TEMPERATURE)

Study of anisokinetic sampling dates back to 1911, when Brady and Touzalin (25) made measurements with coal dust. Numerous articles have appeared since, but the major emphasis has been on the incompressible flow regime. In fact, theoretical or experimental data regarding anisokinetic sampling within the compressible flow regime has not appeared in the literature. Therefore, a brief review of the incompressible results is given and ongoing research investigating isokinetic sampling within compressible flow is discussed.

Determined by numerous investigations was the dependence of the sampling error (difference between the measured particulate concentration and the true particulate concentration) on both the particle's inertia and the ratio of sampling velocity to free stream velocity (26,27,28). Later, Rouillard and Valvona (29) made careful measurements utilizing hot wire anemometry showing the existence of a stagnation zone upstream from the sampling nozzle. Vitols (30) has calculated the entire flow field assuming an ideal frictionless fluid and a nozzle with infinitesimally thin walls. These calculations gave the theoretical sampling errors which compared favorably with previous anisokinetic sampling measurements. Because of the assumption concerning thin walls of the sampling probe, the experimentally varified stagnation zone did not appear in the theoretical results.

Whiteley and Reed (31) performed experiments on nozzles with an outside-to-inside diameter ratio of 1.25 and chamfers of 180^{o}, 120^{o}, and 15^{o}. Significant errors were observed from isokinetic conditions when the chamfer angle varied between 120^{o} and 180^{o}. A negligible effect was measured for smaller chamfer angles. The effect of probe stem distance from the nozzle was also studied. Only a small change in accuracy occurred when changing this distance from 4.8 to 1.6 nozzle diameters. A similar study was conducted by Smith (32) where the larger diameter probes were seen to be more efficient

in sampling particles and the sharp-edged nozzles in all cases performed better than the blunt nozzles. Rouillard and Valvona's measurements (29) indicate that the probe stem should be approximately 10 nozzle diameters downstream.

Fuchs (33) and Parker (34) have proposed an inertial parameter, ψ, to qualitatively describe the adherence of the particles to the gaseous streamlines. The inertial parameter is

$$\psi = \frac{\bar{\rho}_p d_p^2 V_e C}{18 \mu_g D} \qquad [1]$$

where

$\bar{\rho}_p$ = density of particulate material

d_p = particle diameter

V_e = free stream gaseous velocity

C = Cunningham correction factor

μ_g = dynamic viscosity

D = sampling nozzle diameter

Particles that have $\psi < 0.05$ follow the gaseous streamlines and will be sampled correctly. When $\psi > 50$, gaseous flow does not influence the particle trajectories at all. For $0.05 < \psi < 50$, the particle motion is altered to some extent.

Sampling errors resulting from probe alignment are small ($\sim$ 10 percent) with angles approximately 30° or less (26). In addition to probe alignment, turbulent motion within the fluid itself causes some lateral motion of the particles depending upon their inertia. Sampling errors resulting from the level of turbulence relate back to probe alignment because the turbulence causes the particle's trajectory to deviate from the fluid streamlines defined by

the mean motion. For example, assuming a turbulent intensity (normalized velocity of fluctuating component) of 10 percent, the deviation in particle trajectory would be about 5 percent and therefore resulting in negligible sampling error. As the turbulence intensity increases, the particle trajectory deviation would also increase thus increasing the "effective" sampling probe misalignment. However, the turbulent intensity would have to be very large before sampling errors due to misalignment are significant.

The incompressible anisokinetic sampling literature reported here generalizes on two points. First, the sampling nozzle should be as streamlined as practical with sharp edges. Second, the stem should be approximately 10 nozzle diameters downstream.

Two investigations are presently underway concerned with sampling problems in compressible flow. It seems reasonable to suspect that shock and boundary layer effects on small diameter probes could significantly alter the particulate sample collected. One of these studies was mentioned previously - the work of Aerotherm Corporation with the U.S. Navy (12) and the second is the graduate work of a Ph.D. candidate at Oregon State University, Captain Martone (35). Both these studies have not yet generated conclusive results.

The Navy's automated sampler had a particularly difficult requirement to meet - isokinetic sampling up to a Mach number of 1.2. The probe nozzle geometry designed to meet this requirement is shown in Figure 6. The sampling nozzle is 3/16 in. and the material of construction is a special steel alloy. The internal wall of the nozzle within the "shock-down" region is roughened to trip the boundary layer and generate relatively weak shock diamonds before entering a normal shock. Therefore, the sample velocity Mach number at the nozzle entrance can be greater than one. Also, in this manner, damage to the particulate sample is reduced and

pressure recovery is improved. The capability of sampling isokinetically in supersonic flows is not required in the present sampler because at the sampling probe tip, the Mach number reaches a maximum of 1.0 for take-off power settings. Upstream from the probe tip -- at the exit plane of the exhaust nozzle -- the local Mach number could exceeding unity (especially the JT3D and JT9D).

Captain Martone (35) is in the process of constructing test equipment where controlled sampling experiments can be made in a supersonic free jet which also contains a monodispersed aerosol. The influence of sampling velocity and probe-tip geometry will be investigated. Both of these studies will be monitored as the results obtained will define more closely the errors associated with anisokinetic sampling within compressible flows.

Private communication with Klarmen (36) indicates that variations in the sampling velocity at the exit plane of an aircraft turbine engine of $\pm$ 25 percent of the free stream velocity results in negligible sampling error. The EPA Method 5 sampling train was used to make the mass measurements behind the engine. Klarman's results do not include supersonic flows, but do include flows approaching the sonic condition.

At this point, in the absence of refined experimental data, a tolerance of $\pm$ 25 percent in the sampling velocity referenced to the exit plane velocity seems permissible. The effect that anisokinetic sampling up to the $\pm$ 25 percent level has on the particle size distribution is undocumented but is preliminarily investigated in a later section.

2.5 Summary of Literature Review

The literature pertaining to sampling and characterizing exhaust particles generated by aircraft turbine engines is not comprehensive. Aerospace Recommended Practice 1179 (1) gives procedures for determining smoke number which is the only accepted measurement of particulate loading. Mass emission rates from various engines have been measured

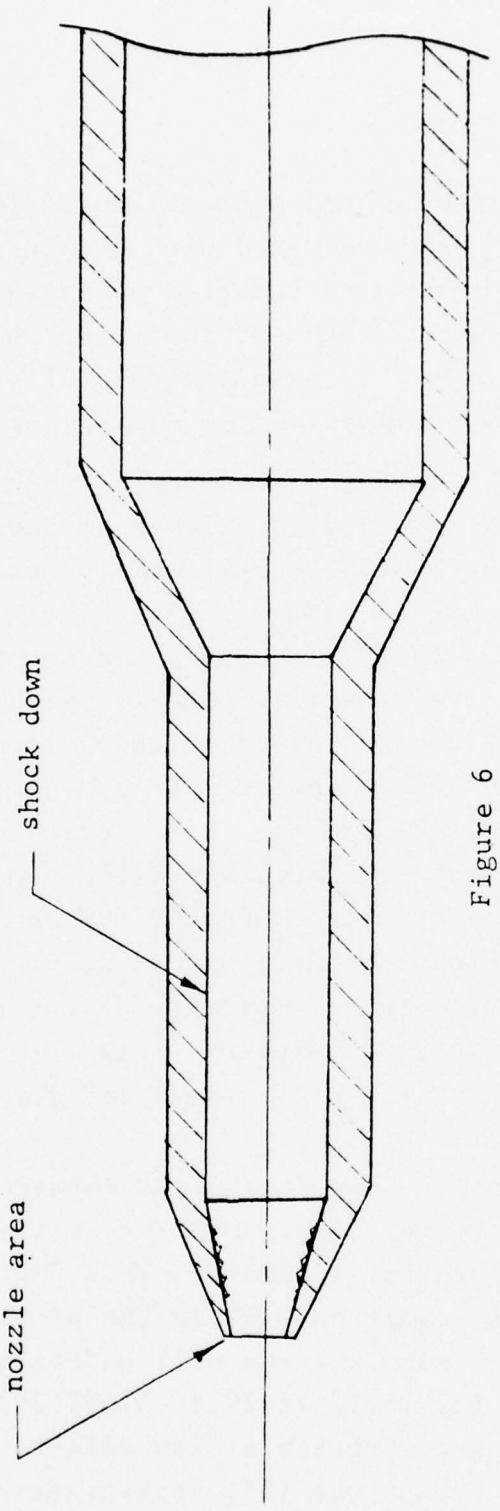

Figure 6

NOZZLE CONFIGURATION FOR THE U.S. NAVY'S AUTOMATED EPA METHOD 5 SAMPLER (12)

(2,4,5,7) but only Johansen and Kumm (5) investigated the experimental difficulties concerned with obtaining reliable data. Sem (10) has informally reported a size distribution of turbine engine generated exhaust particles where the count mean size was 0.023 μm. This mean particle size is also supported by the microscopic analysis of Boderick (11).

Gaseous exhaust sampling of engines is relevant as similar techniques are generally employed. Numerous investigators (17,18,19,20,21,22) have made careful measurements of engine exhaust pollutants: CO, CO_2, NO_x, and total hydrocarbons. The measurements are simplified because the species of interest are gaseous and relatively easy to handle. With gaseous sampling, Klueg and Slusher (18) selected a diamond shaped sample-mixing probe based on engine exit plane traverses (JT8D) to locate the 12 sampling nozzles. Other probe configurations have also been used (area weighted and related modifications) but Souza (20) has investigated three of the common probes and concluded that significant variations do not occur from the probes themselves. Because the majority of the sampling experience occurs with gaseous sampling--this data was used as a guideline in designing the probe specified for the present sampler under consideration.

Since the volumetric flow rates from commercial turbine engines is extremely large, only a portion of the total exhaust flow is required for analysis. This fact raises the question of isokinetic sampling. While the problems associated with isokinetic sampling are well understood for incompressible flows (25,26,27,28,29,30,31,32,34), no results are reported involving compressible flow effects. A current program is conducted by Martone (35) investigating this

question, but results are not yet available. This program is evaluating the influence of nozzle shape on particle capture where the aspiration rate will be varied.

3. CONCEPTUAL DESIGN OF SAMPLER

Before the mechanical details of the exhaust particle sampler can be examined, the overall concept and design philosophy must be discussed. This section presents the engineering analysis used in arriving at the conceptual design of the sampler.

In considering the design of the turbine engine exhaust sampler, the sampling probe must deliver a representative sample of the engine's exhaust particulate material. The second consideration is the location of the particulate sampling equipment. Placing the sampler near the engine, the aerosol transport pipe is eliminated. Otherwise, the aerosol must be transported to the test cell control room where the sampling equipment would be located. The components of the sampling system include:

- Sampling probe
- Diluter
- Electron microscope grid preparation
- Mass emission measurement
- Particulate mass collection for organic chemical analysis

and would essentially be identical regardless of transport. Consequently, the influence of the aerosol transport pipe can be analyzed separately. Also, the sample collection methods and analyses can be examined apart from the transport pipe. The analysis presented here takes the same form -- each component is discussed separately.

3.1 Sampling Probe

The first requirement of the sampler is to withdraw a representative sample of the exhaust particles. The exhaust sample must be obtained by aspiration through a probe fitted with a nozzle and positioned in the upstream direction.

3.1.1 Sampling Nozzle Performance

The literature on isokinetic sampling has already been reviewed. As noted then, no work was found concerning flow details within the compressible regime and several articles were found concerning the flow upstream of the sampling nozzle. Results from the literature did, however, establish that the error due to anisokinetic sampling depended not only on the ratio of the main stream velocity to the sampling velocity, but also depended on particle inertia.

Several additional points in regard to sampling are important. The difference in nozzle performance caused by compressibility is shown in Table 2 with the area and velocity ratios. Table 2 gives the exit plane conditions for each engine as a function of power setting. If incompressible flow is assumed, the area ratio equals the velocity ratio. The deviation between the compressible and incompressible flows is therefore given by the difference between the area and velocity ratios of Table 2. As can be seen, the deviations are not greater than 5 percent relative to the compressible flow condition. On this basis, the inertial parameter commonly used for incompressible flows is useful for anticipating particle trajectories, though not strictly applicable. The inertial parameter (ψ) is given in Equation 1.

Also note from Table 2 the engine exit plane conditions. In no instance is the local Mach number greater than unity. Therefore, the problem of sampling in a supersonic stream does not exist and a straight forward sampling nozzle design is appropriate.

When $\psi < 0.05$, the particle trajectory adheres to the gaseous streamline, and when $\psi > 50$, the particle trajectory is unaffected. Another point is that the distance a streamline is displaced perpendicular to its upstream direction is

Table 2

ENGINE EXIT PLANE CONDITIONS AND PREDICTION* OF SAMPLING FLOW PARAMETERS AT SEA LEVEL

Engine	Power Setting	T_T (°C)	M_e	V_e (ft/sec)†	$\rho_e V_e$ (lb/ft²sec)†	One Design Point: Design $\rho_e V_e$	One Design Point: $\frac{A_p}{A_{st}}$	One Design Point: $\frac{V_e}{V_p}$	Two Design Points: Design $\rho_e V_e$	Two Design Points: $\frac{A_p}{A_{st}}$	Two Design Points: $\frac{V_e}{V_p}$
JT3D	T.O.	505	1.00	1560	53		1.95	2.07		1.23	1.30
	Cli	455	0.87	1502	54		1.98	1.99		1.25	1.25
	Cru	405	0.72	1201	43.2		1.59	1.59	43.2	1	1
	App	365	0.47	755	27.2	27.2	1	1		1.61	1.76
	Idle	290	0.28	430	16.9		0.62	0.57	16.9	1	1
JT8D	T.O.	520	1.00	1609	56.0		1.75	1.82		1.20	1.26
	Cli	485	0.96	1584	53.4		1.67	1.79		1.14	1.24
	Cru	415	0.76	1282	46.8		1.46	1.45	46.8	1	1
	App	365	0.55	885	32.0	32.0	1	1		2.16	2.08
	Idle	350	0.26	425	14.8		0.46	0.48	14.8	1	1
JT9D	T.O.	510	0.70	1440	46.1		1.61	1.73		1.31	1.39
	Cli	460	0.60	1033	35.1		1.22	1.24	35.1	1	1
	Cru	395	0.50	831	28.7	28.7	1	1		0.82	0.80
	App	355	0.34	554	19.9		0.69	0.67		1.31	1.35
	Idle	320	0.25	410	15.2		0.53	0.49	15.2	1	1

* Prediction utilizes compressible flow theory.

† To convert from: ft/sec to m/sec, multiply by 0.305;
lb/ft²sec to kg/m²sec, multiply by 4.87.

$$\Delta x = \frac{D}{2}\left(1 - \frac{\overline{A_{st}}}{A_p}\right) \qquad [2]$$

and is plotted in Figure 7. The important feature is the non-linearity of the relationship. Consequently, it is more desirable to sample at velocities greater than the main stream velocity rather than at smaller velocities. For example, at A_p/A_{st} = 2.0 and 0.5, the corresponding $\Delta x/D$ is 0.15 and -0.20 respectively. The minus sign indicates a streamline displacement away from the axis of the sampling probe.

Practical considerations also influence the performance and operation of the sampling nozzle. The Mach number inside the nozzle itself should be as low as possible. Complications in the flow field due to shock waves and their interactions should be avoided. A constant area probe would exhibit poor performance because at the higher power levels, the flow may accelerate or decelerate depending on the conditions. Hence, the flow could be undergoing a transformation not anticipated and give erroneous results. The area of the probe should be increased downstream from the inlet to reduce the internal flow Mach number. The reduced Mach number should be 0.3 or less because at 0.8, the boundary layer growth is sufficient to decrease the effective flow area (displacement thickness is the effective area restriction). Therefore, the maximum sampling Mach number is 0.8 and is observed in the selection of design flow rates.

Table 3 shows calculation results for ψ, the inertial parameter for each of the three engines and five power settings. Three particle sizes are assumed -- 0.1, 1.0, and 2.0 μm each having a specific gravity of 1.3 (typical of carbonaceous material). For each particle size, two values relating to ψ are given, the left value giving the sampling nozzle diameter corresponding to ψ = 0.05 where the particle trajectory follows

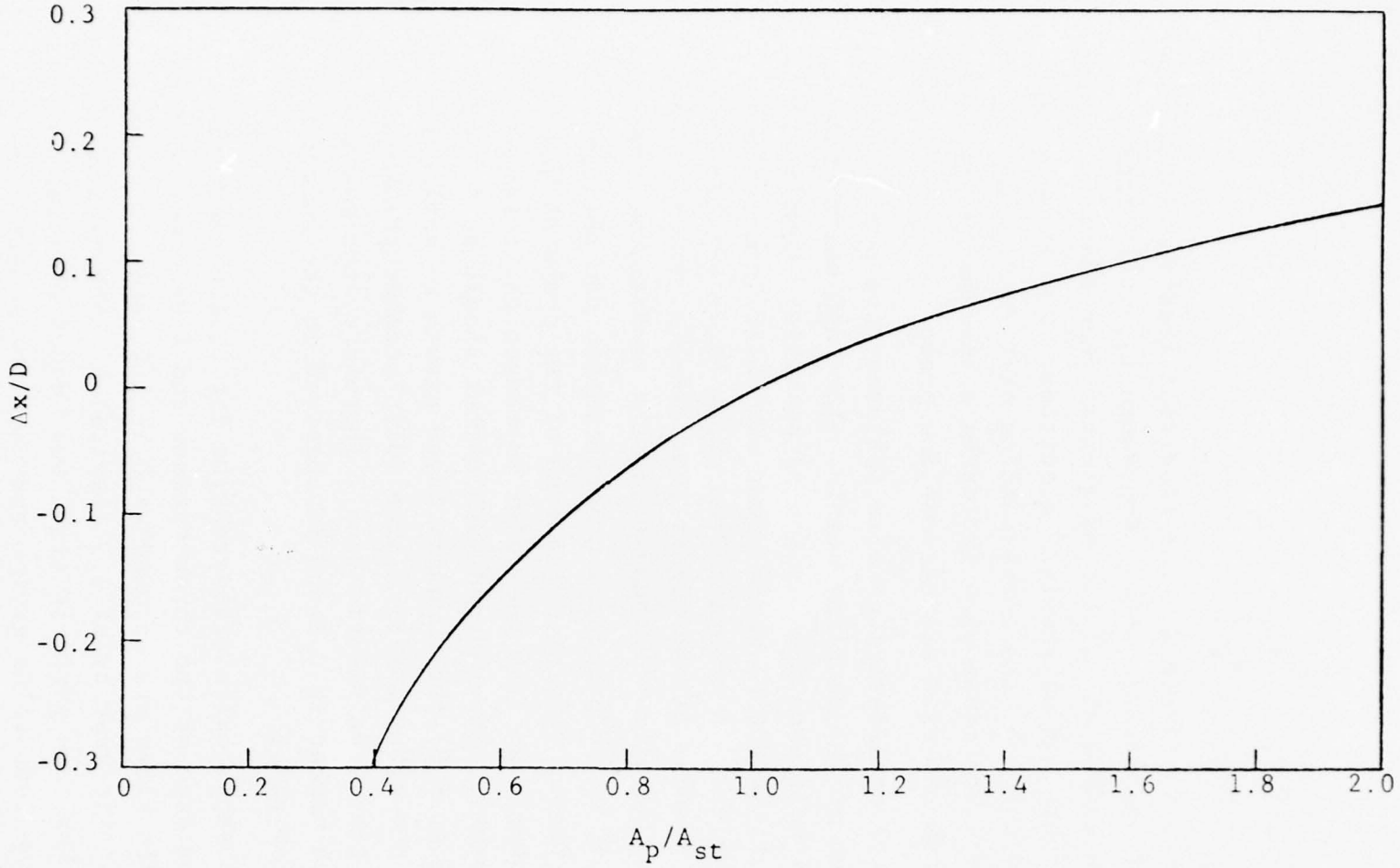

Figure 7

VARIATION OF NORMALIZED DISPLACEMENT WITH SAMPLING AREA RATIO

Table 3

CALCULATIONS FOR INERTIAL PARAMETER
WITH ENGINES OPERATING AT SEA LEVEL

Engine	Power Setting	d_p=0.1 μm		d_p=1.0 μm		d_p=2 μm	
		D for ψ=0.05[2] (cm)	ψ for D=0.1cm[3]	D for ψ=0.05[2] (cm)	ψ for D=0.1cm[3]	D for ψ=0.05[2] (cm)	ψ for D=0.1cm[3]
JT3D	T.O.	0.038	0.019	2.16	1.08	8.6	4.3
	Cli	0.041	0.020	2.14	1.08	8.6	4.3
	Cru	0.036	0.018	1.78	0.90	7.1	3.6
	App	0.027	0.014	1.20	0.60	4.8	2.4
	Idle	0.018	0.0088	0.74	0.38	3.0	1.5
JT8D	T.O.	0.033	0.017	1.90	0.96	7.6	3.8
	Cli	0.035	0.018	1.92	0.96	7.7	3.8
	Cru	0.037	0.019	1.90	0.96	7.6	3.8
	App	0.031	0.015	1.40	0.70	5.6	2.8
	Idle	0.017	0.0084	0.68	0.34	2.7	1.4
JT9D	T.O.	0.039	0.020	2.02	1.01	8.1	4.0
	Cli	0.030	0.015	1.41	0.74	5.6	3.0
	Cru	0.029	0.015	1.26	0.64	5.0	2.6
	App	0.021	0.010	0.88	0.44	3.5	1.8
	Idle	0.017	0.0086	0.72	0.36	2.9	1.4

1. Particulate material specific gravity equals 1.3.

2. Sampling nozzle diameter (D) corresponding to ψ = 0.05.

3. Resulting value of ψ for sampling nozzle diameter equal to 0.1 cm.

Note: d_p = particle diameter, T.O. = take-off, Cli = climb, Cru = cruise, App = approach.

the gaseous streamlines. The right value assumes a sampling nozzle diameter of 0.1 cm and gives the resulting value of ψ. To maintain the acquisition of a representative sample, a necessary condition is $\psi \leq 0.05$. For $\psi \geq 50$, the particle trajectories are not influenced by the gaseous flow at all. For $0.05 < \psi < 50$, the particle trajectory is influenced somewhat. The calculations show that for 0.1 μm particles, the particle trajectory will follow the gaseous streamlines. However, for 1.0 and 2.0 μm diameter particles, the trajectory will not adhere to the streamlines, but will be influenced. For correct sampling of 2.0 μm particles, the sampling nozzle diameter must be approximately 8 cm at the take-off power setting. This is impractical as the flow which would be handled would be entirely too high.

If the diameter of the nozzle is increased to 0.2 cm, then ψ is halved, thus improving the sampling of particles. At this larger diameter, particles 0.2 μm and smaller will be sampled correctly regardless of the sampling velocity. As particle size increases beyond 0.2 μm, the trajectory is affected progressively less. At 1.0 μm, the maximum ψ is about 0.5 -- 10 times greater than the maximum for perfect streamline adherance, but 100 times less than 50 where the particles continue in a straight line. At d_p = 2 μm, the ψ value is intermediate between the defined extremes for particle motion.

The inertial parameter, ψ, is basically the stopping distance of a particle divided by the internal diameter of the nozzle. As such, ψ does not reflect the influence of varying sampling velocities. Therefore, an indication of the particle's motion in the region of the probe's upstream disturbance can be derived from the ratio of the time in which the particle is within this disturbance (Δt) and its relaxation time. The relaxation time is given as

$$\tau = \frac{d_p^2 \bar{\rho}_p}{18\mu_g} \qquad [3]$$

and is basically the time required for a particle to adjust to a new flow condition. Assuming that the disturbance is propagated upstream 6 nozzle diameters*, the ratio of $\Delta t/\tau$ is greater than unity for all particles smaller than 5 μm at all engine operating conditions. This roughly means that particles less than 5 μm will adjust with the gaseous flow and be sampled correctly. However, no experimental evidence exists at this time regarding this assertion.

3.1.2 Analysis of Mixing Probe Configuration

Besides the question of an individual sampling nozzle obtaining a representative sample, the location or the traversing sequence of the sampling nozzles is equally significant. Initially, manual or automated single-point sampling probes are considered undesirable due to the sample at any one time being unrepresentative. In the analysis for particle size, a single representative sample is virtually mandatory. In addition, the single-point traversing mechanisms are cumbersome, require longer sampling times, and are expensive.

Numerous investigators have used four basic sampling probe configurations for the measurement of gaseous emissions. These basic configurations include:

- Area averaged
- Spiral hole pattern
- NAFEC diamond
- Single-point, traversing

---

* This upstream distance was obtained by averaging the results reported in the gaseous sampling literature.

The area averaged probe is also referred to as a multiple-point cruciform where the actual number of sampling points can vary. The Environmental Protection Agency recommends in its source testing regulations that in stack sampling, area-averaged points based on diameter must be used. This procedure allows the unweighted arithmetic summation of the individual point emissions to equal the total emissions from the source. The cruciform probe accomplishes this task through mixing each of the sampling point emissions to achieve one total sample in the end. The sampling nozzles in the cruciform probe are placed on orthogonal arms oriented horizontally and vertically with respect to the engine.

Numerous investigators have employed the cruciform configuration for the determination of gaseous emissions on various engines including the T56, JT3D, JT8D, TF30, and JT9D. The gaseous emission measurements included NO_x, CO, CO_2, and total hydrocarbons. Evaluation of the cruciform's performance was only determined in two instances (2,20) through detailed mapping of the exit plane conditions.

Because variations in particulate mass concentration data at the exit plane is not available, none of the probe configurations can be recommended on this basis. Moreover, relying on probe performance based on gaseous emission measurements only offers reliable data on one engine -- TF30. A reasonable assumption to make is that exit plane variations in the gaseous emissions (especially total hydrocarbons) correspond to variations in particulate material emissions. This assumption is necessary if the gaseous data is to be used.

Because none of the probe configurations offered significantly better gaseous performance, the simplest geometry would be the best choice. This is the NAFEC diamond where the sampling nozzles are located 62 percent outward from the center of the exit plane. Important to note is that the NAFEC diamond

was specifically designed in conjunction with JT8D engine. The JT3D engine is about the same in exit plane area and a similar probe configuration should yield a representative sample. Probes have been used interchangeably between the JT3D and JT8D with acceptable results (2). For this study, however, separate probes will be fabricated to suit the JT3D and JT8D engines. For the JT8D, four sampling nozzles (0.20 cm diameter) will be located as specified (18). With the JT3D, the same configuration will be used but the gas generator flow is the stream sampled. The JT9D presents mechanical design problems by virtue of the afterbody, but the same approach is taken -- the gas generator flow will be sampled approximately 2-4 inches downstream from the outer annular lip. Expansion of the flow and its effect on emission concentrations is therefore minimized. For each engine then, four sampling nozzles will be employed.

Examining the 4-point configuration more closely, exit plane maps of gaseous emissions are given for each of the three engines in Figures 8 through 16 (37). The CO and total hydrocarbon data is given for the idle power setting and the NO_x data is given for maximum continuous. The points indicated correspond to the sampling locations for the NAFEC diamond. The center sampling nozzle location is the selection for the probe recommended in this study. Table 4 summarizes the results of the exit plane data. The percent deviations in the two right-hand columns give the relative performance of the NAFEC diamond and the 4-point modification. The overall deviation summed from all the measurements is less than 5 percent for both probes. However, considering only the total hydrocarbon data, the 4-point configuration and the NAFEC diamond are both 34 percent below the mean. Since both probes have similar performance, the 4-point probe is still acceptable.

Further justification for only four sampling nozzles in the probe configuration results from the problem in "handling"

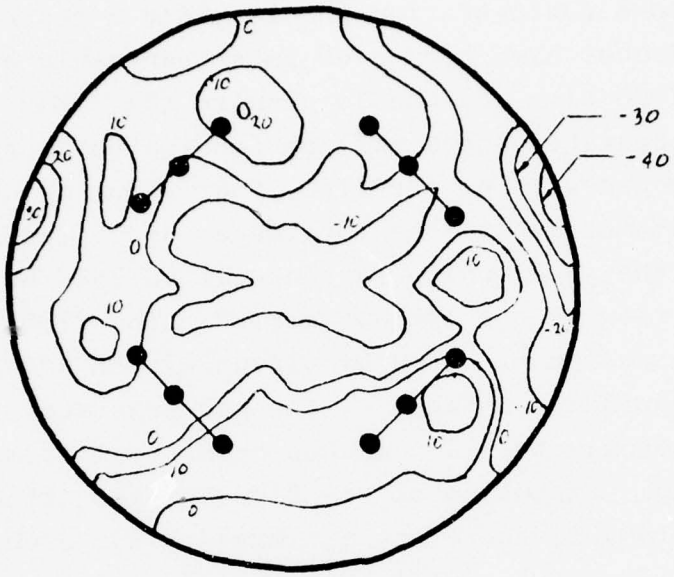

Figure 8

JT3D ISOPLETH FOR CARBON MONOXIDE AT IDLE WITH NAFEC SAMPLING NOZZLE LOCATIONS (37)

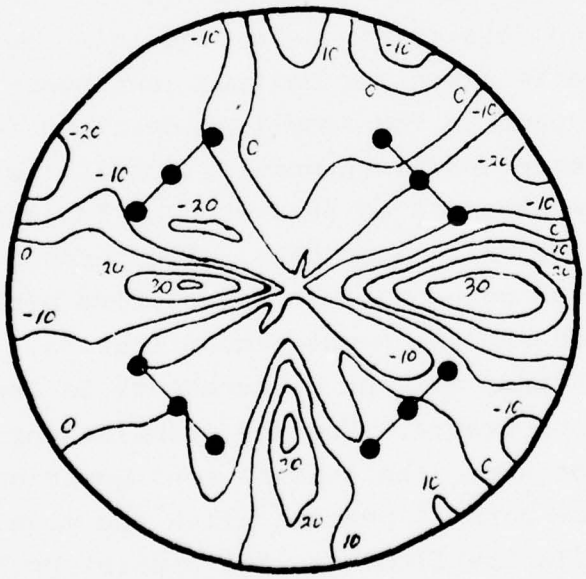

Figure 9

JT3D ISOPLETH FOR TOTAL HYDROCARBONS AT IDLE WITH NAFEC SAMPLING NOZZLE LOCATIONS (37)

Note: Isopleth values are given as percent deviation from area weighted average

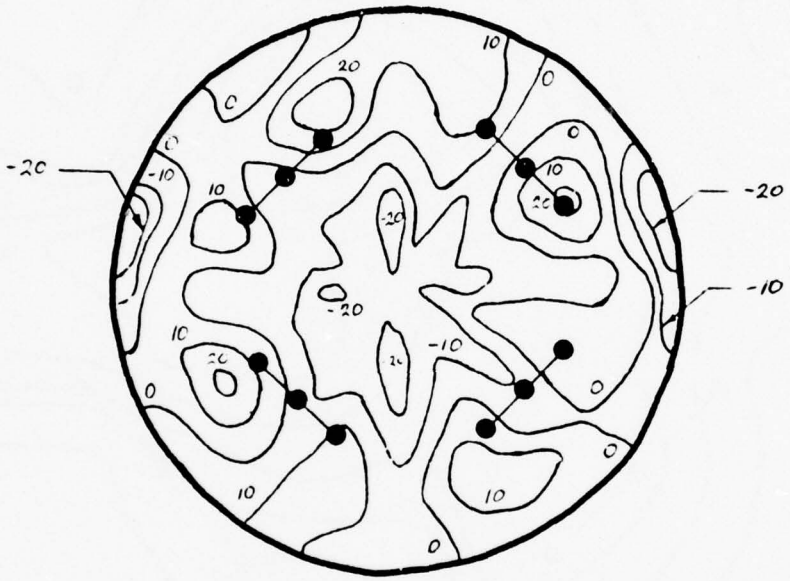

Figure 10

JT3D ISOPLETH FOR OXIDES OF NITROGEN AT MAXIMUM CONTINUOUS WITH NAFEC SAMPLING NOZZLE LOCATIONS (37)

Note: Isopleth values are given as percent deviation from area weighted average

Figure 11

JT8D ISOPLETH FOR TOTAL HYDROCARBONS AT IDLE WITH NAFEC SAMPLING NOZZLE LOCATIONS (37)

Note: Isopleth values are given as percent deviation from area weighted average

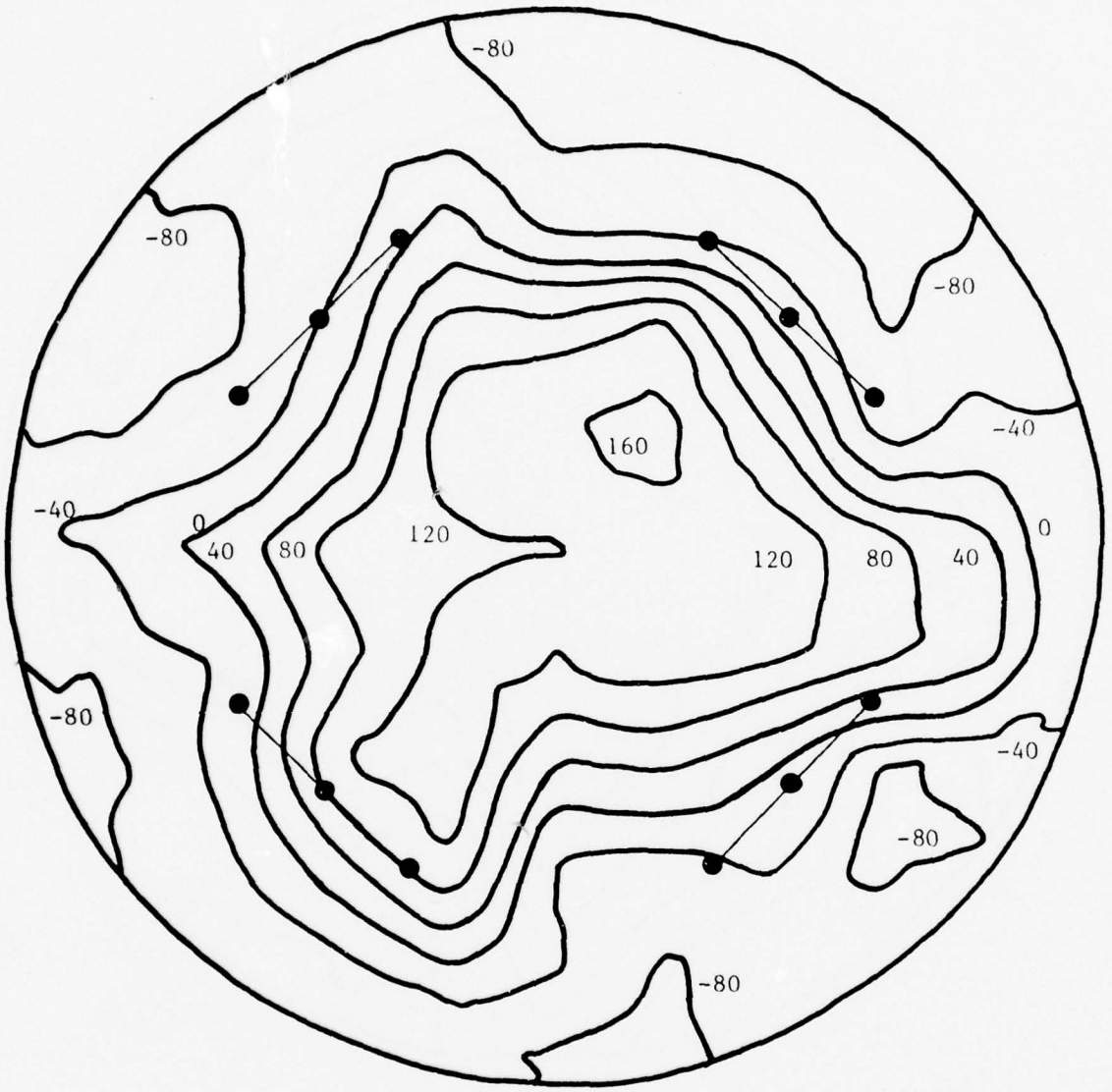

Figure 12

JT8D ISOPLETH FOR CARBON MONOXIDE AT IDLE WITH NAFEC SAMPLING NOZZLE LOCATIONS (37)

Note: Isopleth values are given as percent deviation from area weighted average

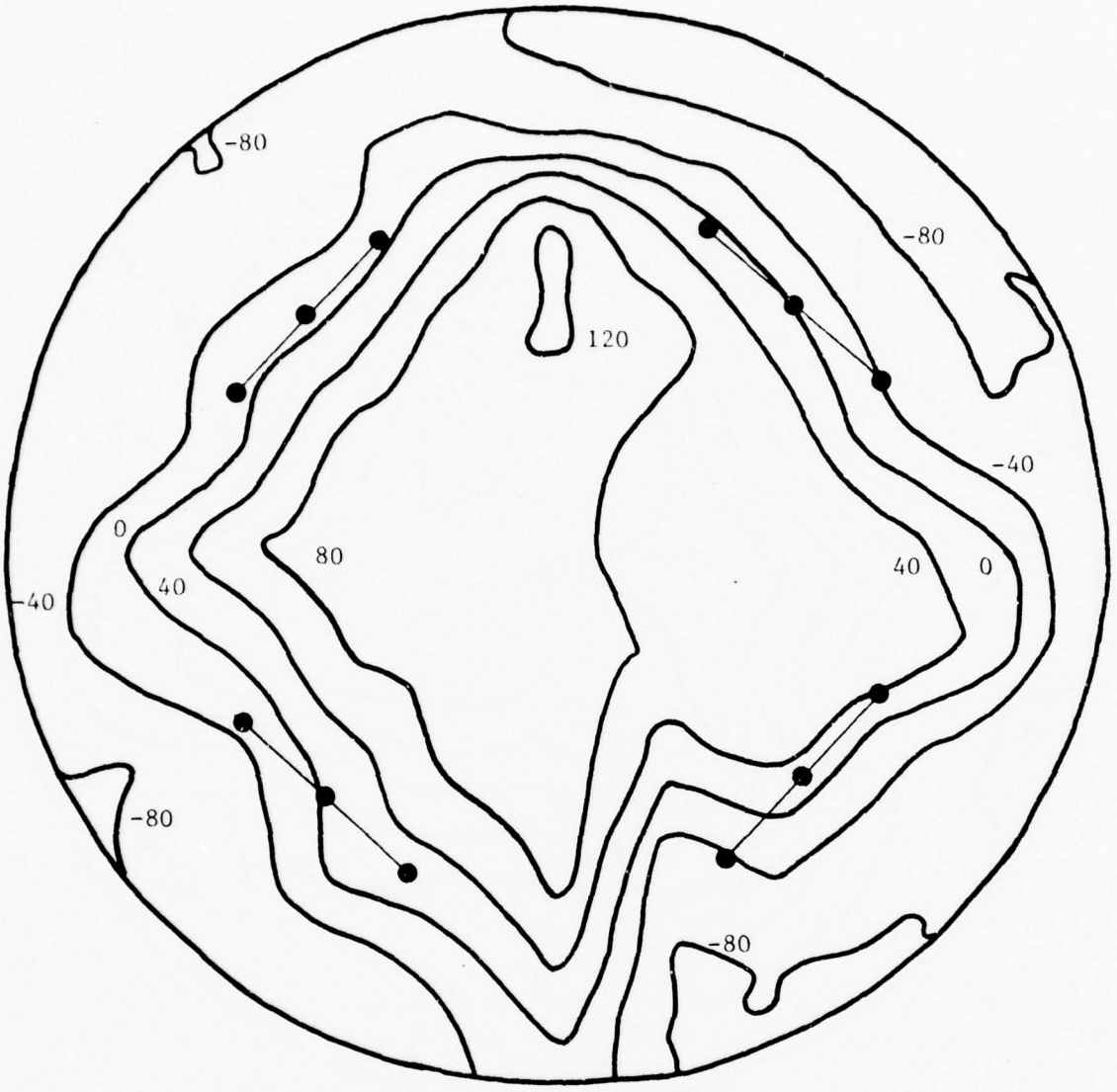

Figure 13

JT8D ISOPLETH FOR OXIDES OF NITROGEN AT MAXIMUM CONTINUOUS
WITH NAFEC SAMPLING NOZZLE LOCATIONS (37)

Note: Isopleth values given as percent deviation from area weighted average

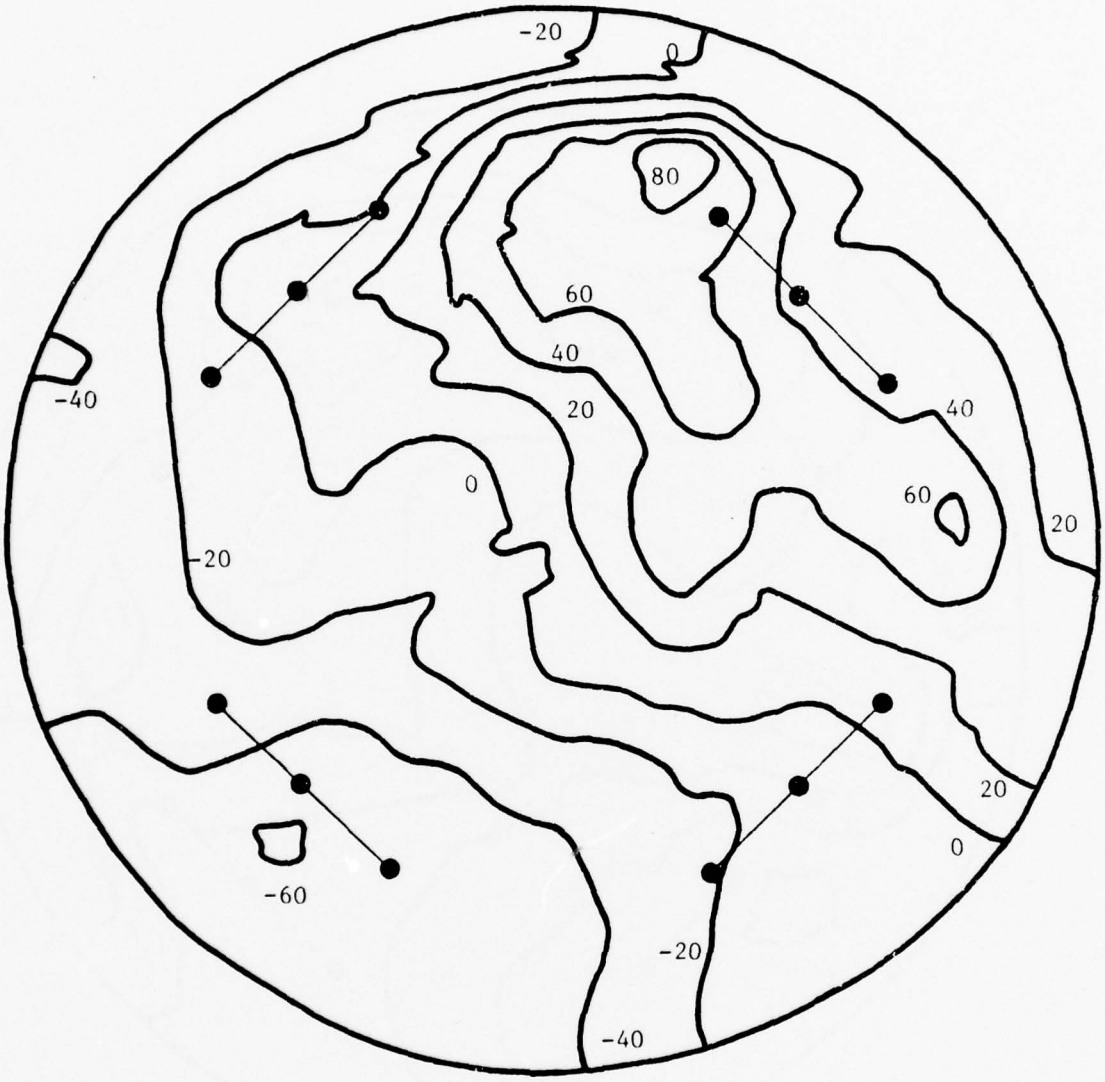

Figure 14

JT9D ISOPLETH FOR TOTAL HYDROCARBONS AT IDLE WITH NAFEC SAMPLING NOZZLE LOCATIONS (37)

Note: Isopleth values given as percent deviation from area weighted average

Figure 15

JT9D ISOPLETH FOR CARBON MONOXIDE AT IDLE WITH NAFEC SAMPLING NOZZLE LOCATIONS (37)

Note: Isopleth values given as percent deviation from area weighted average

Figure 16

JT9D ISOPLETH FOR OXIDES OF NITROGEN AT MAXIMUM CONTINUOUS
WITH NAFEC SAMPLING NOZZLE LOCATIONS (37)

Note: Isopleth values given as percent deviation from area weighted average

Table 4

PERFORMANCE COMPARISON OF NAFEC DIAMOND AND 4-POINT EXHAUST SAMPLING PROBES

Engine Type	Power Setting	Species Measured	NAFEC Diamond - 12-Point (% deviation from mean)	4-Point (% deviation from mean)
JT3D	idle	THC	-5.0	-5.0
	idle	CO	+6.0	+3.8
	max. cont.	NO_x	+6.0	0.0
JT8D	idle	THC	-14	-2.5
	idle	CO	-7.0	+2.5
	idle	NO_x	-6.5	+10
	max. cont.	THC	-14	-23
	max. cont.	CO	-3.5	+2.5
	max. cont.	NO_x	-19	+3.3
JT9D	idle	THC	-0.8	-3.8
	idle	CO	+1.0	-1.3
	max. cont.	NO_x	+2.3	+2.3
			-4.8	+0.8
			Average Deviation	Average Deviation

particulates against maintaining low probe-blockage effects. This means that a compromise is best achieved by use of the four sampling nozzle configuration. The total passage length of the sampling tubes within the engine's flow field is minimized, thus allowing for larger diameter tubes to reduce deposition.

Details regarding the geometery of the internal support struts was obtained from Nelson (38) directly. The information is as follows

JT3D: nozzle diameter = 67.1 cm (26.4 in.), four struts located 90° apart both vertically and horizontally, strut trailing edge distance to thrust reverser exit plane is 129.5 cm (51.0 in.)

JT8D: nozzle diameter = 75.9 cm (29.9 in.), four angled struts support inner core and have profiles similar to air foils, struts extend through fan case causing "diamond" profiles for exhaust profiles, strut trailing edge distance to thrust reverser exit plane is 159.8 cm (62.9 in.)

JT9D: nozzle diameter = 123.4 cm (48.6 in.), 15 struts equally spaced, top most strut located slightly closkwise, profile of strut similar to exit guide vanes, strut configuration varies with engine model, strut trailing edge distance to thrust reverser exit plane is 111.0 cm (43.7 in.)

and may be important in establishing the configuration of the sampling probe. However, performance evaluation of the 4-point sampling configuration has been made on actual exit plane mappings thus incorporating the strut geometry of each engine.

3.1.3 Operation of Sampling Probe

Before calculations can proceed concerning the sampling conditions near the exit plane of a turbojet engine, the conditions at the exit plane must be known, Table 2 gives the total temperature (T_T), exit Mach number (M_e), and the exit velocity (V_e), for the JT3D, JT8D, and the JT9D at each of five power sttings, The quantity $\rho_e V_e$, where ρ_e is the gaseous density, is the gaseous mass flux at the exit plane of the engine of a per unit area basis. As can be seen, $\rho_e V_e$ varies significantly with power setting.

Two design possibilities are also shown in Table 2. The design points assume a sampling condition and then calculate the performance at the other conditions. In the calculations, compressibility effects are taken into account for both the area and velocity ratios. The area ratio is taken as the sampling nozzle internal area (A_p) divided by the area of the undisturbed stream tube (A_{st}) which enters the sampling nozzle. Similarly, the velocity ratio is the exit plane velocity divided by the velocity at the entrance of the sampling nozzle (V_p).

With one design sampling condition, the selection of a Mach number equal to 0.5 offers the best compromise. The area and velocity ratios are both doubled or halved at the extreme operating conditions. The corresponding power settings are approach on the JT3D and JT8D engines, and cruise on the JT9D. Arguing against this selection is the relatively large deviation from isokinetic conditions -- four power settings would not be sampled incorrectly. Also, little of the engine operation time occurs at the approach power setting ($\sim$14%) -- a significant amount of engine time is spent at cruise power. Only the JT9D is sampled at cruise.

Alternatively, two design sampling conditions can be defined where the most typical power settings are selected. The sampling performance of the nozzle is also given in Table 2 where the cruise and idle power settings are assumed for the JT3D and JT8D. For the JT9D, climb and idle is selected because climb corresponds to a Mach number of 0.6 -- intermediate between take-off and cruise. Idle is selected for each engine, the reason being that idle is at the low extreme of the engine operating range. In the performance of the sampling nozzle, the maximum area ratio occurs at the approach power setting for the JT8D and JT3D engines. As discussed earilier, variations up to 25 percent of the sampling velocity relative to the main stream velocity result in negligible

sampling error for jet engine exhaust. With the two design sampling conditions here, the maximum deviation in sampling velocity is 39 percent (JT9D at take-off). This excludes the approach condition for the JT8D and JT3D. As a consequence, a significant error could result with restricting the sample flow rate to two values.

In recommending an approach to the isokinetic sampling question, four alternatives exist. The first two are given in Table 2 and have already been discussed. The third is to provide three sampling design flow rates. The fourth possibility is to allow the flow rate to be fully variable. In each alternative, the limiting Mach number of 0.8 in the sampling nozzle cannot be violated as the consequences could be severe. Therefore, the climb and take-off power settings for the JT3D and JT8D cannot be sampled isokinetically. The maximum relative velocity ratio occurring here is 30 percent (JT3D at take-off). As was noted earlier, this is near the 25 percent value where negligible effects were measured (36). Now, if 30 percent is taken as a tolerable limit, a single flow rate is seen not to meet the 30 percent criteria. Also, with the two flow rate designs, the approach power setting for the JT3D, JT8D, and JT9D, in addition to the JT9D at take-off, do not meet the criteria. Adding a third flow rate would put the velocity ratio within the 30 percent criteria. Here, the approach power setting would be matched, thus giving the JT3D and JT8D adequate sampling according to the criteria. With the JT9D, the maximum flow rate would be between take-off and climb, the intermediate at cruise, and the lowest at idle. A completely variable control over flow rate would in reality not provide a significantly improved adherence to isokinetic sampling because of the Mach 0.8 limitation and the correspondence in exit flow rates among the engines.

Another factor weighing in the decision is complexity of construction and operation of the sampler. Since a completely

variable sample flow rate offers no advantage over fixed flow rates, it is considered undesirable from the fabrication standpoint. On the other hand, a single fixed flow rate is not good because of the large deviations in sampling velocity relative to the main stream velocity and the unknown effects on particles greater than 0.2 μm (the effects should be small). Two flow rates would be better than one flow rate but the approach power setting is not sampled near to isokinetic conditions. Other than this power setting, isokinetic sampling is approximated.

Therefore, the best compromise is the three flow rate design. The three flow rates ($\rho_e V_e$) selected are approximately 216, 145, and 73 kg m^{-2} sec^{-1} and from Table 2 are seen to correspond to the power settings for each engine in a convenient manner. The approach condition is properly selected for the JT3D and JT8D. The JT9D has a different power setting correspondence -- take-off, climb, and idle. In all cases, the sampling velocity ratio is less than the 30 percent criteria already mentioned. Moreover, the best indications are that all particles as large as 5 μm should be sampled with a minimum of bias (inlet probe diameter = 0.2 cm). The magnitude of the bias is not possible to predict, but based on the particle relaxation time, is negligible. More elaborate flow control systems are costly and do not materially improve the sampling situation.

Selection of the 0.2 cm diameter sampling nozzle provides a total sample flow of 5, 10, and 19 actual m^3/hr from the engine. These flow values are calculated from the exhaust gas mass fluxes ($\rho_e V_e$) selected for operation of the sampler.

3.2 Aerosol Transport Pipe

As discussed previously, there are basically two approaches in locating the sampler. The first is to provide a transport pipe to bring the exhaust particles from the sampling probe to the point of collection. The consequences of the transport

pipe are analyzed here. The alternative is to place the particle collection equipment near the engine and eliminate the transport pipe. This alternative approach comes with a disadvantage -- the particle collection equipment must be acoustically isolated from the engine and test cell to properly operate and not fail prematurely.

Deposition of aerosol particles can occur from turbulent streams by the following mechanisms: particle inertia, gravitational settling, brownian diffusion, space charge precipitation, and image force attraction. Assuming the aerosol particles to be electrically neutral, (a particulate system possessing a net electrical charge has greater tendency for deposition), particles larger than 1 μm deposit predominantly by inertia (39) and bleow 0.1 μm by Brownian diffusion (40). Gravity settling only becomes important for very large particles -- the settling velicity for a 100 μm particle is 25 cm/sec (quiscent fluid and unit density). Consequently, for consideration of the transport pipe, only two deposition mechanisms are important, particle inertia and Brownian diffusion.

Experiments concerned with the deposition of aerosols are difficult to conduct accurately. Aerosol generation, electrical neutralization, sampling, and measurement of aerosols, in addition to particle re-entrainment, influence of pipe joints, and the effects of surface roughness all confound the results. Upon reviewing the particle deposition literature, Liu and Agarwal (41) provide the most credible experimental data within the inertial deposition regime. The calculation procedure for determining the penetration (defined as the fraction of material not deposited in the pipe) depends on both the particle's relaxation time, τ, and the Reynold's number based on pipe diameter. The relaxation time is given (equivalent to Equation 3) as

$$\tau = \frac{d_p^2 \bar{\rho}_p}{18 \mu_g} \qquad [4]$$

where the Cunningham correction is unity, d_p the particle diameter, $\bar{\rho}_p$ the density of the particle material, and μ_g the dynamic viscosity of the gas. As in several studies concerning deposition (42,43,44,45), the relaxation time is made dimensionless by

$$\tau_t = \frac{\tau u_*^2}{\nu_g} \qquad [5]$$

where u_* is the friction velocity and ν_g the kinematic viscosity of the gas. The friction velocity is defined as

$$u_* = \sqrt{\frac{\tau}{\rho}} \qquad [6]$$

and is related to the pipe friction factor, f, as

$$u_* = \left(\frac{f}{2}\right)^{1/2} U_{avg} \qquad [7]$$

where U_{avg} is the mean velocity. For $N_R < 10^5$

$$f = \frac{0.316}{f\left(N_R\right)^{1/4}} \qquad [8]$$

assuming a smooth pipe (46). Defining the dimensionless deposition velocity as

$$V_t = \frac{V}{u_*} \qquad [9]$$

where V is the actual deposition velocity. V is given by

$$V = \frac{Q}{\pi DL} \ln\left(\frac{1}{P}\right) \qquad [10]$$

where Q is the volumetric flow rate, L the length of pipe, D the diameter of the transport pipe, and P the penetration. Figure 17 shows the relationship between V_t and τ_t as given by Liu and Agarwal (41). By rearranging the above equation, the penetration is

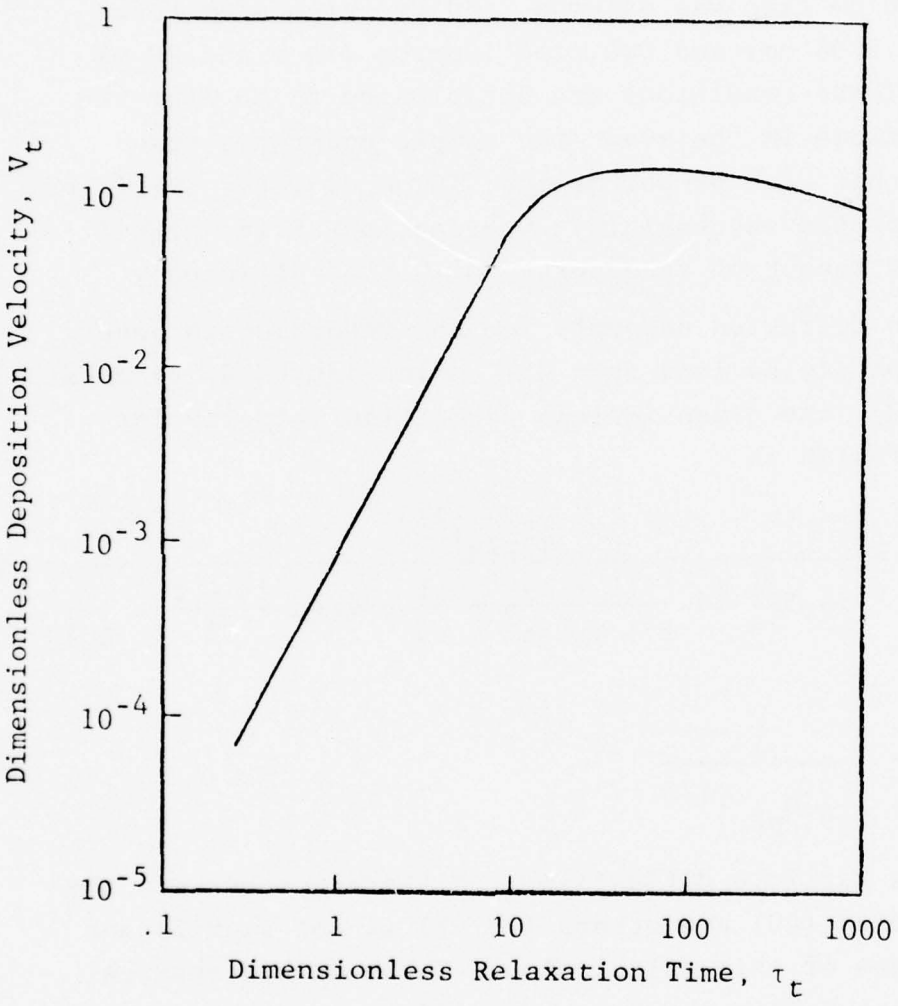

Figure 17

VARIATION OF DIMENSIONLESS DEPOSITION VELOCITY WITH NORMALIZED PARTICLE RELAXATION TIME (41)

$$P = \exp\left(-\frac{\pi DVL}{Q}\right) \qquad [11]$$

Figure 18 shows the results of calculations for particle deposition within the transport pipe. Particle inertia is seen to strongly influence deposition for particles greater than approximately 1 μm. In the calculations, an actual flow rate of 4,720 cm^3/sec was assumed, and two pipe diameters (2.54 cm and 5.08 cm) and two pipe lengths (10 m and 20 m) were used. These conditions are anticipated to be near the design conditions in the event the sample undergoes transport. Note that with proper design, 10 μm diameter particles can be transported successfully, whereas, particles significantly larger cannot be transported with good efficiency.

Brownian diffusion accounts for the reduction in penetration for particles less than 0.1 μm in Figure 18. According to Davies (40), the dimensionless deposition velocity for Brownian diffusion is

$$V_t = \frac{\left(D_{p/\nu}\right)^{2/3}}{14.5\left(\frac{1}{6}\ln\frac{(1+\phi)}{1-\phi+\phi^2} + \frac{1}{\sqrt{3}}\arctan\frac{2\phi-1}{\sqrt{3}} + \frac{\pi}{6\sqrt{3}}\right)} \qquad [12]$$

where

$$\phi = \frac{1}{2.9\left(D_{p/\nu}\right)^{1/3}}$$

and D_p is the particle diffusivity. Differences between the theory of Davies (40) and others (43,47) is not significant for the purpose of this calculation. The same hypothetical conditions are used in the Brownian diffusion calculations as in the inertial deposition predictions. Note that the penetration is on the order of 0.5 for particles approximately 0.01 μm in diameter. Particles smaller than this possess an even smaller penetration rate. Increasing the transport pipe length reduces further the penetration. To overcome bias in

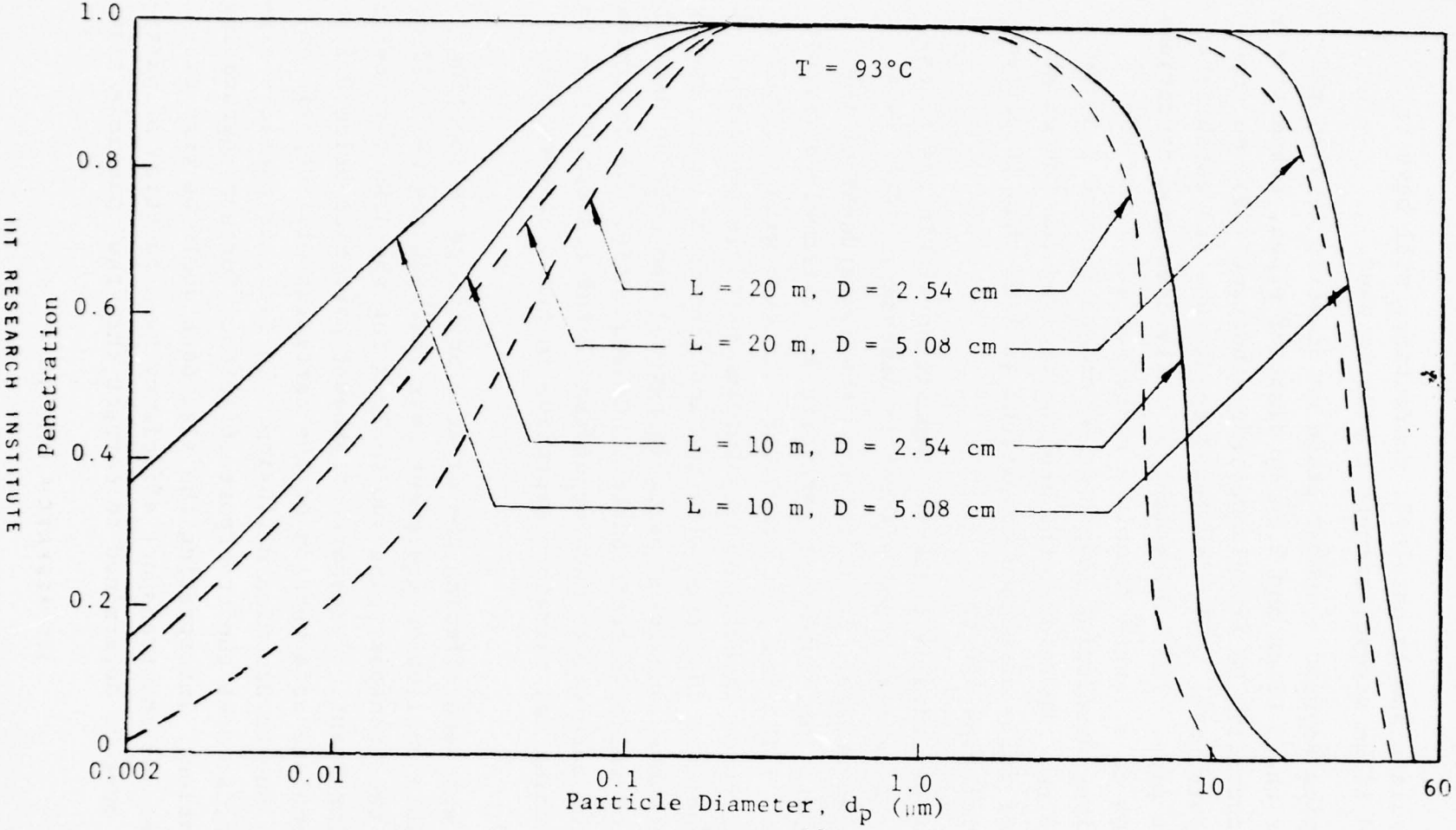

Figure 18

PENETRATION OF AN AEROSOL AS A FUNCTION OF PARTICLE SIZE FOR TYPICAL CONDITIONS

the particulate sample obtained, corrections will have to be applied if an aerosol transport pipe is used.

The pipe Reynold's number based on diameter is 5330 and 10,650 for the 5.08 cm and 2.54 cm diameter pipes, respectively. However, according to Friedlander and Johnstone (39), no deposition occurs until fully developed conditions are established within the pipe. The achievement of fully developed conditions corresponds to a length Reynold's number of 10^5. For the 5.08 cm pipe, developing length is 95 cm and for the 2.54 cm pipe, 23.8 cm. Therefore, the length required for the establishment of fully developed conditions is less than 10 percent of the total pipe length.

To experimentally check the deposition within the transport pipe, disassembly and washing is necessary. This is a strong disadvantage. In addition to the awkwardness of the washing operation, submicron particles are extremely difficult to remove. IITRI has just completed a program with the United States Air Force investigating submicron particle separation (48). Results indicate that even with the application of sonic energy and surfactants, submicron particle removal can only be described in terms of relative efficiencies. Consequently, the determination of the particulate mass deposited in the transport pipe is time consuming and therefore expensive in terms of test cell operation.

The approach offering the greater advantage is locating the particle collection equipment near the test engine. Eliminating the transport pipe (up to 10 m for the JT9D test cell) is very important. Transport of exhaust particles below 0.1 μm is not complete as a portion of the particles will deposit on the walls due to Brownian diffusion. In fact, as particle size decreases, so does the transport efficiency further aggravating the situation. Interpreting the size data would be very difficult because the transport efficiency as a function of particle size must be determined to correct the "raw" particle size

data. Although the theoretical predictions are reliable, experiments would be required to quantify the rate of deposition for the actual conditions of the sampler. Two methods could be used: subject a monodispersed test aerosol to the transport pipe and sampler and carefully measure the particulate mass deposited or operate the sampler in conjunction with a turbine engine and by washing the transport pipe clean, quantify the mass of the deposit. Both methods are time consuming and not necessarily guaranteed to give useful results.

Another important factor is the modification to the particles as they are transported through the pipe. Alternate deposition and re-entrainment plus particle-particle collisions would change the size and shape of the exhaust particles. These possible particle modifications are impossible to predict accurately. As can be seen, the use of a transport pipe poses problems which are best avoided.

Placing the particle collection equipment near the turbine engine does not occur without penalty. The test cell environment is quite harsh acoustically and access to the collected samples is limited. However, a long transport pipe is not required and the attending problems are eliminated. The short transport length that is required can be incorporated with the sample dilution system.

To overcome the environmental penalty, the sample collection equipment must be surrounded by a barrier capable of sufficiently attenuating the test cell noise ($\sim$160 Db). This requires an acoustically treated box. Good attenuation is possible with the construction of two boxes, an inner and an outer, from plywood sheets 1.9 cm thick. The gap between the inner and outer box is approximately 15 cm. On the outside of the inner box, sheet lead or other acoustically absorbing material should be installed. Plastic foam within the inner box offers a final barrier. The test equipment will be located within the final plastic foam barrier. Rubber gromets are necessary to surround pipes and electrical leads leaving

and entering the acoustically treated box. Before the box can be completely specified, the components inside must be carefully studied as to their upper acoustic limit.

Locating the sampler "box" near the engine may be fortunate as the minimum noise of an aircraft-mounted engine occurs within a region 45° on either side of a line perpendicualr to the axis. However, in the test cell environment, the noise "levels" could be relatively uniform throughout the cell, thus reducing the sampler location to one of convenience. Engine noise data is not presently available to resolve this question. Consequently, the sampler will be located within the "ambient" minimum noise envelope. The sampler itself will only be used on a limited number of engine tests to complete the program and therefore, reducing the location problem.

Control of the sampler operation within the test cell is possible through the use of remote controlled valves, turrets, etc. The cost is increased, but in relation to the test cell charges becomes relatively small. Anticipated in the design of the sampler is the remote operation for the sample collection of all five power settings. This minimizes test cell time.

An added advantage of locating the sampler near the engine is the portability of the sampling system itself. The only equipment specific for each engine will be sampling probe and transport pipe to the dilution system. The particle collection equipment and controls are portable and can be transported between test cells.

3.3 Diluter-Conditioner

Due to the high temperature of the exhaust gas, the sample will require conditioning to permit compatibility with the particle collection equipment. The dew point of the extracted sample must be considered in respect to possible water vapor condensation. Also, the conditioning action must be gentle to not alter the configuration of the particles. From the above requirements, dilution of the sample with dry filtered ambient air appears the most suitable.

Performing an energy balance on the diluter schematically shown as below

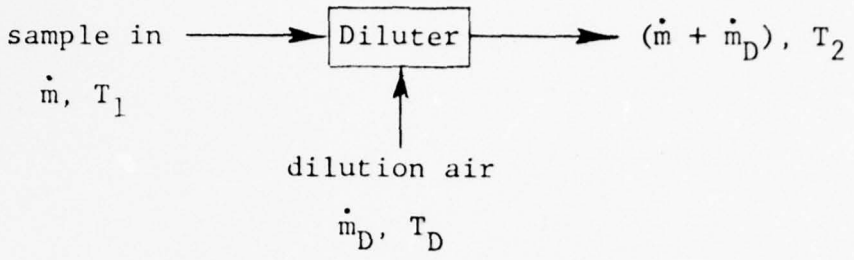

results in the following expression for mass flow ratio

$$\frac{\dot{m}_D}{\dot{m}} = \frac{T_1 - T_2}{T_2 - T_D} \text{ or } T_2 = \frac{\dot{m}T_1 + \dot{m}_D T_D}{\dot{m} + \dot{m}_D} \qquad [13]$$

Assuming that the exhaust temperature 520°C (maximum value) and the dilution air temperature as 20°C, Table 5 gives the resulting temperature after dilution is complete. As can be seen, significant temperature reductions are possible. A rough estimate of the resulting dew point is also given where saturation was assumed at 100°C for the exhaust gas. For any mass ratio of dilution, maintaining the sample temperature above the dew point will eliminate condensation of water vapor.

Further analysis of the dilution process is necessary to resolve the temperature history of the sample within the diluter. Taking into account the flow rates selected for each engine power setting and the corresponding dilution air flow rate, the temperature of the sample can be calculated as a function of diluter tube length. The tube length is non-dimensionalized so that the plotted results are applicable to any length. The temperature at maximum continuous is taken to be 520°C and the temperature at idle is taken as 300°C -- these temperatures are typical of all three engines. The dew point temperature is assumed to be 70°C and decreases along the diluter tube length. In the calculations, complete mixing of the sample gas and dilution air is assumed. Results

Table 5

TEMPERATURE AND DEW POINT AS
A FUNCTION OF DILUTION
MASS FLOW RATIO

$\frac{\dot{m}_D}{\dot{m}}$	T_2 (°C)	Dew Point Estimate (°C)
1	270	73
3	145	43
5	103	34
7	83	27
10	65	23

are plotted in Figure 19. More detailed calculations are possible, but a solution does not exist in closed form, thus, requiring computer aided finite difference techniques. For the present purpose, a sophisticated analysis is unwarranted.

Diluters have been used in conjunction with samplers designed for mobile combustion sources and all subject the aerosol to highly turbulent flow conditions (49,50). This is done to insure adequate mixing and, consequently, good dilution. Unfortunately, under these flow conditions, deposition and agglomeration are a significant problem. IITRI has developed a procedure for transporting aerosols over short distances with minimum deposition (51). The technique is not available commercially, but has been successful for many aerosol systems. To achieve high penetration, clean transpiration air is introduced through a porous tube perpendicular to the flow of the aerosol. The transpiration air then generates a "clean" boundary layer, thus, isolating the aerosol from the walls. Figure 20 shows the percentage of particle deposition as a function of particle size and transpiration flow rate. Figure 21 shows the influence of particle size on percent of particle deposition. Note that the penetration is one minus the percent particle deposition divided by 100.

Utilizing the transpiration technique to enhance aerosol transport also provides a means of gentle dilution. The dilution action is gentle because transpiration air is introduced continuously along the tube length. Only distances of several meters can accomodate a diluter of this type -- a complete transport pipe is much too long. A maximum design length exists because a minimum of transpiration air is required per unit distance of the pipe. Therefore, the diluter would be ideally suited for the approach where the particle collection equipment is located near the aircraft engine.

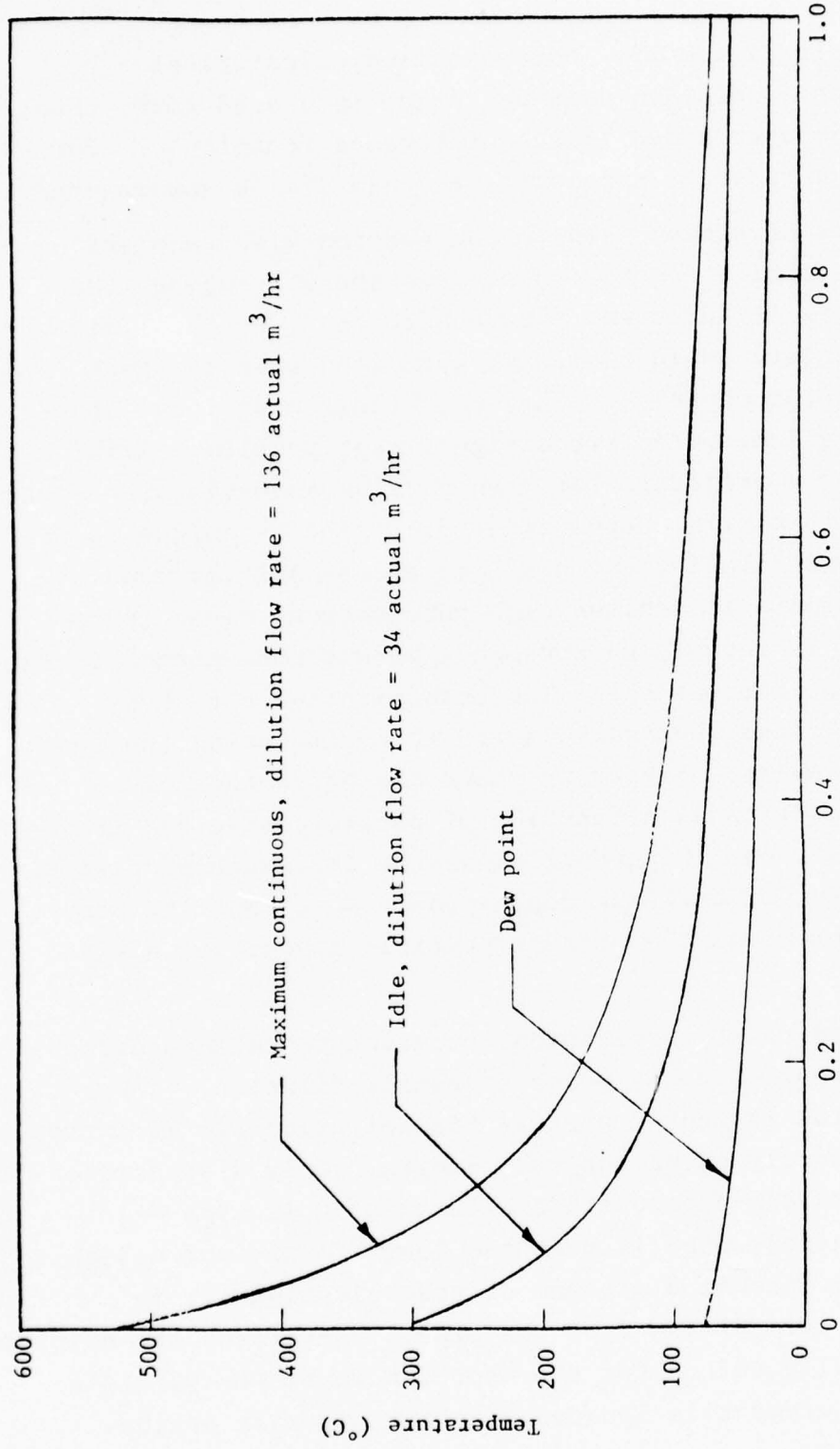

Figure 19

TEMPERATURE HISTORY IN MAIN SAMPLE DILUTER AS A FUNCTION OF ENGINE POWER LEVEL

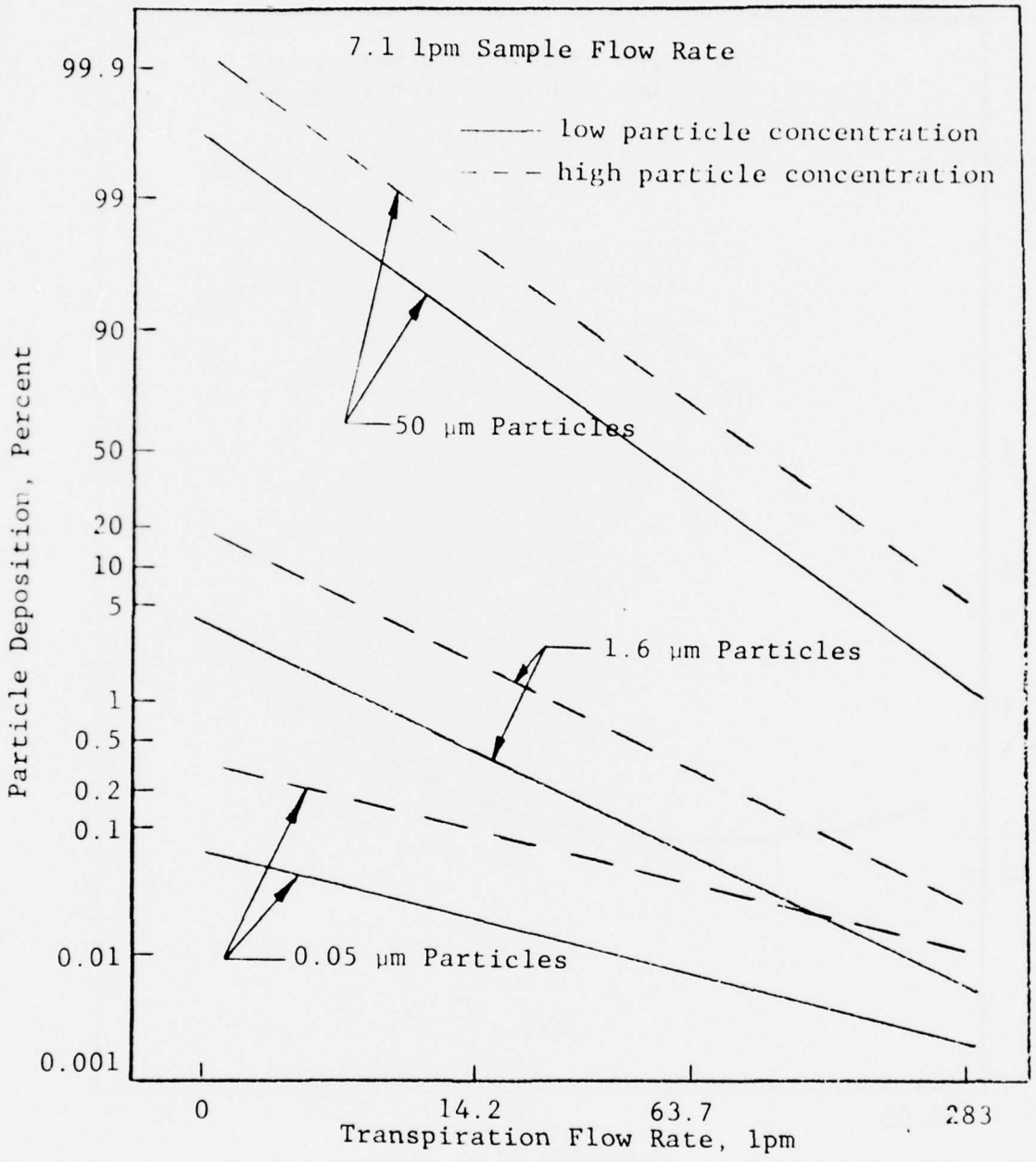

Figure 20

DEPOSITION OF SMALL, MEDIUM, AND LARGE PARTICLES vs. TRANSPIRATION FLOW RATE WITH VARYING PARTICLE CONCENTRATION (51)

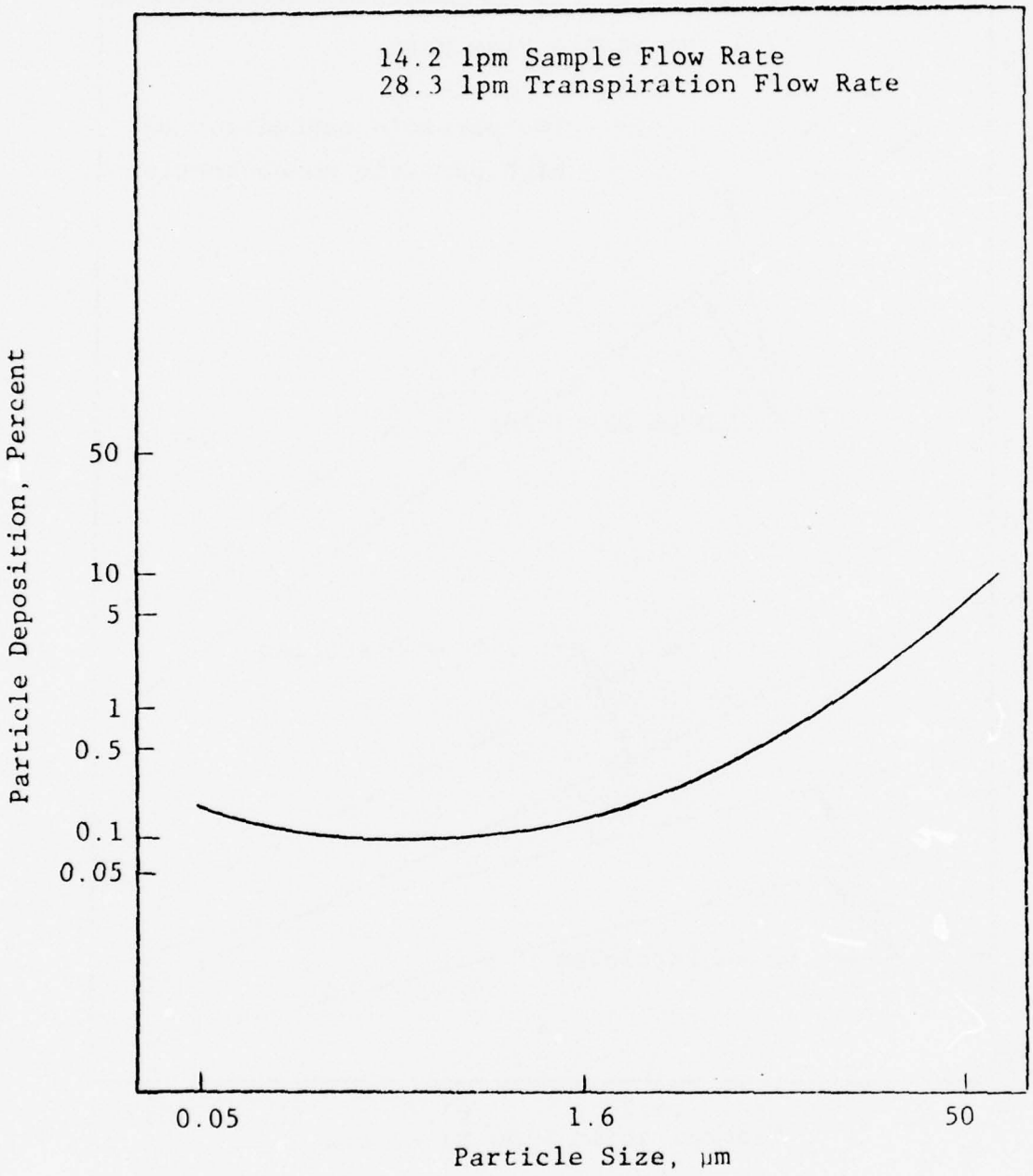

Figure 21

DEPOSITION OF PARTICLES IN RELATION TO PARTICLE SIZE AT INTERMEDIATE LEVELS OF PARTICLE CONCENTRATION, SAMPLE FLOW RATE, AND TRANSPIRATION FLOW RATE (51)

3.4 Mass Emission Measurement

Once a representative sample is captured by the sampling probe and transported by the main diluter, the particulate sample must be collected and/or analyzed. One of the required measurements that the sampler must make is particulate mass concentration. This measurement is necessary to determine the mass emission rate of the engine.

Only techniques which measure mass directly were considered because other measurement techniques based on various correlations would involve large systematic errors and would therefore require calibration. Gravimetric weighing has been demonstrated to give good results by Johansen and Kumm (5) where direct filtration and differential weighing were employed. Accurate measurement of exhaust particulate mass concentration based on a gaseous sample volume of 0.028 m^3 is possible with direct weighing. Disadvantages are the lack of a real-time measurement capability and the requirement of filter removal after each measurement. Although these may not be serious disadvantages with the collection equipment located in the test cell control room, they would present difficulty if the equipment were located near the engine.

A significant consideration is the advantage of real-time mass concentration information. With this, the operating condition of the sampler can be monitored, thus avoiding the chance of faulty sampler operation. The overall operating condition of the sampler would be known insuring good samples and, thus, minimizing usage of the test cell and engine running time.

Other techniques of direct measurement can provide real-time data. The techniques include inertial impaction, filtration, and electrostatic deposition to place the particles onto the measurement surface. Two surfaces are commercially used: filter material and piezoelectric crystals. Table 6 shows the combinations of deposition and sensing techniques

Table 6

INSTRUMENTS FOR DIRECT MEASUREMENT OF AEROSOL MASS CONCENTRATION

Method	Resolution (μg)	Mass Concentration Range (mg/m^3)	Minimum Particle Size Collected (μg)	Real-Time	Approx. Cost
Gravimetric Weighing	0.1	-	(function of filter)	no	-
Beta Radiation Attenuation					
GCA (RDM 101)	100	1 - 25	0.4	no	$ 3,400
Phillips	-	0.1 - 4	0.3	yes	$11,000
Lear-Siegler	-	0.1 - 100	0.3	yes	$14,000
Piezoelectric Microbalance					
Celesco (PM 37)	0.01	0.001 - 2	0.2 - 100*	yes**	$ 4,000
Thermo-Systems	0.01	0.002 - 20	0.01 - 10*	yes**	$ 4,320

* Particle size range collected.

** Modifications necessary.

commercially available. Note that gravimetric weighing itself is not commercially available in the form of a complete unit.

The three commercial instruments utilizing beta radiation attenuation shown in Table 6 use either impaction to deposit the particles as in the GCA instrument, or filtration as in the Phillips or Lear-Siegler equipment. The disadvantage of using an impactor is the limitation on the minimum particle size collected. Particles below this size are not collected and the contribution to the total mass concentration is unknown. If an instrument of this type were to be used, determination of the losses is required because a significant portion of the particulate mass is anticipated to be less than 0.1 μm. With filtration, the collection efficiency is defined at a certain particle size (given in Table 6) and is typically 99%. Particles below this size will also be collected but at a varying efficiency. Although the efficiency curve is unknown as a function of particle size, Brownian diffusion coupled with a reasonable face velocity should give high efficiencies. Both the Phillips and Lear-Siegler indicate the same collection efficiency at 0.3 μm and are completely automatic. The Lear-Siegler requires approximately two minutes for a measurement cycle.

Advantages of beta radiation include good reliability, freedom from calibration drift, and long term unattended operation. This results from the fact that the particles are deposited onto a moving filter strip and subsequently measured (not true for GCA RDM 101). Cleaning problems resulting from the deposited material are thus eliminated and therefore allowing a large number of measurements to be made -- more than 100. The sensitivity of the beta radiation technique is somewhat less than the piezoelectric microbalance, but not significantly so for application to turbine engine exhaust particles.

The piezoelectric microbalance was only developed recently but has received wide usage. The principle of operation depends on the shift in resonant frequency of a solid as the solid's mass changes. In the two commercial instruments listed, a quartz wafer is employed as the vibrating solid. The particles are deposited directly onto the solid (vibrating crystal) by two mechanisms. The Celesco instrument uses inertial impaction and the Thermo-Systems unit electrostatic deposition.

The sensitivity of the piezoelectric microbalance is greater than that of the "beta gage" leading to short sampling times. However, in the sample application here, dilution will be necessary to reduce the aerosol mass concentration to levels allowing sufficiently long sampling times (15 sec). Additional dilution will reduce the accuracy of the mass concentration measurement primarily because of the uncertainty in the dilution flow measurement. A significant disadvantage of the piezoelectric technique is the necessity of periodic cleaning of the crystal sensor. The cleaning must be performed manually since the instrument is partially disassembled to apply a sticky coating to the crystal. The Celesco instrument has a large cut-off particle size and for this reason, not applicable to the engine sampler's requirements. The size range captured by the Thermo-Systems device is expanded greatly in the submicron region (Table 2) and therefore applicable to this study. Rough calculations indicate that an aerosol mass concentration of 1 mg/m^3 would permit 1 hr of sampling with the Thermo-Systems instrument. Remote operation of both piezoelectric microbalances would require the addition of remotely operated valves and switches. The cost indicated does not include the modifications for automatic operation. Good reliability and lack of calibration drift characterize both instruments.

Recently, Daley and Lundgren (52) have evaluated the relative performance of the Celesco and Thermo-Systems

instruments. Concluded from the work was that in either instrument, both temperature and humidity variations were not compensated by the second "reference" quartz crystal isolated from the aerosol. The humidity affected the indicated mass through moisture absorption and evaporation from the particulate deposit itself. The electrostatic precipitator on the Thermo-Systems device had significant improvement over the Celesco for collecting particles below 0.5 μm.

Gravimetric weighing is seen to offer the best choice for the determination of the engine's mass emission rate. At the idle condition, a 10 minute sampling interval will give about 40 mg while at take-off, a 5 minute interval will give over 150 mg. These are weighable samples and apply to all three engines. The emission rate would be obtained by dividing the weight of the particulate mass collected by the exhaust gas volume passing through the filters and multiplying by the total volumetric exhaust flow generated by the engine. The actual "weighing" itself should be immediately at the conclusion of the test run. United Airlines has available an analytical balance with a 0.1 mg sensitivity. Afterwards, the filter sample should be placed in a pyrex petri dish and kept in the dark to reduce decomposition.

A typical glass fiber filter is the Gelman Type A/E*. This filter material is free from organic binders and commonly used in the gravimetric analysis of air pollutants. Particle retention under normal conditions (moderate face velocities) is approximately 98% for particles between 0.05 to 0.3 μm. As the face velocity increases, particle retention decreases. Reliable theoretical estimates regarding the magnitude of the level of particle retention cannot be made because large extrapolations are required.

---

* Gelman Instrument Co.; 600 South Wagner Road, Ann Arbor, Michigan

Chemical analysis in addition to the elemental analysis provided by the electron microscope (EM) can be performed on the collected particulate material. With the real-time techniques, insufficient quantities of particulate material are collected for chemical analysis. Using a glass fiber filter allows extractions suitable for organic analysis but could prove difficult for a trace element analysis because of the difficulty in extracting all the exhaust particles. The particulate material must be removed in order to eliminate the high background provided by the glass fiber filter. A plausible extraction scheme would use hot nitric acid, subsequent stages of concentration, and deposition onto a cellulose filter.

3.5 Techniques for Particle Size Analysis

Numerous methods are available for the analysis of particle size. All methods, except one, require the collection of the particles and subsequent analysis by electron microscopy. Analysis under the electron microscope (EM) will meet the sizing requirements of the program -- resolution to 0.001 μm. Also, the EM provides data ragarding the morphology of the particles and their shape. The one method which takes exception to the EM is the electrical aerosol analyzer (EAA) or particle mobility analyzer. Although the size range is restricted (0.01 to 0.7 μm) and no shape data is possible, the results are essentially real-time.

Each technique, except for the EAA, has a common goal -- deposit onto an EM grid a representative sample of the aerosol particles. A list of the techniques available is given below:

- Diffusion onto EM grid directly
- Thermophoretic collection
- Electrostatic deposition
- Membrane filter

- Aerosol spectrometer
- Measurement of particle mobility (EAA)

In this section of the report, each technique will be described and discussed in relation to the goals of the turbine engine exhaust sampler.

With each of the collection techniques, special provisions are required for remote operation. This consideration is important because the particle collection equipment will be located adjacent to the engine. Anticipated in the collection of particulate samples is the necessity of multiple samples of varying mass loadings. This will insure the acquisition of a sample appropriate for microscopic analysis. If the deposit is too dense, artificial agglomeration will be introduced and if too low a deposit, not enough particles will be observed for reliable results.

However, during operation of the sampler, real-time information on the particle deposit is available indirectly. Either the aerosol mass concentration or the particle number concentration based on the EAA could provide this data. The measurement of the aerosol mass concentration is redundant with the mass emission measurement while the EAA can provide real-time particle analysis as well. Consequently, the EAA appears the appropriate choice for the acquisition of real-time information. Real-time data would indicate the general operation of the sampler and could save the repeating of several test conditions and therefore cover its additional expense.

3.5.1 Diffusion onto Electron Microscope (EM) Grid

The placement of an EM grid in the flow field of an aerosol will cause particles to deposit. Two mechanisms are involved -- Brownian diffusion and inertial impaction which are fundamentally incompatible. On the one hand, Brownian diffusion requires low flow velocities to allow time for particle deposition, while on the other, inertial impaction requires high velocities. The flow velocities necessary for effective Brownian diffusion result in negligible inertial impaction.

Assuming the flow velocity to be 1 cm/sec and the temperature to be 93°C, the Reynold's number based on the diameter of the EM grid is 1.4 and is within the Stokes flow regime. In related work with diffusion in solutions (as in aerosol problems, large Schmidt numbers), Levich (53) gives the rate of diffusion towards a sphere in Stokes flow as

$$\phi = 7.9 n_o D_p^{2/3} U^{1/3} R^{4/3} \qquad [14]$$

where n_o is the number concentration of the aerosol, D_p the diffusion coefficient, U the velocity, and R the radius of the sphere. In work with aerosols, investigators report varying values for the coefficient the average of which is given by Fuchs (33) to be 7.8. To predict the collection efficiency of the EM grid in the 1 cm/sec flow field, the collection efficiency for a given particle size is defined as

$$\eta = \frac{\text{equivalent stream tube of collection}}{\text{projected area stream tube flow}}$$

and with substitution of the relation given by Levich (53) becomes

$$\eta = \frac{7.8}{\pi}\left(\frac{D_p}{UR}\right)^{2/3} \qquad [15]$$

where R is the radius of the EM grid. This relation is only valid for deposition by Brownian diffusion onto a sphere. However, the EM grid in practice is placed onto a filter support, thus allowing flow to pass by the grid similar to that of a sphere. On this basis, the above equation approximates the collection efficiency of an EM grid. Figure 22 gives the collection efficiencies as a function of particle size. Above 0.01 μm the collection is less than 10%, but at 0.001 μm is about 100%. Consequently, effective use can be made of Brownian diffusion for depositing small particles (less than 0.001 μm). Particles greater than 0.01 μm exhibit very low efficiencies.

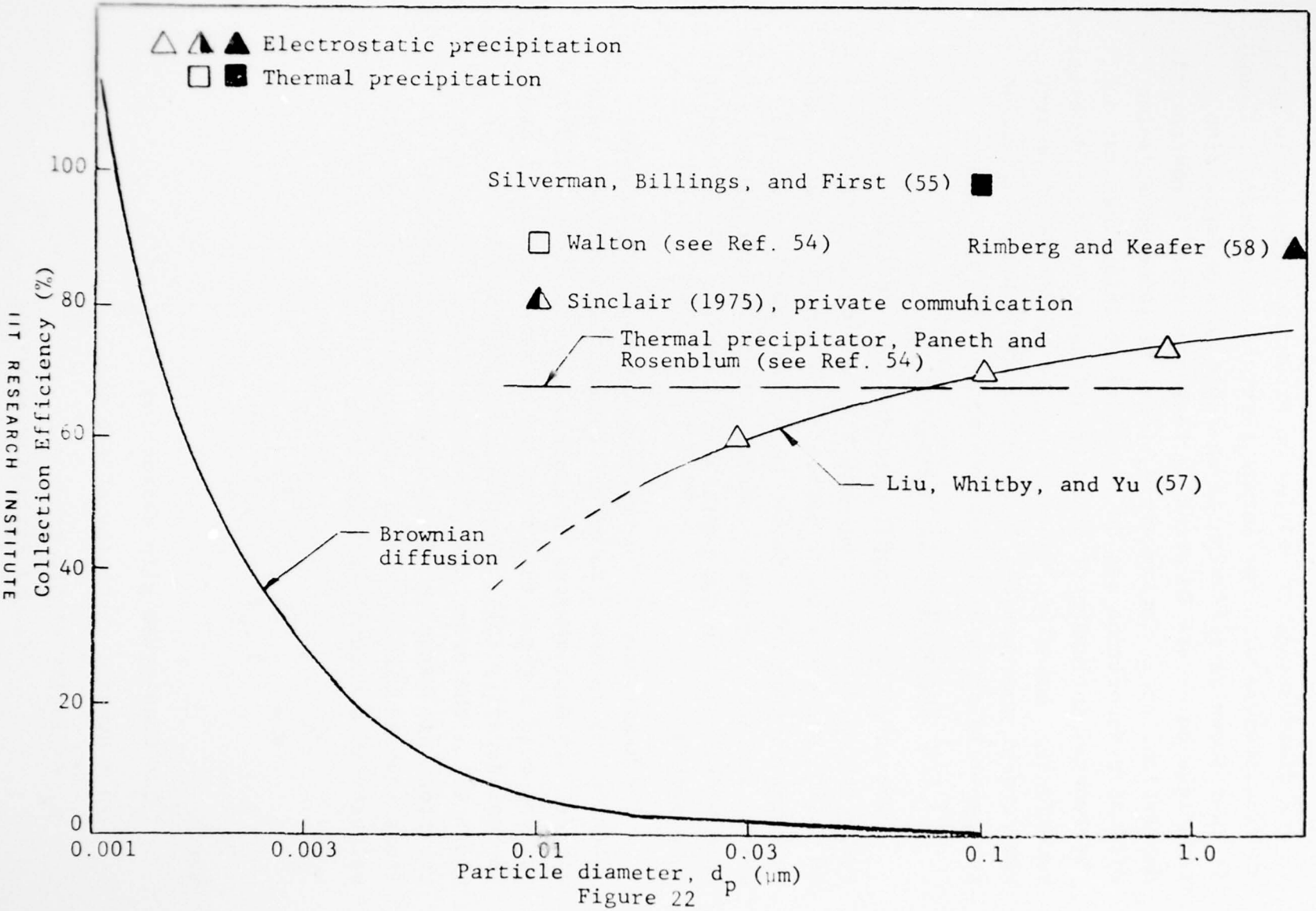

Figure 22

PARTICLE COLLECTION EFFICIENCY AS A FUNCTION OF PARTICLE SIZE

A disadvantage of relying on Brownian diffusion is its ineffectiveness with the larger particles. Important, though, is that Brownian diffusion is operable in any deposition technique to obtain EM grids -- thermophoresis, electrostatic deposition, etc. Consequently, total reliance on Brownian diffusion deposition can be discarded at this time, but not the general influence of Brownian diffusion on other deposition techniques. Actually, the performance of any device except the aerosol spectrometer is dominated by Brownian diffusion for particle sizes below approximately 0.003 μm.

3.5.2 Thermophoretic Deposition

The so-called "thermal precipitator" utilizes a strong temperature gradient to collect the particles. The direction of motion for the aerosol particles is opposite that of the temperature gradient. Hence, particles deposit onto the colder surface. Several commercial thermal precipitators have been widely used in the past, and the device can be readily constructed.

The magnitude of the thermal gradient must be large (~4000°C/cm) in order to effect reasonable deposition velocities. In most devices, a central wire is heated (100°C) and the cold surface is maintained by metal blocks of high thermal capacity (54). With this configuration, the gap width is on the order of 0.025 to 0.05 cm. Consequently, the flow rate capacity of the thermal precipitator is low (less than 10 ml/min) and is a disadvantage. The particle velocity in a thermal gradient is

$$V = -\frac{3}{2}\frac{C\mu_g}{\rho_g T}\,2 + \left(\frac{k_p}{k_g}\right)^{-1}\frac{dT}{dx} \qquad [16]$$

where

C = Cunningham slip correction

μ = dynamic viscosity of the gas

ρ_g = density of the gas

k_p = thermal conductivity of the particulate material

k_g = thermal conductivity of the gas

dT/dx = magnitude of thermal gradient

The Cunningham slip correction factor is as follows (55)

$$C = 1 + \frac{\left(2 \cdot 10^{-4}\right)}{pd_p} \; 6.23 + 2.01 \exp\left(-1095pd_p\right) \quad [17]$$

where p is the gaseous pressure. From the relationship for the velocity, the motion of the particle is not a function of its size -- as long as the slip correction is equal to unity. However, for particles less than 0.5 μm, the slip correction is significantly greater than one, and at 0.1 μm for example, equals 3.0 (approximately) at atmospheric conditions. Therefore, deposition effectiveness is inversely proportional to particle size, thermal conductivity of the particle, and the aerosol flow rate. On the basis of the velocity relationship, the flow rate and geometrical configuration of a thermal precipitator can be established for this application.

In using a thermal precipitator, the sample is usually deposited onto a glass microscopy cover slip located adjacent to the heated wire. In general, the glass slides are precoated with a carbon film vacuum deposited onto the surface to facilitate transfer to an electron microscope sample grid. EM grids cannot be placed directly into the thermal precipitator because the thermal field near the grid wires is greatly distorted. Therefore, the temperature gradient varies from the grid wire to the carbon film suspended between two grid wires. Since conduction is greater through the wires than the carbon film itself, particles preferentially deposit onto the grid wires.

Because of the non-uniform deposition pattern, the entire substrate would have to undergo analysis. This is time consuming and expensive, but the substrate dimensions are much

reduced over the aerosol spectrometer. The heat generated in the operation of the thermal precipitator could evaporate some liquids and oxidize organic materials.

Disadvantages of the thermal precipitator include the following:

- Low gaseous flow rate (<10 ml/min)
- Unknown effects of thermal gradient and elevated temperature
- Non-uniform deposition of particles onto substrate
- Substrate limitations -- EM grids introduce errors

The most valuable feature of the thermal precipitator is the high collection efficiency for particles smaller than 0.1 μm; collection efficiencies are reported to be in the vicinity of 90% and has no lower particle sized limit (54). Mr. Warren Hendricks of Micromeritics Instrument Corporation (past manufacturer of a thermal precipitator) indicates that contrary to the literature, the collection efficiency is a function of the aerosol's mass concentration (56). Figure 22 shows some reported collection efficiencies of the thermal precipitator, but none include careful tests with monodisperse aerosols. The efficiency data is reported in the text by Green and Lane (54).

3.5.3 Electrostatic Deposition

An electrostatic precipitator utilizes particle charging and an electric field to deposit particles onto a substrate. Early designs of the electrostatic precipitator operated continuously and therefore produced a non-uniform particle deposit with respect to particle size. Later, Liu, et al. (57) deisgned and tested an electrostatic precipitator which deposits uniformly through intermittent charging and application of the electric field. This design is available commercially through Thermo-Systems.

Careful experiments were conducted by Liu, et al. (57) and Rimberg and Keafer (58) using monodisperse test aerosols to determine the collection efficiency. Figure 22 shows the collection efficiency as a function of particle size. The

experiments performed with the electrostatic precipitator are more reliable than those of the thermal precipitator mainly because of the use of well-defined test aerosols. However, as the particle size decreases, the collection efficiency decreases in the electrostatic precipitator. This is a result of the decreased charging rate for particles decreasing in size. For particles below 0.2 μm, the predominant mechanism is diffusion charging given approximately as

$$n = \frac{d_p kT}{2e^2} \ln\left(1 + \frac{\pi d_p c N_o e^2 t}{2kT}\right) \qquad [18]$$

where

n = number of charges on an initially neutral particle after time t

k = Boltzmann's constant (1.38×10^{-16} erg/molecule °K)

N_o = ion density (ions/cm^3)

c = ion velocity (root mean square)

t = time

e = one electronic charge (4.8×10^{-10} statcoulomb)

The velocity of deposition within the Stokes regime is given as

$$V = \frac{EneC}{3\pi\mu_g d_p} \qquad [19]$$

where E is the electric field strength. From the equation for n, which gives the charge accepted by a particle, the charging rate decreases rapidly because of the natural log term. Collection efficiency in the region of 0.01-0.001 μm is very low for electrostatic precipitation. In fact, Brownian diffusion will probably dominate particle deposition in sizes below 0.003 μm.

An important advantage of the Thermo-Systems precipitator is that regardless of the collection efficiency for a given particle size, the deposit for that particle size is uniform.

EM grids can be used directly as the collecting substrate, and the deposition action is gentle. Flow rate capacity is on the order of 4-6 ℓ/min -- much higher than the thermal precipitator and the membrane filter approach.

To operate the Thermo-Systems precipitator remotely is possible for one set of samples (one run), but multiple runs will require multiple sampler units and remotely operated valves. This consideration is important because for any given engine power setting, several samples are required to insure an optimum deposit for subsequent microscopic analysis. Three electrostatic precipitators will, for example, allow three samples of each engine power level setting. Anticipated is that at least one of these sample sets will be appropriate for microscopic analysis. After the samples are taken, the substrates must be retrieved and fresh substrates installed. Of course, the same is true for the thermal precipitator.

3.5.4 Membrane Filtration

Membrane filters are manufactured from cellulose ester gels dried to form thin, porous films of controlled pore size. Tests involved with atmospheric dust have demonstrated the capability of membrane filters to trap particles as small as 0.001 μm. The depth of penetration is usually less than 10 μm which pemits *in situ* microscopic examination. Maintaining a low filter face velocity and the appropriate particle loading, agglomerated particles should not shatter. The minimum pore size available is 0.01 μm and approximately 80% of the total filter volume is occupied by the pores.

Our experience with cellulose membrane filters indicates that difficulties will be experienced analyzing the exhaust particles. The surface of the cellulose filters is extremely rough -- identification of particles would not be easy. The identification problem would be compounded by the slight contrast difference between the particles and filter (both are predominantly carbon). On the other hand, Nuclepore membrane

filters have a flat surface with the pores uniformly spaced. Both the Nuclepore's flat appearance and chemical composition would aid in particle identification. Nuclepore membrane filters are available in diameters up to 293 mm with a 0.03 μm pore size. Nuclepore filters are also more resistant to high temperature than the cellulose filters -- Nuclepore, 150°C and cellulose, 100°C.

The resistance to air flow through the small pore size membrane filters is high -- the filters must be specially supported to eliminate rupture (once rupture occurs, the sample must be discarded). Supports of fine mesh stainless steel are in common use today. EM grids can be placed directly onto the membrane filter to make effective use of Brownian diffusion to collect the very small particles. Also, to achieve greater flow capacity, the filter should be as large as possible. For a 0.03 μm pore size Nuclepore filter, the air flow rate is approximately 0.4 $\ell/min/cm^2$ at 25°C and 70 cm Hg pressure drop.

To use the membrane filter with electron microscopy, the filter after receiving a particle deposit is cut into approximately 2 mm squares. The particles on the filter are then transferred to an EM grid using acetone to dissolve the filter. The use of acetone could significantly alter the particles and must be examined before the dissolving approach can be taken. Using the electron microscope in the scanning mode will permit direct use of the filter in the instrument. In the scanning mode, X-ray elemental analysis is possible. Comparisons between the EM grids placed on the membrane filter and those generated from dissolving the filter must be made to determine the approximate relative collection efficiencies. Large differences are not anticipated, however, because of the action of Brownian motion on particles below 0.001 μm.

A clear advantage with the membrane filter is its simplicity -- no electronic gear subject to failure. Also, the

technique will collect particles uniformly for sizes greater than 0.1 μm for the cellulose filter and 0.03 μm for the Nuclepore. Below this size, a portion of the particles will escape but will reduce as the particle size decreases even smaller. Remote operation of the filtration technique is possible through a turret mechanism capable of being advanced at the completion of sampling. Conceivably, many filters can be placed onto the turret, thus minimizing the time required for removing collected samples and installing fresh substrates.

3.5.5 Aerosol Spectrometer

The aerosol spectrometer is essentially a spiral centrifuge capable of separating particles by aerodynamic diameter in the size range 0.03 to 1.0 μm. The lower portion of the size range is achievable through the use of either radioactive or colored particulate materials (59). Otherwise, the lower size limit is approximately 0.1 μm (60,61,62).

To achieve the lower end of the particle size range, high rotational speeds are used (~24,000 rpm). With speeds of this magnitude, deposition of particles is violent relative to other methods -- electrostatic and thermophoretic deposition, membrane filtration. The influence of the spectrometer's effect on agglomerates can only be determined by comparison to another method.

The particles are separated and deposited onto a strip of metal foil approximately 200 cm in length. Consequently, the entire strip is the sample which must be analyzed to determine a size distribution and shape characteristics. A disadvantage of the aerosol spectrometer is that the aerosol sample does not enter the measuring channel a fixed distance above the substrate (metal foil) and therefore, the separation of the particle sizes is not complete. In fact, each size of particle from entry to the sedimentation channel will commence depositing near the point of entry and will form a layer

finishing at the point where the particles furthest from the substrate are deposited. Because of variations within the flow channel, the thickness of the particle layer is not constant. The varying thickness has been predicted by Stöber (63) and later experimentally verified by Dyment (60). Stöber expresses reservations about the possibility of determining accurately the size distributions of polydisperse aerosols with the spectrometer. Consequently, use of the spectrometer with the engine exhaust aerosol would prove difficult in determining size distributions.

Three factors effect the accuracy of the aerosol spectrometer:

1. Entry losses -- Rapid changes in direction and turbulent flow increase deposition prior to the aerosol entering the sedimentation chamber. Downstream, transition to laminar flow occurs, thus eliminating turbulent deposition. Banst (64) has identified the following entry losses:

   d_p = 1 μm, loss = 50%

   d_p = 0.1 μm, loss = 15%

2. Exit losses -- Undeposited particles pass from the system. At 24,000 rpm and the minimum flow rate, all particles below 0.025 μm escape.

3. Assumption of linearity -- The depth of the deposit layer is a linear function of distance up to the "cut-off" point. The cut-off is not sharp and varies with particle size.

Application of the aerosol spectrometer to the collection of particles for subsequent EM analysis appears limited. Particles below 0.025 μm are not captured and offer a severe limitation of the method. Awkwardness of changing the strip after every sample will require care and, therefore, be time consuming. In addition, because of the sample strip's large size, a significant amount of electron microscope time would be involved in analyzing each strip.

3.5.6 Electrical Aerosol Analyzer (EAA)

The electrical aerosol analyzer (EAA) is capable of measuring particle size distributions in situ over the diameter range of 0.01 to 0.7 μm. Three operations occur in the measurement technique:

- Electrical charging
- Precipitation or classification by electric mobility
- Aerosol detection

Three basic electrical charging processes can be used, but the only commercial instrument available utilizes charging by unipolar positive ions. The relationship between the particle charging and electrical mobility is monotonic between the geometric particle size and particle mobility. This relationship is therefore used to infer the particle size distribution from the measured mobility distribution.

Figure 23 is a schematic diagram of the EAA marketed by Thermo-Systems, Inc.* The major components include the aerosol charger, mobility analyzer tube, current sensor, and associated electronic and flow controls. The sample flow rate to the instrument is 4 ℓ/min with an additional 45 ℓ/min of clean air needed to operate the EAA.

Space charge and diffusion losses within the charger account for the major portion of the losses within the instrument. Results from detailed analysis (65) indicate that because of these losses, the smallest particle size range is about 0.006 μm and that sizing down to 0.003 μm is possible under certain circumstances.

Figure 24 gives a comparison of the EAA's output against a monodispersed aerosol input. The correlation is seen to be excellent in the particle size range from 0.006 μm to

---

* 2500 Cleveland Ave. North, St. Paul, Minn. 55113

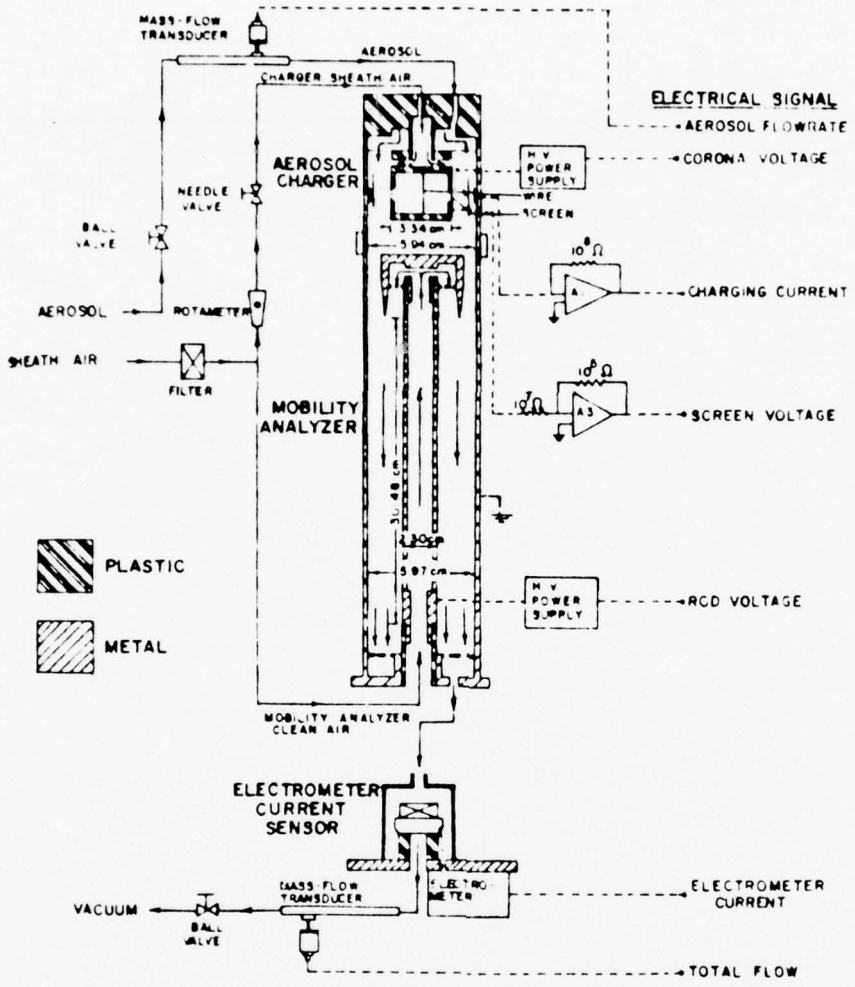

Figure 23

SCHEMATIC OF THE THERMO-SYSTEM MODEL 3030
ELECTRICAL AEROSOL ANALYZER

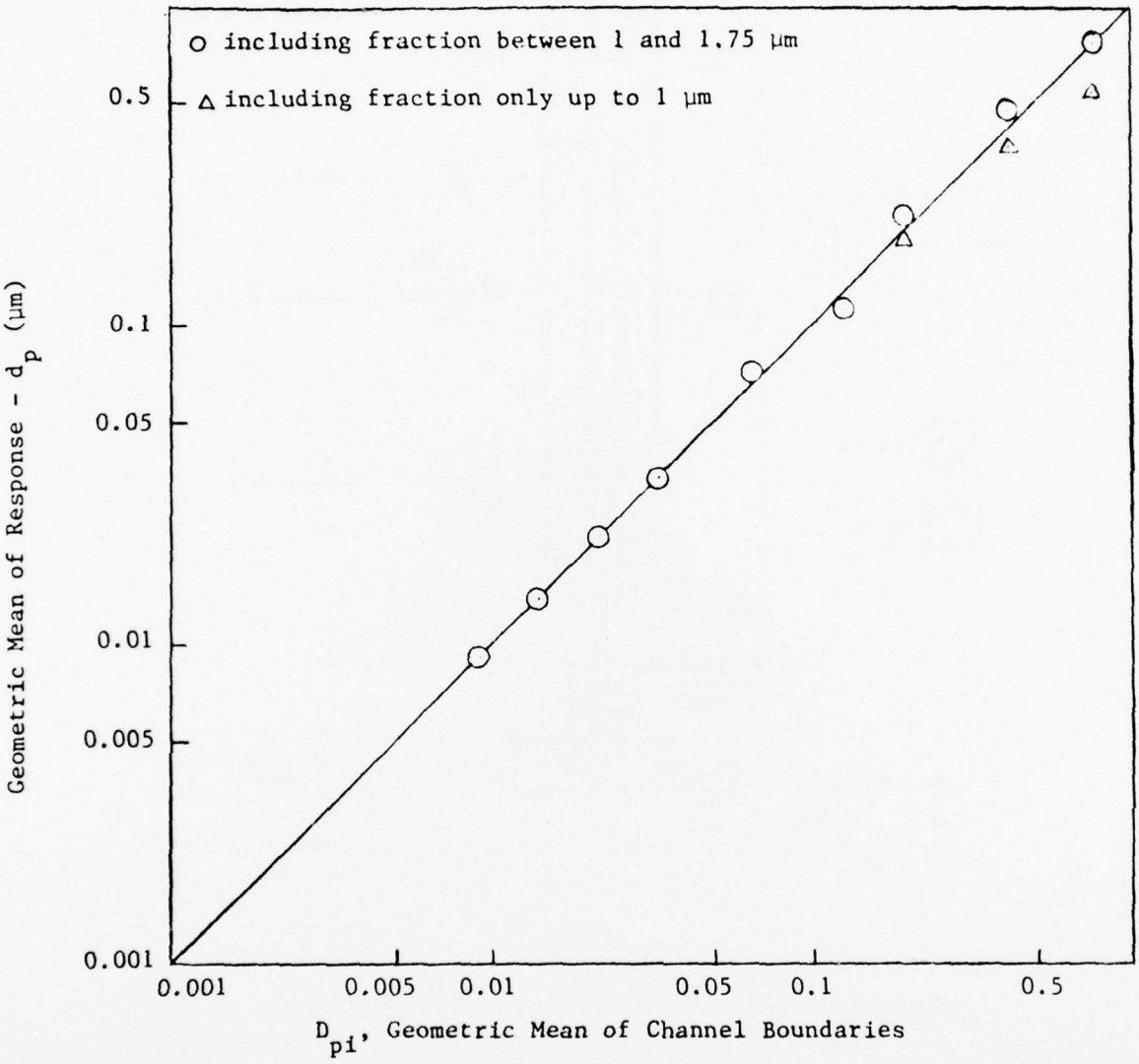

Figure 24

COMPARISON OF THE INSTRUMENT INDICATION WITH THE RESPONSE TO MONODISPERSE AEROSOLS FOR THE MODEL 3030 ELECTRICAL AEROSOL ANALYZER (65)

0.6 μm. However, within the 0.6 to 1.0 μm particle size range, the instrument's response is reduced about 35 percent.

Stability of the EAA during the measurement cycle is difficult to predict and control. Changes in the aerosol concentration as a function time tend to cause errors in the calculated particle numbers (65). Magnitude's involved with this error are unknown, therefore requiring that the aerosol's concentration be as stable as possible. A "damping" chamber can be used (20-50 liters) to minimize fluctuations of this type.

Other non-ideal effects have been observed in the past with the commercial EAA, but are not fully understood. One effect is negative currents for several of the smallest particle size ranges. Instrument to instrument variations have also been observed and are probably due to insulator charging effects in the mobility analyzer.

3.5.7 Recommendations for Particle Size Analysis

The design configuration of the sampler is constrained to deliver information regarding particle size, particle shape, and chemical composition. The particulate mass concentration (mass loading) of the engine's exhaust is also required. Because different engines, power settings, fuel types, and atmospheric conditions are the important variables, multiple samples are mandatory.

The techniques available for particle sizing have been reviewed. The only real-time instrument available is the Electrical Aerosol Analyzer (EAA) offered by Thermo-Systems. It has a usable particle size range of 0.01 to 0.7 μm. The electron microscope (EM) can in itself meet the program requirements -- 0.001 μm to 2 μm -- but suffers from elaborate sample preparation. The samples must also be stored for a period before analysis. The EM is the only method by which complete shape characteristics can be obtained. Also, the EM

through the X-ray probe can provide data on elemental composition where the concentration of the element exceeds the technique's sensitivity. The EM is the only instrument capable of performing these tasks and therefore indispensable in the task of sample analysis.

Upon selection of the most appropriate method of particle size analysis, the EAA is considered necessary for two reasons. Real-time data is highly useful in operating the sampler in the test cell. This has direct implication to the preparation of EM samples (grids) as discussed later. Second is that the size range covered is nearly two orders of magnitude -- considerable when compared to other techniques. The EAA is well documented in the literature and widely used.

Many techniques are available for the preparation of EM grids. These have been reviewed and the most suitable for this application is the use of Nuclepore filters with EM grids attached directly to the filter substrate. Both the grids and Nuclepore material are compatible with EM analysis. Also, the technique is totally mechanical in nature, thus avoiding the complication of electrical circuitry. The EM is sensitive to the particle loading on the grid. If the particles are too sparse, a large number of fields must be analyzed absorbing valuable time. On the other hand, if the particle loading is too dense, the particle's characteristics are masked because of close proximity to each other. Therefore, the correct particle loading must be achieved to obtain the best results. The EAA is very useful in this regard, as a direct reading of the particulate concentration is available allowing modification of the sample before collecting. This should maximize the number of good samples and minimize the number of repeat samplings.

AD-A041 499 IIT RESEARCH INST CHICAGO ILL F/G 21/5
TURBINE ENGINE PARTICULATE EMISSION CHARACTERIZATION.(U)
SEP 76 D L FENTON DOT-FA75-WA-3722
UNCLASSIFIED IITRI-C6352-10 FAA/RD-76-141 NL

2 OF 2
ADA
041499

END

DATE
FILMED
7-77

4. SAMPLER DATA AND SAMPLE HANDLING PROTOCOL

The sampler's components have been discussed. Basically, information from the sampler will come from three sources: analysis through the elctron microscope, electrical aerosol analyzer, and glass fiber filters. A list of the data available from each source is given below:

- Nuclepore filter and EM grids -- Particle size and shape data from 0.001 μm to approximately 2 μm. Particle morphology and elemental analysis on individual or group particle basis.
- Electrical Aerosol Analyzer -- Real-time particle size distribution based on electrical mobility from 0.01 to 0.7 μm. Time required for a measurement cycle is about three minutes.
- Glass fiber filter -- Rate of total mass emission. Analysis of deposit gives organic chemical content and analysis of trace elements. The elemental analysis performed on the deposit augments the analysis done under the EM.

The particulate sample deposited on the Nuclepore filter and EM grids will require handling and storage after collection. The samples obtained after a test run must be removed from the sampler and placed inside protective packages. Shipment of the samples (after properly labeled) back to IITRI can be accomplished in two ways. The first is by separate freight and the second is with the sampling team upon their return. The samples should not undergo any degradation for the short time periods involved. Upon receipt of the samples at IITRI in Chicago, analysis is initiated by sample preparation. Subsequent to this, size, shape, and composition data are obtained with the electron microscope. The size data obtained will augment the data generated by the EAA.

The glass fiber filter will yield the total mass emission rate by gravimetric analysis. The filters must be weighed initially and subsequent to sample collection. Control filters are also required to assess the effects of relative

humidity. The weighing is to be performed at United Airlines on a normal analytical balance. After this, the filter will be placed inside pyrex petri dishes and kept in the dark. Where convenient, samples undergoing organic chemical analysis will be kept as cool as practical to minimize losses due to volatization. To be noted is that filter removal from the sampler must be immediate.

Selection of the best glass fiber filter material is difficult because the analyses performed require different substrates. Whereas glass fiber filters are appropriate for organic analysis, they are not appropriate for metallic analysis. For trace element analysis, cellulose filters are the most suitable*.

Cleaning the sampling probe and transport lines to the main diluter is necessary at least once to quantify the internal particulate deposition. An organic solvent -- chloroform -- should be used to rinse the inner walls of the sample line and sampling probe assembly. Chloroform is desirable because evaporation occurs rapidly in air without leaving an apparent residue. Before the next run is initiated, the internal surfaces should be dry. The solvent-particulate material mixture can be placed into a glass bottle for subsequent mass analysis.

---

* To overcome the dilema, pre-washed glass fiber filters should be used to minimize extraneous metals and organic binders present in the filter material. Then an extraction procedure (probably using hot nitric acid) should be used to remove the particualte material from the glass fiber filter. Filtration of the particulate material onto a small cellulose filter will both concentrate the sample and permit convenient analysis.

5. MECHANICAL DESIGN OF SAMPLER

An overall configuration of the sampler is given in Figure 25. The main components of the exhaust sampler are indicated on the diagram. The exhaust gas sample flow rate extracted by the probe will be either 5, 10, or 19 actual m^3/hr depending on the engine's power setting. These flow rates correspond to idle, approach, and a nozzle inlet Mach number of 0.8. The inside nozzle diameter planned for each of the three probes is 0.2 cm. Design details of the sampling probe, sample line, and main sample diluter are given in this section.

5.1 Component Design

Supply air to the main sample diluter is available through existing facilities at United Airline's engine test cells. The supply air auxiliary equipment is commercially available except for the five-orifice cartridge necessary to control the dilution air flow rate. The nominal flow rates anticipated are 34, 60, 85, 110, and 140 actual m^3/hr. The orifice cartridge assembly will be fabricated at IITRI and is comprised of a plate within which is machined a series of orifices. Positioning the plate to any one of the orifices effectively regulates the air flow. The filter selected is an absolute type capable of very high (98%) collection efficiencies. The dryer is composed of a bed of water adsorbing materials (dririte) capable of being recycled. A line heater is also necessary to maintain the sample above the dew point and is not shown on Figure 25.

In the design of the flow control system, remote control and readout systems will be used throughout. The three-way ball valve used to divert the flow through the bypass circuit is motorized. The three shut-off valves are all 1/2 solenoid operated. The two inch ball valve on the secondary sampling circuit (electrical aerosol analyzer and five-position turret for the electron microscope grid samples) is also motorized.

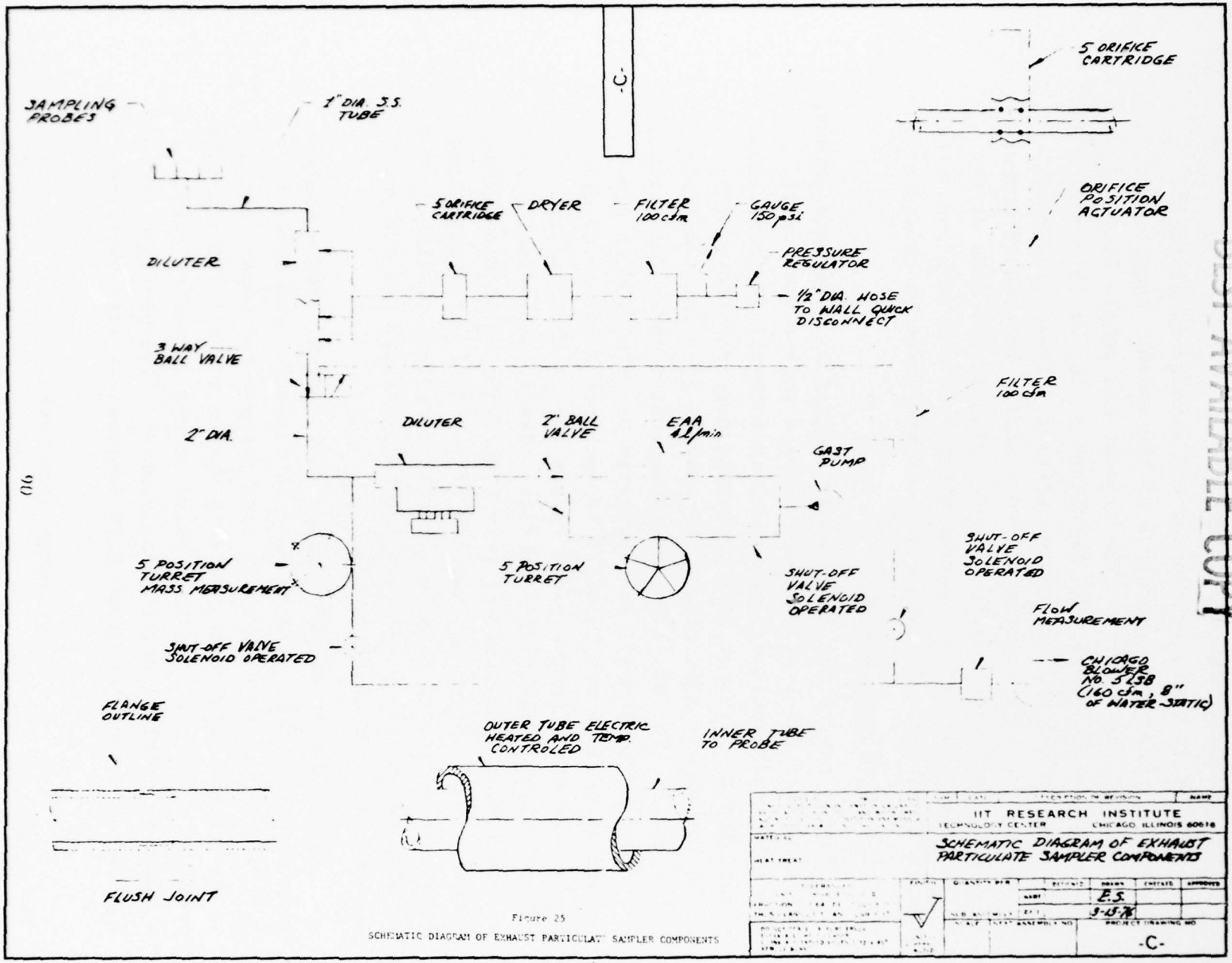

Figure 25

SCHEMATIC DIAGRAM OF EXHAUST PARTICULATE SAMPLER COMPONENTS

BEST AVAILABLE COPY

Turrets are employed for both the mass measurement and in the preparation of the electron microscope grid samples. The use of five positions allows the sampler to be operated for each of the five engine power settings without any manual attendance. As a consequence, engine operation time is minimized. The method of activation for both turrets is through an ordinary pneumatic ratchet. Motorized indexing systems are more costly while pneumatic systems require greater set-up time. For a single unit, which is our case, the pneumatic approach is cost effective.

A small aliquot of the main sample stream will be diverted to the EAA and EM grid preparation stage (less than 5%). A special diluter will be made to provide a variable dilution in order to provide a suitable loading to the EAA and EM grid station. The excess material must be dumped because the flow to the sampling equipment is restricted to low values. The operating sequence should permit only one of the systems to function at any particular time. This way the EAA can give a tentative mass loading in addition to a particle size distribution. Also, the particulate mass concentration applied to the EM grids will be known, affording the opportunity to adjust the exposure time to maximize the chance of a good sample.

The second diluter is necessary to further reduce the concentration of the exhaust particles. The design of this diluter is not yet complete. The basic concept is similar to the main sample diluter except that the dilution ratios vary over a wider range. Critical flow orifices operated by solenoid valves control the flow giving precise levels affording accurate knowledge of the dilution ratios at all times. Only a portion of the diluted sample will be used by either the electrical aerosol analyzer or the EM grid turret. Therefore, part of the flow must be diverted. Filtered compressed air supplies the dilution air. The concentration ratio between stages is varied by changing the

flow rate of the spillover exhaust from the end of the system. The dilution ratio for any stage is governed by the following relationship

$$R_n = 1 + \frac{q_{an}}{q_e + q_{bn} - q_{an}}$$

where

R_n = ratio of concentration in state n to that in the prior state (n - 1)

q_{an} = dilution air flow rate introduced just prior to state n

q_{bn} = air flow rate withdrawn from stage n

q_e = exhaust overflow rate from end of system

The dilution ratios between sucessive stages can be varied. For this application, the use of four stages with concentration ratios between stages equal to five gives dilutions varying from 5 to 625. However, the dilution steps are large and the addition of a fifth dilution stage designed to reduce the concentration by a factor of 2 would afford greater operating flexibility. Also, the maximum dilution ratio avaliable increases to 1250. Calculations indicate that this range is adequate. Therefore, the secondary diluter will utilize five dilution stages, any of which can be used to give the desired dilution.

The fan package consists of the fan itself, flow controls, and measurements for temperature and pressure. The flow controls and measurements are placed downstream of the bypass and sample union.

Facility for purging (clean compressed air) the sampling probe is necessary to maintain the cleanliness of the sampling lines during engine starts. Clouds of atomized fuel have been observed upon engine starting and ingestion of this material would surely compromise the exhaust sample collected later.

Deposition within the short transport pipe between the probe and diluter could be significant. A Reynolds number of 2,800 is indicated by Strom (66) to result in minimum deposition. Assuming the fluid properties at the exit plane of the engine, back calculation gives the following for the extreme power settings:

Take-off -- D = 1 in. -- N_R = 4,080
Idle -- D = 1 in. -- N_R = 1,420

As seen in the deviation from the nominal 2,800, the 1 inch diameter is the best compromise. Downstream from the main dilution, the flow is much higher requiring a larger diameter tube. A diameter of 2 inches gives a take-off N_R of 42,400 and a N_R value of 14,800 at idle, both larger than 2,800. However, deposition is minimized because the particles are focused toward the pipe centerline and the transport length is short. These pipe sizes are reasonable and readily available in 316 stainless.

Bends in the transport tube promote deposition and are considered sharp (66) if

$$R < \frac{\bar{\rho}_p d_p^2 UC}{(1.8)\mu_g}$$

where the variables have already been defined.

The maximum velocity within the 1 inch transport pipe will be approximately 12 m/sec (40 ft/sec). Assuming d_p is equal to 2.0 μm, and substituting typical exit plane values, results in R < 0.18 cm (0.07 in.). In a practical sense, values for R this small result in no constraints at all. Downstream from the main diluter, the maximum velocity in a 2 inch pipe is about 30 m/sec (100 ft/sec) resulting in a R < 0.5 cm (0.2 in.). Again, this results in no practical limitation.

A tentative design of the sampling nozzle is given in Figure 26. The leading edge of the nozzle is sharp as practical to result in minimum disturbance to the flow and

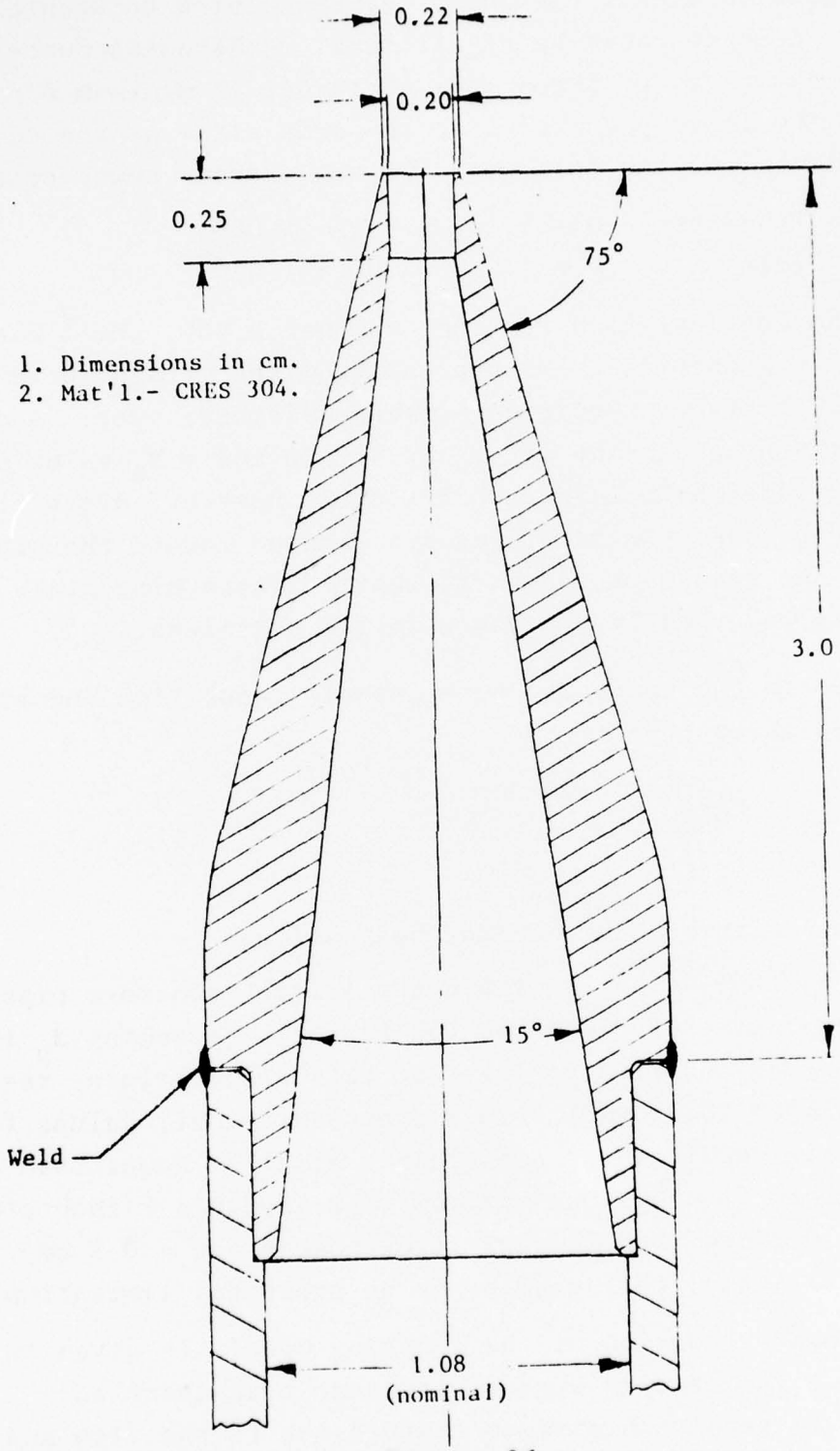

Note: 1. Dimensions in cm.
2. Mat'l.- CRES 304.

Figure 26

PROBE INLET DESIGN

and particles. Tine (67) reports that, in practice, the external conical surface taper of the nozzle usually ranges from 10° to 45° relative to the centerline. An angle of 15° seems to be the practical limit of the taper given the harsh environment at the engine's exit plane. The area expansion inside the nozzle is of sufficient magnitude to decelerate the flow and avoid the problems associated with shock-wave and boundary-layer interactions. The outside taper of the nozzle is gradual to reduce the flow disturbance caused by the probe and to locate the leading edge of the nozzle 10 diameters (2 cm) upstream from the probe support structure.

Additional drawings are given to show details in the probe and sampler design. Figure 27 indicates the method of securing the upper two sampling nozzles to the support frame. Note that a clamp is provided near the probe tip to prevent bending and avoid complications arising from vibration. The sampling tube is secured to the trailing edge of the probe support structure. Figure 28 indicates the sampling tube geometry for the lower two sampling nozzles. Probes for each of the three engines will be fabricated in an identical fashion.

The fixture holding the sampling probe to the engine is identical to the present technique used by United Airlines. The technique is time proven and already meets their approval. Also, the support structure of the probe will be identical to that presently used by United Airlines. This is desirable as design time is reduced and affords greater reliability. The United Airlines drawing numbers corresponding to the three engines under investigation giving design details are:

JT3D -- 9SF6666-78-OOT
JT8D -- 9SR6576-78-OON
JT9D -- 9SF6720-78-OOP

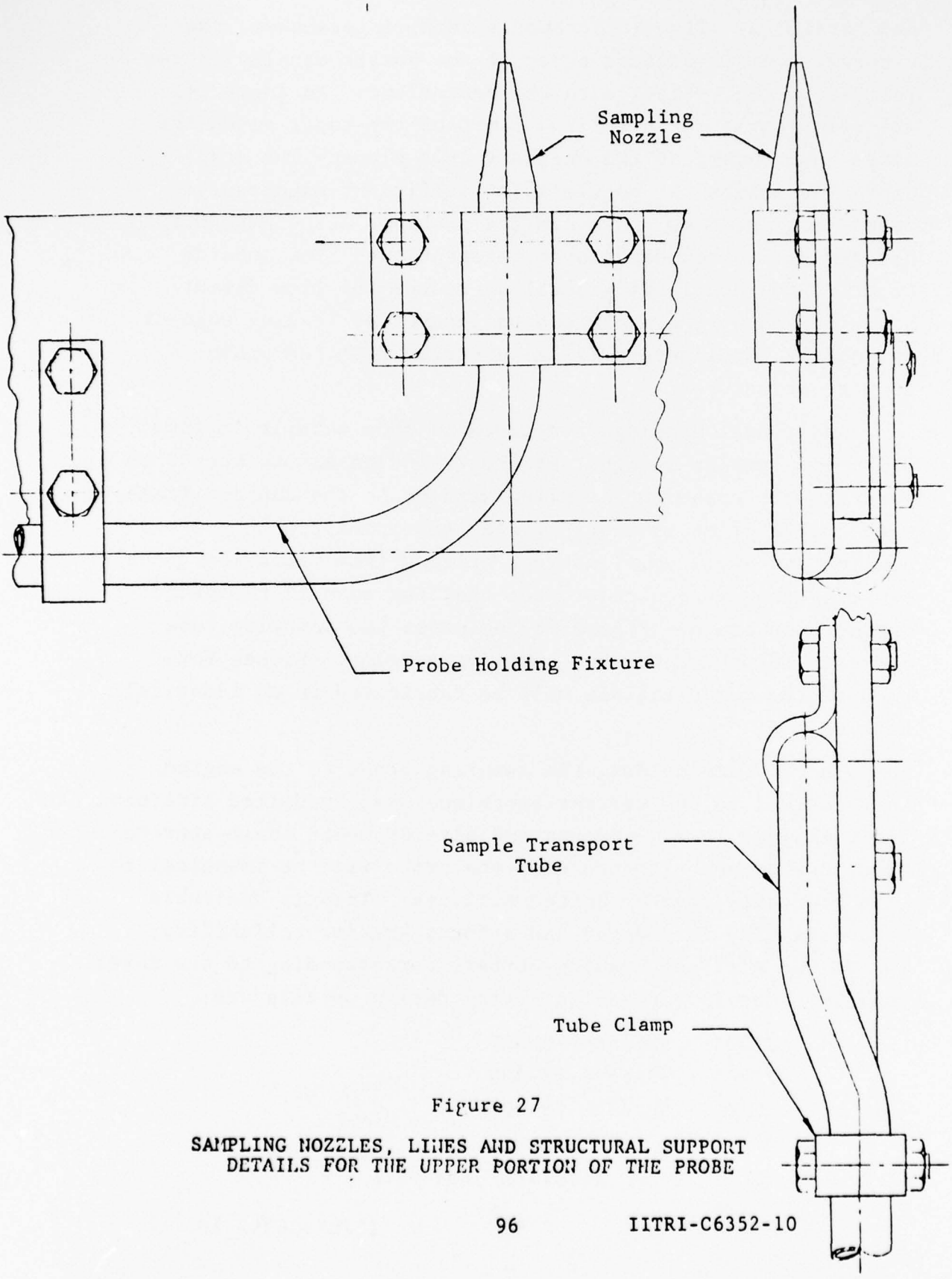

Figure 27

SAMPLING NOZZLES, LINES AND STRUCTURAL SUPPORT DETAILS FOR THE UPPER PORTION OF THE PROBE

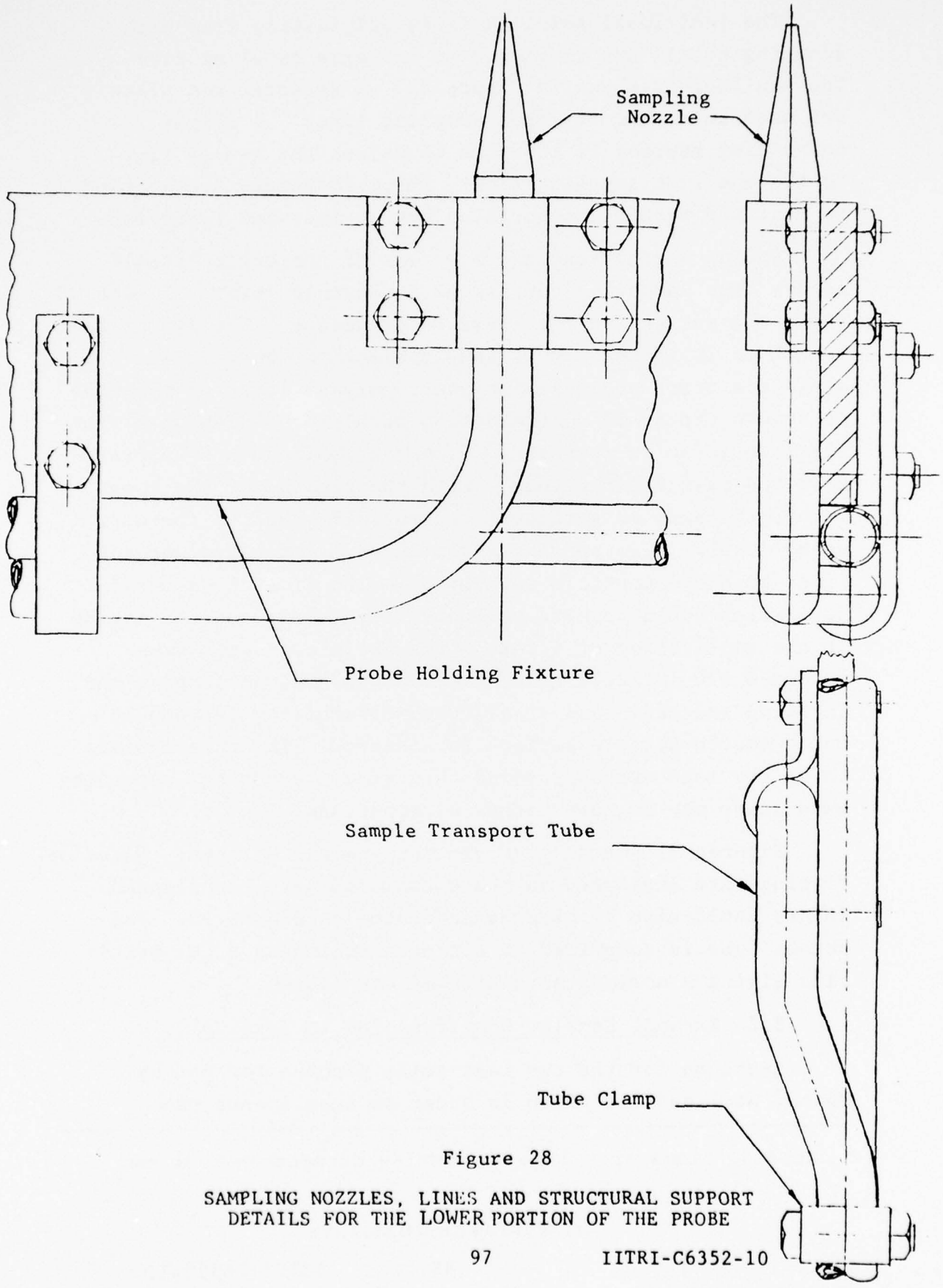

Figure 28

SAMPLING NOZZLES, LINES AND STRUCTURAL SUPPORT DETAILS FOR THE LOWER PORTION OF THE PROBE

The individual sampling lines originating from each sampling nozzle are converged to a single sampling line. The manifold is shown in Figure 29. A setscrew and plate are used to anchor the four sampling lines. A slight converging section is required to adjust the sample flow to the one inch sampling line. Sharp shoulders are avoided to minimize particle deposition due to inertial impaction.

During engine testing, movement of the engine itself occurs thus mandating the use of a flexible joint. Figure 30 shows the design for the flexible connector. The approximate length is 36 inches and is compatible with schedule 40 stainless steel tubing* The inner polymer layer of the hose is removed to avoid contamination problems. Location of the flexible joint is downstream from the manifold and upstream from the main diluter tube. With the removal of the inner liner, the exposed surface is essentially that of the wire weave itself. Two options exist in terms of a replacement liner to avoid particle deposition. The first is a metal foil which would require periodic replacement and the second is the application of a thin gauge stainless steel tube (0.010-0.020 in. wall thickness) to serve as an inner liner. In using the stainless steel tube, flexibility is reduced but a smooth durable surface is achieved. The tube appears to be the most appropriate at this time. Practical operating experience may suggest better alternatives.

Figures 31 and 32 give the main sample diluter. Swagelock fittings are indicated on these two drawings, but flanged joints could also be used as indicated on Figure 23. The porous tube is comprised of sintered stainless steel particles giving a nominal pore size of one micron.

5.2 Exhaust Sampler Congifuration in Test Cell

Sketches for the two test cells planned for use by United Airlines are given in order to best locate the

---

* Outside diameter = 3.34 cm, inside diameter = 2.66 cm.

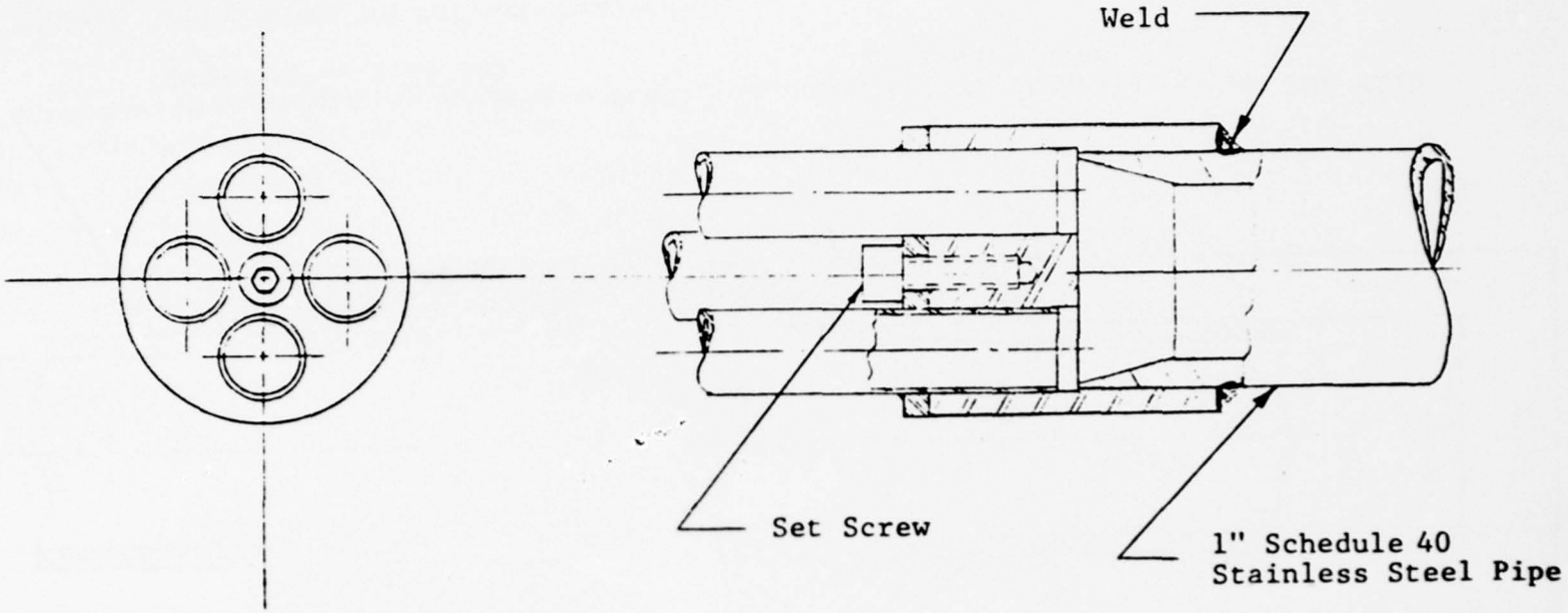

Figure 29

SAMPLING LINE MANIFOLD ASSEMBLY FOR TRANSITION TO ONE INCH TUBE

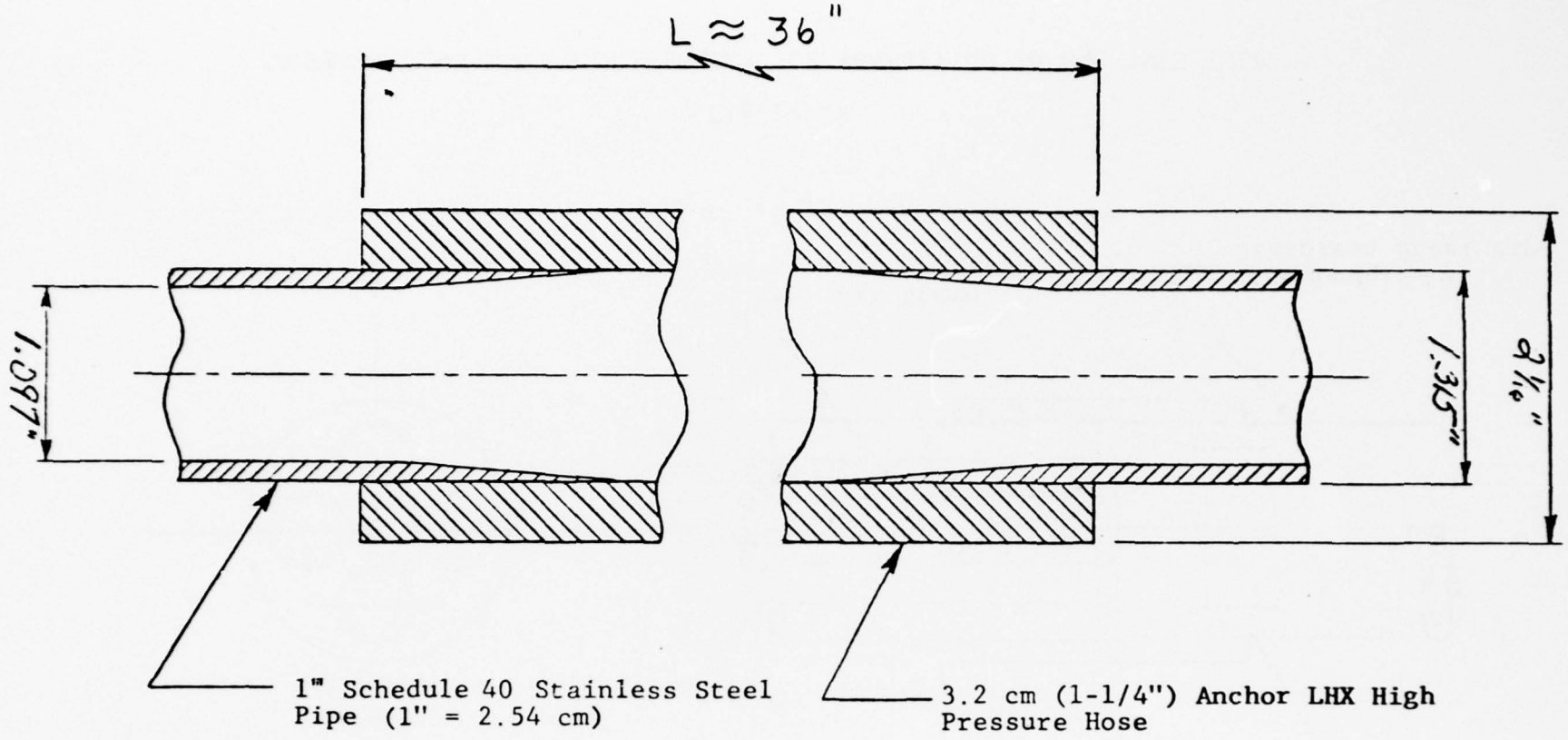

Figure 30

FLEXIBLE CONNECTOR

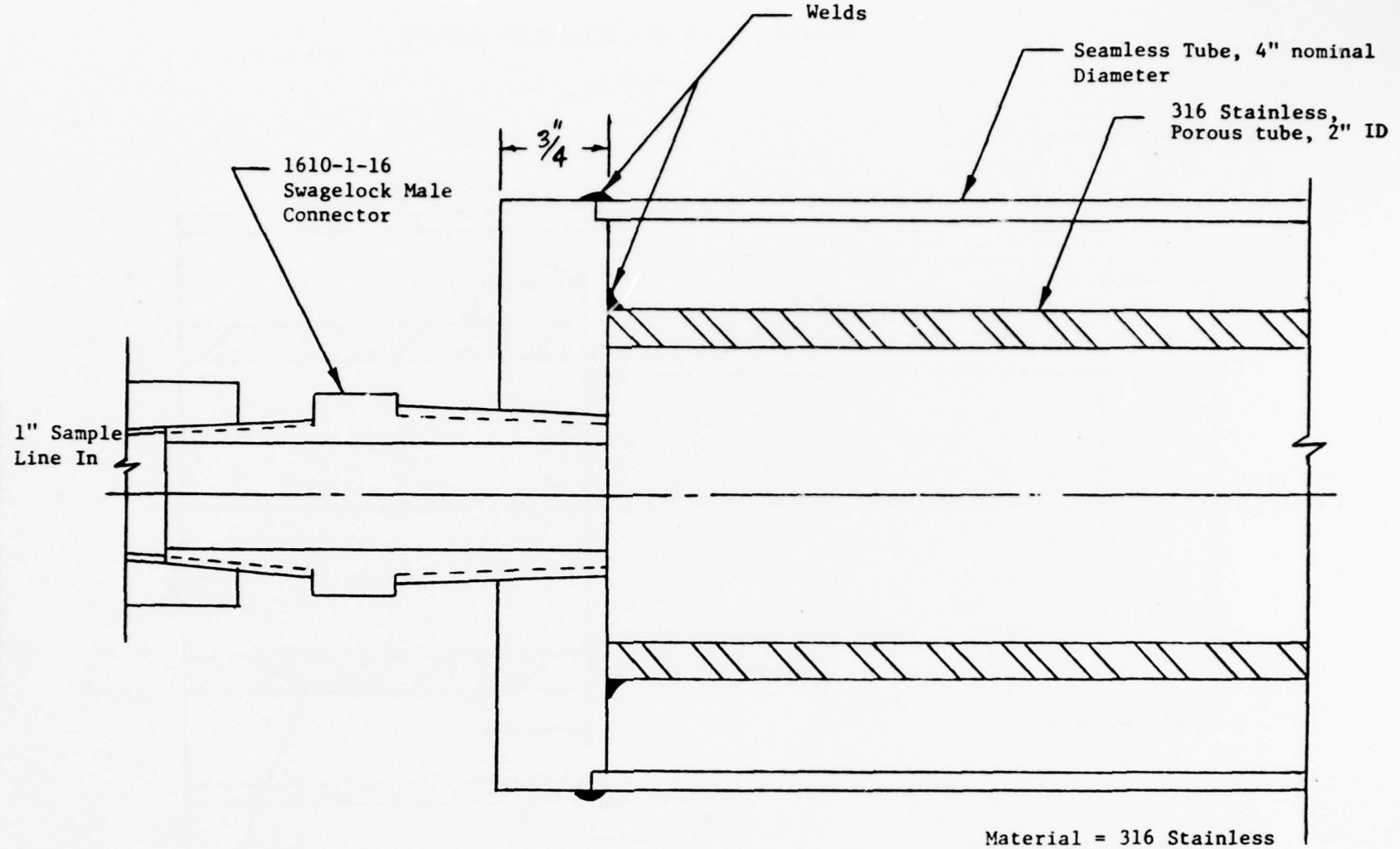

Figure 31

INLET ASSEMBLY FOR MAIN DILUTER

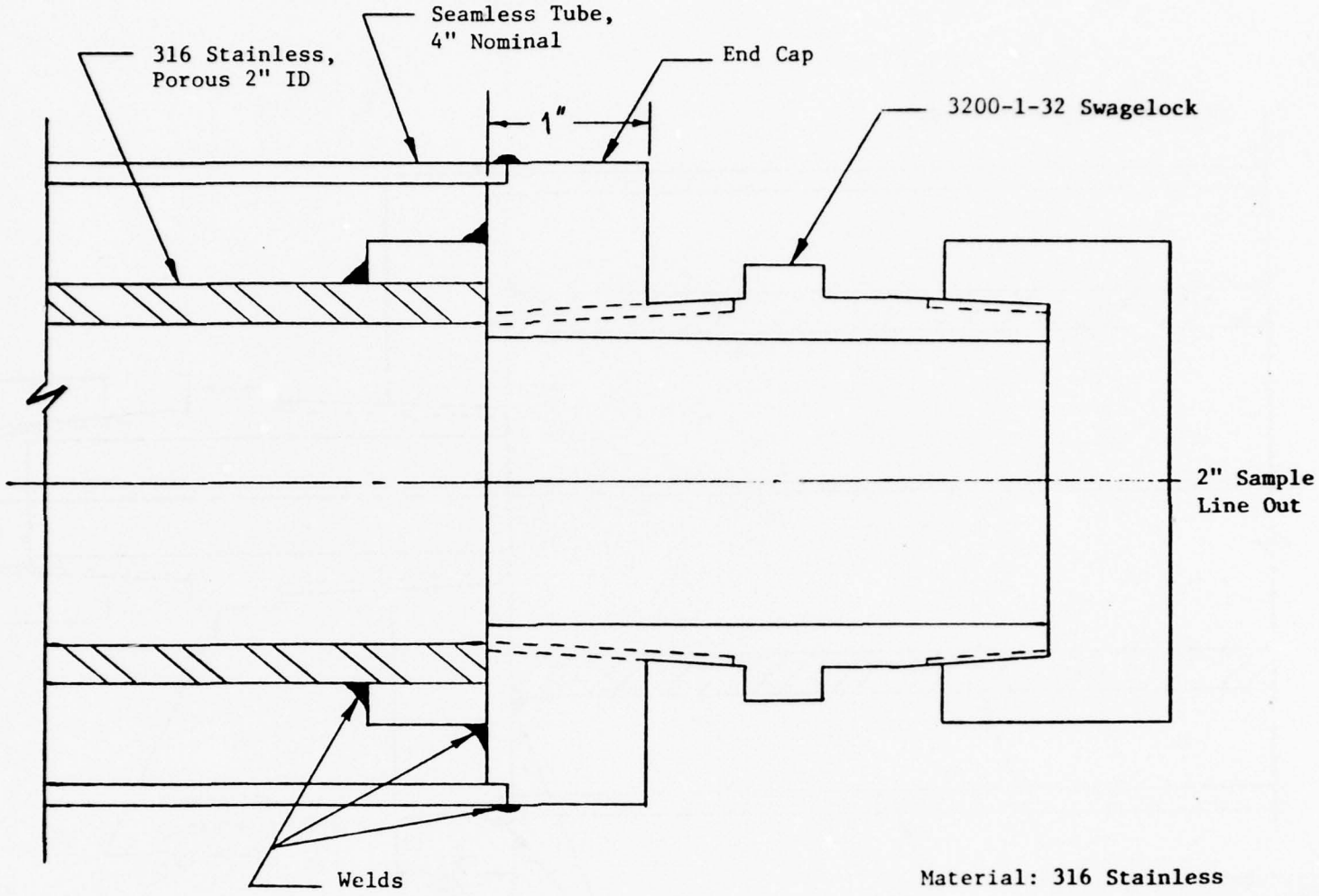

Figure 32

OUTLET ASSEMBLY FOR MAIN DILUTER

sampler under design. An important consideration in this regard is the transport length the exhaust sample must undergo. This length must be minimized. In conjunction with transport length is the practical considerations involving mechanical support for the sampler box and main diluter.

Figure 33 shows a sketch of the test cell geometry applicable to the JT3D and JT8D engines. In this case, the sampler box is positioned along the side of the engine at approximately the mid-point. The main diluter transports the sample on a diagonal both downward and forward. The length of the main diluter itself is approximately 5 feet. In the test cell where the JT3D and JT8D engines will be sampled, tie-down loops are installed in the floor, thus providing adequate support for the sampling box. An alternative location exists for the sampler box in this test cell -- behind the cell's exhaust tube. Air flow in this region of the test cell is considerably reduced from the engine mid-point location, but a significant turn and longer distance in the sample line is necessary to accomodate the alternative location.

In addition, the secondary air flow velocity near the cell's exhaust tube may be high, thus indicating large forces on the sampling line passing through this region.

A sketch of the test cell geometry where the JT9D is operated is given in Figure 34. Two acceptable locations exist for the sampler box based on acoustical energy patterns about an engine. One is along the staircase leading to the floor of the cell and the second is on the floor of the movable platform. Both locations occur forward of the engine's exit plane and thus are favorable acoustically. Also, the distance the sampling line exposure to the "fan air" is minimized. However, the staircase platform (specially constructed) is a much more convenient location

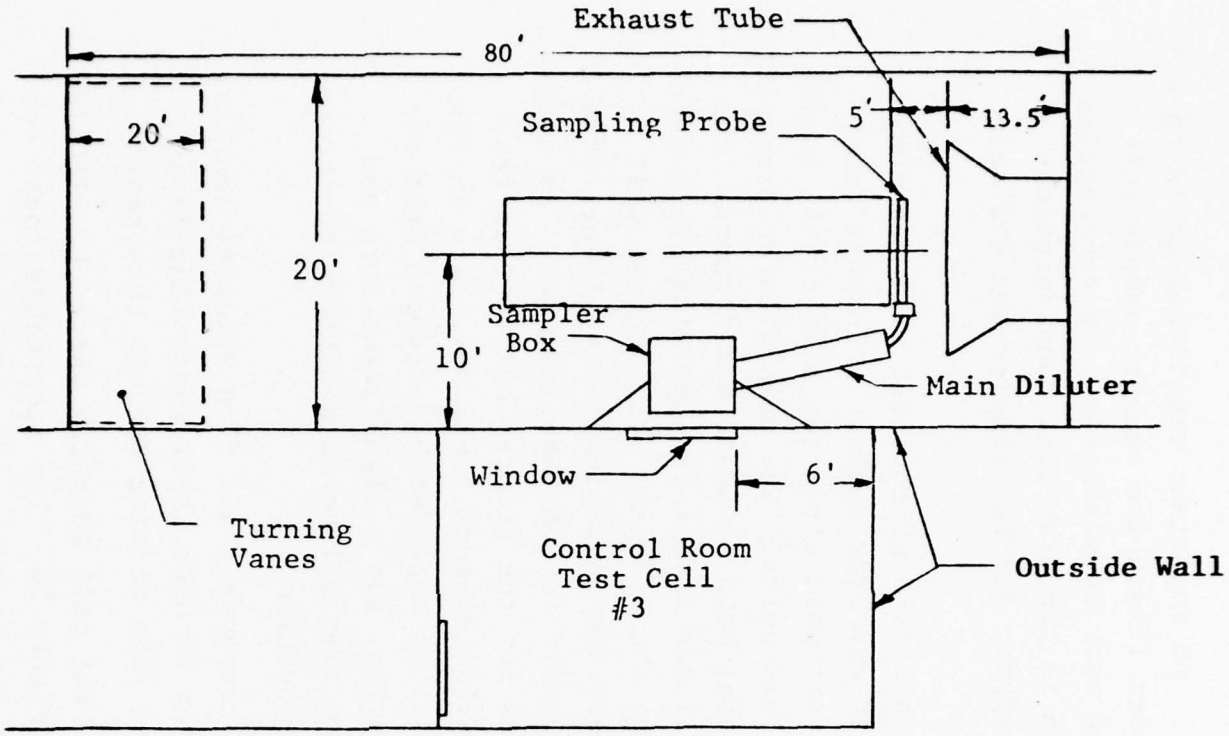

Approximate Dimensions Sketch Not to Scale

Note: 1. Engine centerline height above floor is 7 ft.
2. Length of main diluter tube is approximately 5 ft.

Figure 33

TOP VIEW SKETCH OF UNITED AIRLINES TEST CELL #3 WHERE JT3D AND JT8D ARE OPERATED WITH EXHAUST SAMPLER LAYOUT

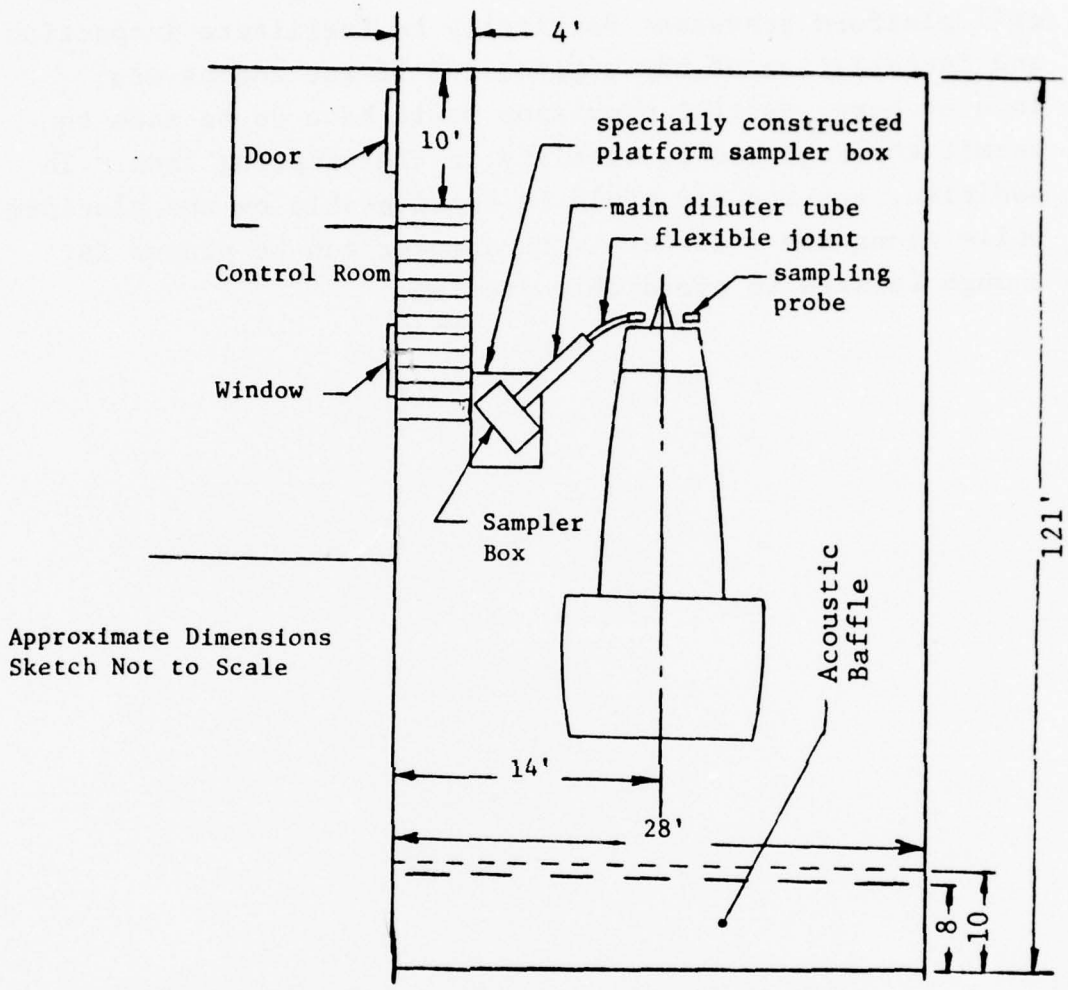

Note: 1. Engine centerline height above floor is 14 ft.

2. Length of main diluter tube is approximately 7 ft.

Figure 34

TOP VIEW SKETCH OF UNITED AIRLINES TEST CELL #4
WHERE THE JT9D ENGINE IS OPERATED
WITH EXHAUST SAMPLER LAYOUT

as the sampler is fixed relative to the engine. The test cell platform traverses vertically to facilitate inspection and installation of the engine, and if the engine was located here, special provision would have to be made to permit the required flexibility in the sampling line. In addition, the fan air would be considerable on the platform, while along the staircase, the sampler can be placed far enough forward to avoid this problem.

REFERENCES

1. Aerospace Recommended Practice 1179, Soc. of Automotive Engineers, Inc., May 1970.

2. Nelson, A. W., "Collection and Assessment of Aircraft Emissions Baseline Data-Turbine Engines", Final Report, EPA Contract No. 68-02-0027, Feb. 1972.

3. Devorkin, H., Chass. R. L., Fundwich, A. P., and Kanter, C. V., Air Pollution Source Testing Manual, Los Angeles County Air Pollution Control District, Nov. 1965.

4. Klarman, A. F., "Evaluation of a Sampling Train Procedure for Measuring Gas Turbine Engine Particulates", Final Report, NAPTC-LR-76-8, Naval Air Propulsion Test Center, New Jersey, April 30, 1976.

5. Johansen, K. M. and Kumm, E. L., "Determination of Aircraft Turbine Engine Particulates", Final Report, AiResearch Manufacturing Company, Phoenix, Ariz., EPA Contract No. 68-02-1236, May 1975.

6. Johansen, K. M., private communication, AiResearch Manufacturing Company, Phoenix, Ariz., Feb. 1976.

7. Davidson, D. L. and Domal, A. F., "Emission Measurements of a J93 Turbojet Engine", Final Report, Report No. AEDC-TR-73-132, Arnold Engineering Development Center, Arnold Air Force Station, Tenn., 1972.

8. Hall, R. L. and Shaffermocker, W. M., "Engine Failure Prediction (Ion) Probe Program", Final Report, Report No. AFAPL-TR-74-46, Air Force Aero. Propulsion Lab., Wright-Patterson AFB, Ohio, June 1974.

9. Teller, A., "Turbine Emission Control - A Systems Approach", 68th Annual Meeting of the Air Pollut. Control Assoc., Boston, Mass., Paper No. 75-03.2, June 1975.

10. Sem, G. J., "Design and Application of an Electrical Size Analyzer for Submicron Aerosol Particles", 21st Annual ISA Analysis Instrumentation Symposium, Instrument Society of America, Philadelphia, Penn., May 6-8, 1975.

11. Boderick, A., private communication, Dept. of Trans., Boston, Mass., Oct. 10, 1975.

12. "Development of an Automated EPA Method 5 Stack Sampler", Report No. AESO-161-1-76, Naval Environmental Protections Support Service, Naval Air Rework Facility, North Island, Calif., July 1975.

13. Shabod, L. M. and Smirnov, G. A., "Aircraft Engines as a Source of Carcinogenic Pollution of the Environment [Benzo(a)pyrene Studies]", Atmos. Envir., 6:153-164, 1972.

14. Fenton, D. L., "Design Study for Turbine Engine Particulate Sampler", IITRI Report No. C6330-5, IITRI, Air Force Contract No. F41609-75-C-0024, Brooks Air Force Base, Texas, July 1975.

15. Conkle, J. P., Lackey, W. W., and Miller, R. L., "Cryogenic Sampling of Turbine Engine Exhaust", Prog. Report No. SAM-TR-74-54, USAF School of Aerospace Medicine, Nov. 1974.

16. Gearhart, J. and Benek, J. A., "Measurement of Pollutant Emissions from an Afterburning Turbojet Engine at Ground Level - Part I. Particulate Emissions", Final Report, Arnold Engineering Development Center, Arnold Air Force Station, Tenn., 1971.

17. Vaught, J., Parks, W., Johnsen, S., and Johnson, R., "Collection and Assessment of Aircraft Emissions Baseline Data Turboprop Engines (Allison T56-A-15)", Final Report, EPA Contract No. 68-04-0029, Sept. 1971.

18. Klueg, E. P. and Slusher, G. R., "Exhaust Emission Probe Investigation of a Mixed Flow Turbofan Engine", Fed. Aviation Admin., Atlantic City, N.J.

19. Souza, A. F., "A Study of Aircraft Powerplant Emissions", EPA Report, EPA Contract No. 68-04-0037, NTIS No. PB-207 107, Jan. 1971.

20. Souza, A. F., "Further Investigation into the Causes of Variability in Aircraft Turbine Engine Emission Measurement", EPA Report, EPA-460/3-75-011, Nov. 1975.

21. Aerospace Recommended Practice 1256, Soc. of Automotive Engineers, Inc., May 1971.

22. Lyon, T. F., "Development of Emission Measurement Techniques for Afterburning Turbine Engines", presented at Air Force Aero. Propulsion Lab., Wright-Patterson AFB, Ohio, Contract No. F33615-73-C-2047, Aug. 27, 1975.

23. Souza, A. F. and Reckner, L. R., "Variability in Aircraft Turbine Engine Emissions Measurements", EPA Report, EPA-460/3-74-006, Jan. 1974.

24. Vaught, J. M., "The Effect of Inlet Temperature and Pressure on an Industrial Turbine Engine Exhaust Emission", ASME Paper No. 75-WA/67-11, Gas Turbine Division, Amer. Soc. of Mech. Engrs., Winter Annual Meeting, Houston, Texas, Nov. 30-Dec. 4, 1975.

25. Brady, W. and Touzalin, L. A., "The Determination of Dust in Blast Furnace Gas", J. Ind. Engr. Chem., 3:662-70, 1911.

26. Hemeon, W. C. L. and Haines, G. F., "The Magnitude of Errors in Stack Dust Sampling", Air Repair, 4(3):159-64, 1954.

27. Watson, H. H., "Errors Due to Anisokinetic Sampling of Aerosols", Amer. Ind. Hyg. Assoc. Quart., 15(54):21-5, 1954.

28. Badzioch, S., "Collection of Gas-Borne Dust Particles by Means of an Aspirated Sampling Nozzle", Brit. J. Appl. Phys., 10(1):26-32, 1959.

29. Rouillard, E. E. A. and Valvona, P. J., "Flow Patterns Upstream of Isokinetic Dust Sampling Probes", Chem. Engr. Res. Group, Council for Scientific and Industrial Research, Pretoria, South Africa, Report No. 109, 1974.

30. Vitols, V., "Theoretical Limits of Errors Due to Anisokinetic Sampling of Particulate Matter", J. Air Pollution Contr. Assoc., 16(2):79-84, 1966.

31. Whiteley, A. B. and Reed, L. E., "The Effect of Probe Shape on the Accuracy of Sampling Flue Gases for Dust Content", J. Inst. Fuel, 32:316-20, 1959.

32. Smith, F. H., "The Effects of Nozzle Design and Sampling Techniques on Aerosol Measurements", EPA Report No. EPA-650/2-7-070, July 1974.

33. Fuchs, N. A., The Mechanics of Aerosols, Pergamon Press, New York, pp. 142-151, 1964.

34. Parker, G. T., "Some Factors Governing the Design of Probes for Sampling in Particle-and-Drop-Laden Streams", Atmos. Env., 6:133-142, 1972.

35. Martone, J. A., private communication, Dept. of Mech. Engr., Oregon State Univ., Corvallis, Oregon, March 18, 1972.

36. Klarman, A. T., Naval Air Prop. Test Center, Trenton, N.J., private communication, Aug. 27, 1975.

37. "Detailed Comments on 40 CFR Part 87 Proposed Standards for Control of Air Pollution from Aircraft and Aircraft Engines", Vol. 1, Ref. No. 73-9171, Pratt and Whitney Aircraft, East Hartford, Conn., Feb. 12, 1973.

38. Nelson, A. W., private communication, Pratt and Whitney Aircraft, East Hartford, Conn., Apr. 14, 1976.

39. Friedlander, S. K. and Johnstone, H. F., "Deposition of Suspended Particles from Turbulent Gas Streams", Indust. and Engr. Chem., 49(7):1151-1156, July 1957.

40. Davies, C. N., "Deposition from Moving Aerosols", Aerosol Science (edited by Davies, C. N.), Academic Press, New York, pp. 407-440, 1966.

41. Liu, B. Y. H. and Agarwal, J. K., "Experimental Observation of Aerosol Deposition in Turbulent Flow", Aerosol Science, 5:145-155, 1974.

42. Montgomery, T. L. and Corn, M., "Aerosol Deposition in a Pipe with Turbulent Air Flow", Aerosol Science, 1(3):185-213, 1970.

43. Beal, S. K., "Deposition of Particles in Turbulent Flow on Channel or Pipe Walls", Nuc. Sci. and Engr., 40:1-11, 1970.

44. Rouhiainer, P. O. and Stachiewicz, J. W., "On the Deposition of Small Particles from Turbulent Streams", ASME Paper No. 68-HT-41, Presented at ASME-AICHE Heat Transfer Conference, Minneapolis, Minn., Aug. 3-6, 1969.

45. Sehmel, G. A., "Particle Sampling Bias Introduced by Anisokinetic Sampling and Deposition Within the Sampling Line", Amer. Ind. Hyg. Assoc. J., 31(6):358-771, Nov. 1970.

46. Schlichting, H., Boundary-Layer Theory, McGraw-Hill Book Company, New York, 1968.

47. Lin, C. S., Moulton, R. W., and Putnam, G. L., "Mass Transfer Between Solid Wall and Fluid Streams: Mechanism and Eddy Distribution Relationships in Turbulent Flow", Indust. Engr. Chem., 45(3):636-640, 1953.

48. Davies, R., Ranade, M. B., and Puretz, J., "Submicron Separation and Data", IITRI Project No. 6239, Aug. 1974.

49. Spindt, R. S., "Polynuclear Aromatic Content of Heavy Duty Diesel Engine Exhaust Gases", First Annual Report, Coord. Res. Council, Project No. CAPE-24-72, July 1974.

50. Bradow, R. L., Carpenter, D. A., and King, F. G., "CRC Exhaust Particulates Program EPA Data Summary and Discussion", EPA Project 26ACV, Task 19, Nat'l. Envir. Res. Center, Research Triangle Park, N.C. Dec., 1974.

51. Ranade, M. B., "Sampling Interface for Quantitative Transport of Aerosols", EPA Contract No. 68-02-0579, Nat'l. Envir. Res. Center, Research Triangle Park, N.C., Dec. 1973.

52. Daley, P. S. and Lundgren, D. A., "The Performance of Piezoelectric Crystal Sensors Used to Determine Aerosol Mass Concentrations", Amer. Ind. Hyg. Assoc. J., 36(7):518-532, 1975.

53. Levich, V. G., Physiochemical Hydrodynamics, Prentice-Hall, Inc., Englewood Cliffs, N.J., pp. 30-37, 1962.

54. Green, H. L. and Lane, W. R., Particulate Clouds: Dusts, Smokes, and Mists, E. & F.N. Spon. Ltd., London, England, pp. 188-190, 1957.

55. Silverman, L., Billings, C. E., and First, M. W., Particle Size Analysis in Industrial Hgyiene, Academic Press, New York, pp. 12-22, 34-49, 109-123, 1971.

56. Hendricks, W., private communication, Micromeretics Instrument Co., Atlanta, Georgia, Oct. 17, 1975.

57. Liu, B. Y. H., Whitby, K. T., and Yu, H. H. S., "Electrostatic Aerosol Sampler for Light and Electron Microscopy", Review of Sci. Instruments, 38(1):100-102, 1967.

58. Rimberg, D. and Keafer, D., "Evaluation of a Commercial Electrostatic Aerosol Sampler", Atmos. Env., 5:65-66, 1971.

59. Dyment, J., "Use of a Goetz Aerosol Spectrometer for Measuring the Penetration of Aerosols through Filters as a Function of Particle Size", Aerosol Science, 1(1):53-67, 1970.

60. Stöber, W., Flachsbart, H., and Boose, C., "Distribution Analysis of the Aerodynamic Size and the Mass of Aerosol Particles by Means of the Spiral Centrifuge in Comparison to Other Aerosol Precipitators", J. Colloid and Interface Sci., 39(1):109-120, 1972.

61. Kops, J., Hermans, L., and Van de Vate, J. F., "Calibration of a Stöber Centrifugal Aerosol Spectrometer", Aerosol Science, 5(4):379-386, 1974.

62. Heyder, J. and Porstendörfer, J., "Comparison of Optical and Centrifugal Aerosol Spectrometry: Liquid and Non-Spherical Particles", Aerosol Science, 5(4):387-400, 1974.

63. Stöber, W. and Zessack, U., "Zur Theorie either Konischen Aerosolzentrifuge", Staub, 24(8):295-304, 1964, in German.

64. Baust, E., "Use of the Goetz Aerosol Spectrometer to Measure the Size Spectra of Polydispersed Aerosols", Staub, 27(4):16-22, 1967.

65. Whitby, K. T., "Electrical Measurement of Aerosols", in Fine Particles Aerosol Generation, Measurement, Sampling, and Analysis, ed. by B. H. V. Liu, Academic Press, Inc., New York, pp. 581-624, 1975.

66. Strom, L., "Transmission Efficiency of Aerosol Sampling Lines", Atmos. Env., 6:133-142, Feb. 1972.

67. Tine, G., "Gas Sampling and Chemical Analysis in Combustion Processes", Advisory Group for Aeronautical Research and Development, North Atlantic Treaty Organization, Pergamon Press, New York, 1961.

68. Draftz, R.G., Private Communication, IIT Research Institute, Chicago, Illinois, April 19, 1976.

Appendix A

ANALYSIS BY ELECTRON MICROSCOPY OF J-93 TEST SAMPLES

ANALYSIS BY ELECTRON MICROSCOPY OF J-93 TEST SAMPLES

Particle samples from the J-93 tests were received from Dr. Tony Broderick of the U.S. Department of Transportation, Transportation Systems Center. These particle samples were collected on carbon film substrates -- copper electron microscope (EM) grids. Electrostatic precipitation was the mechanism used to deposit the exhaust particles onto the EM grids.

The analysis of these samples at IITRI had the following objectives:

1. To familiarize ourselves with the types and morphology of the various jet engine exhausts in order to recommend useful sample collection methodology.

2. To determine the best operating mode or combination of electron microscopy modes in order to maximize acquisition of information on particle samples (morphology and other characteristics).

3. To correlate image results and operating mode to automatic image analysis.

4. To determine elemental composition and electron diffraction analysis versus particle morphology.

5. To identify the information acquisition potential of various electron microscope operating modes.

The JEOL 100C Scanning Transmission Electron Microscope (STEM) at IITRI has the following instrument capabilities or modes of operation:

1. Conventional Transmission Electron Microscopy (CTEM) in brightfield, as well as darkfield, illumination

2. Secondary Electron Microscope (SEM)

3. Scanning Transmission Electron Microscope (STEM)

4. Elemental Analysis by energy dispersive X-ray analysis.

5. Electron Diffraction Analysis.

With the provided jet exhaust samples, the system capability for these samples was evaluated.

J-93 TEST SAMPLES AND ANALYSIS PROCEDURE

A total of 15 samples were received for study and Table A1 gives the corresponding conditions and figure numbers for typical photomicrographs. The copper grid was broken in sample II-69 and no film substrate was observed on the grid in sample III-5.

Samples I-10 and II-68 were used in comparing the various operating modes of the microscope to learn which mode produced the best results. The basic modes compared were the CTEM, SEM, and STEM using various aperture, accelerating voltages, and instrument settings to maximize image quality and information. The selected mode and operating conditions were then used to observe the rest of the samples.

RESULTS OF ELECTRON MICROSCOPE ANALYSIS

The conventional transmission electron microscope (CTEM) was found to give the best results in regard to the J-93 samples. Operating conditions of the microscope include an accelerating voltage of 60 kv, an illuminating spot size of #2, a condenser aperture of #1, and an objective aperture of #3 were found to produce well-defined images. Several problem areas in the STEM and SEM operating modes were identified. These problems were due to the presence of the grid and the nature of the sample. The most useful samples were observed with the CTEM mode.

Observation of all samples showed that the samples could be divided into two basic types -- wet (liquid drops) and dry (clusters and individual particles). The afterburning power setting samples were extremely wet and the presence

Table A1

J-93 EXHAUST PARTICLE SAMPLES*

Sample Number	Engine Operating Condition	Respective Figure Number
I-10, 11, 12	Military Power 65,000 ft M = 2	
I-25,26	Afterburning 65,000 ft M = 2	I-25, Figure No. A1 I-26, Figure No. A2, A3
I-39, 69, 74	Military Power 75,000 ft M = 2	
II-68, 69, 74	Military Power 55,000 ft M = 2	II-68, Figure No. A4, A5, A6
III-20, 31	Military Power 65,000 ft M = 2.7	III-20, Figure No. A7, A8
III-5	Military Power 35,000 ft M = 1.4	Figure A9, no carbon film

* Obtained from Dr. Anthony J. Broderick, Environmental Measurements Branch, U.S. Department of Transportation, Cambridge, Massachusetts 02142.

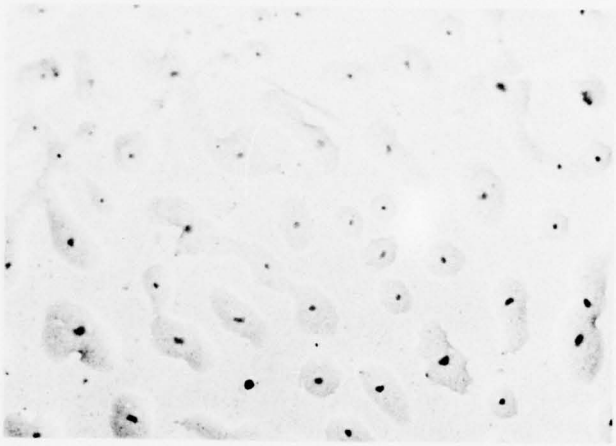

Figure A1

SAMPLE I-25, J-93: AFTERBURNING, 65,000 FT.,
M = 2; MAGNIFICATION = 1.6K

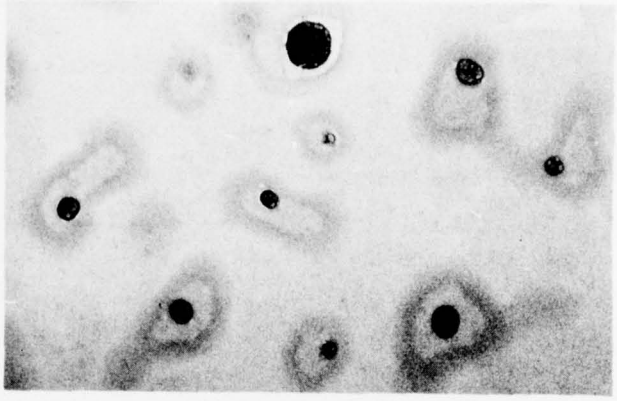

Figure A2

SAMPLE I-26; J-93: AFTERBURNING, 65,000 FT., M = 2;
MAGNIFICATION = 20K (FIRST PHOTOMICROGRAPH)

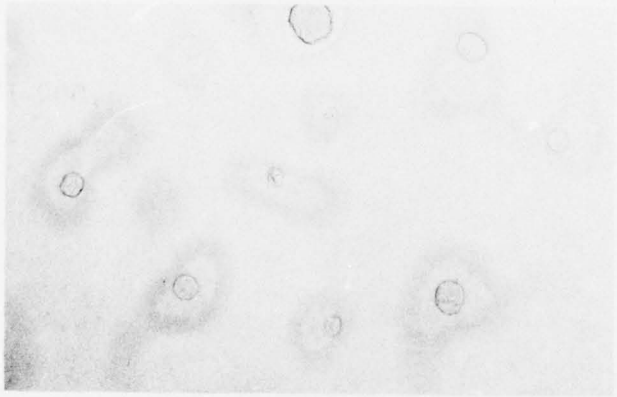

Figure A3

SAMPLE I-26; J-93: AFTERBURNING, 65,000 FT., M = 2;
MAGNIFICATION = 20K (SECOND PHOTOMICROGRAPH)

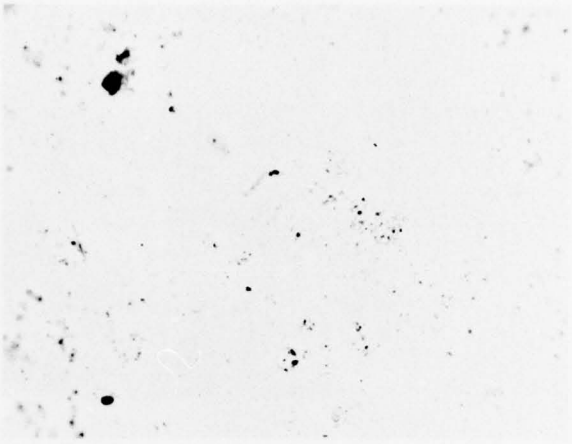

Figure A4

SAMPLE II-68; J-93: MILITARY POWER, 55,000 FT., M = 2; MAGNIFICATION = 1,000X

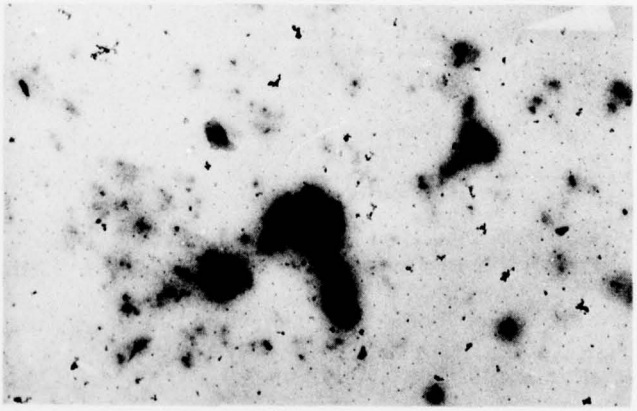

Figure A5

SAMPLE II-68; J-93: MILITARY POWER, 55,000 FT., M = 2; MAGNIFICATION = 6.6K

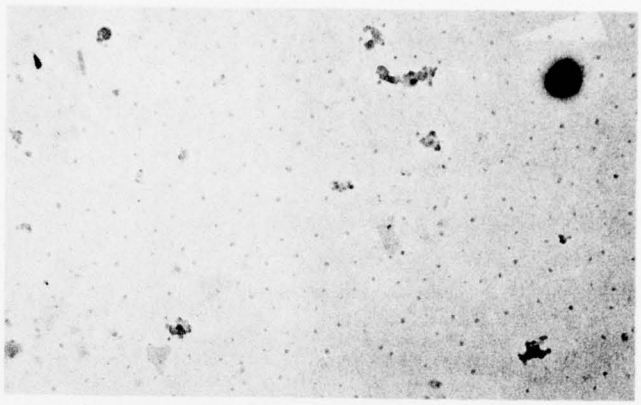

Figure A6

SAMPLE II-68; J-93: MILITARY POWER, 55,000 FT., M = 2: MAGNIFICATION = 20K

Figure A7

SAMPLE III-20; J-93: MILITARY POWER, 65,000FT., M = 2.7; MAGNIFICATION = 10K

Figure A8

SAMPLE III-20; J-93: MILITARY POWER, 65,000 FT.
M = 2.7; MAGNIFICATION = 20K

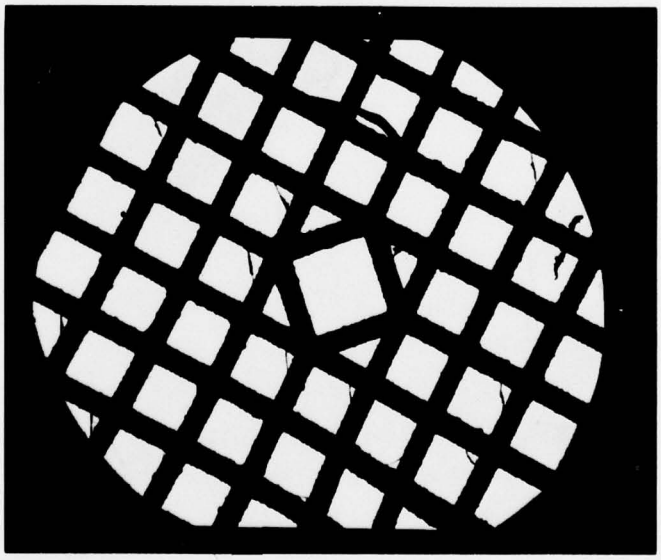

Figure A9

SAMPLE III-5; J-93: MILITARY POWER, 35,000 FT.,
M = 1.4; MAGNIFICATION = 90X

of liquid was obvious. Photographs were taken to indicate the presence of liquid drops and the evaporation of these drops on exposure to the electron beam (Figures A2 and A3).

The stereotyped clusters and chainlike particles (dry) attributed to combustion generated emissions that were observed on sample III-20, as shown in Figures A7 and A8, and on sample III-31. Photomicrographs of the various samples indicate that this type of particle was observed.

The electron diffraction analysis of a few particles indicated the typical amorphous pattern of a carbonaceous nature. No metallic elements were observed during X-ray imaging of a few dry particles.

On the basis of the observed samples, sizing of the particulates (solid and liquid) in the jet exhaust by use of the electron microscope will be difficult. However, this may be attributed to the age of the sample and possible subsequent liquid adsorption which may have affected the particle characteristics.

The aircraft engines of interest in the present study include the JT3D, JT8D, and JT9D -- all commercial subsonic engines. Because afterburning is not employed with these engines, wet particle samples similar to those of Figures A1, A2, and A3 should not be encountered. However, storage for long periods of time should be avoided as the nature of the particle samples obtained from these engines is unknown. The electron microscope is the only instrument available for direct observation of the extremely small particles (particles less than 0.01 μm in diameter). Consequently, the electron microscope is necessary for sizing, calibration of the other measurement techniques, and spot checking of sampling methodology.

Appendix B

ORGANIC CHEMICAL ANALYSIS OF COLLECTED ENGINE SOOT SAMPLE

ORGANIC CHEMICAL ANALYSIS OF COLLECTED ENGINE SOOT SAMPLE

In order to anticipate the quantity of exhaust particulate necessary for a full organic chemical analysis, an actual soot sample was scraped from the exhaust nozzle of a JT8D engine. The acquisition of this sample included only soot from the inside surface of the nozzle. Soot on the outside of the nozzle appeared physically different -- an agglomerated mass of material.

Analytical studies conducted on the carbon residue involved a preliminary extraction of the adsorbed material with methanol. For this extraction, a weighed amount of sample (397 mg) was placed in a 10 ml volumetric flask and filled to volume with absolute methanol. The flask was allowed to sit for 24 hours at room temperature with intermittent mixing. This sample, which was dark brown in color, served as the stock solution for the subsequent analysis performed.

Initial screening was carried out by scanning the attenuated (UV) region in order to obtain some information as to the presence of polynuclear aromatic (PNA) and other possible aromatic species present. The spectrum shown in Figure B1 indicates the presence of low levels of materials out to 350 nm. Such components are typically associated with condensed ring systems of the PNA type molecules. The absorption below 250 nm suggests the presence of highly polar and/or relatively simple ring systems. In view of the relatively large background, absorption throughout the entire UV region would suggest the presence of numerous aromatic species yielding a very general background spectrum. In order to separate and characterize the general nature of the components present, high pressure liquid chromatography was explored.

A DuPont Model 830 high pressure liquid chromatography (HPLC) fitted with a 1 m x 2.1 m Permaphase ODS column (octadecylsine coating on 30 μm particles of silica; reverse

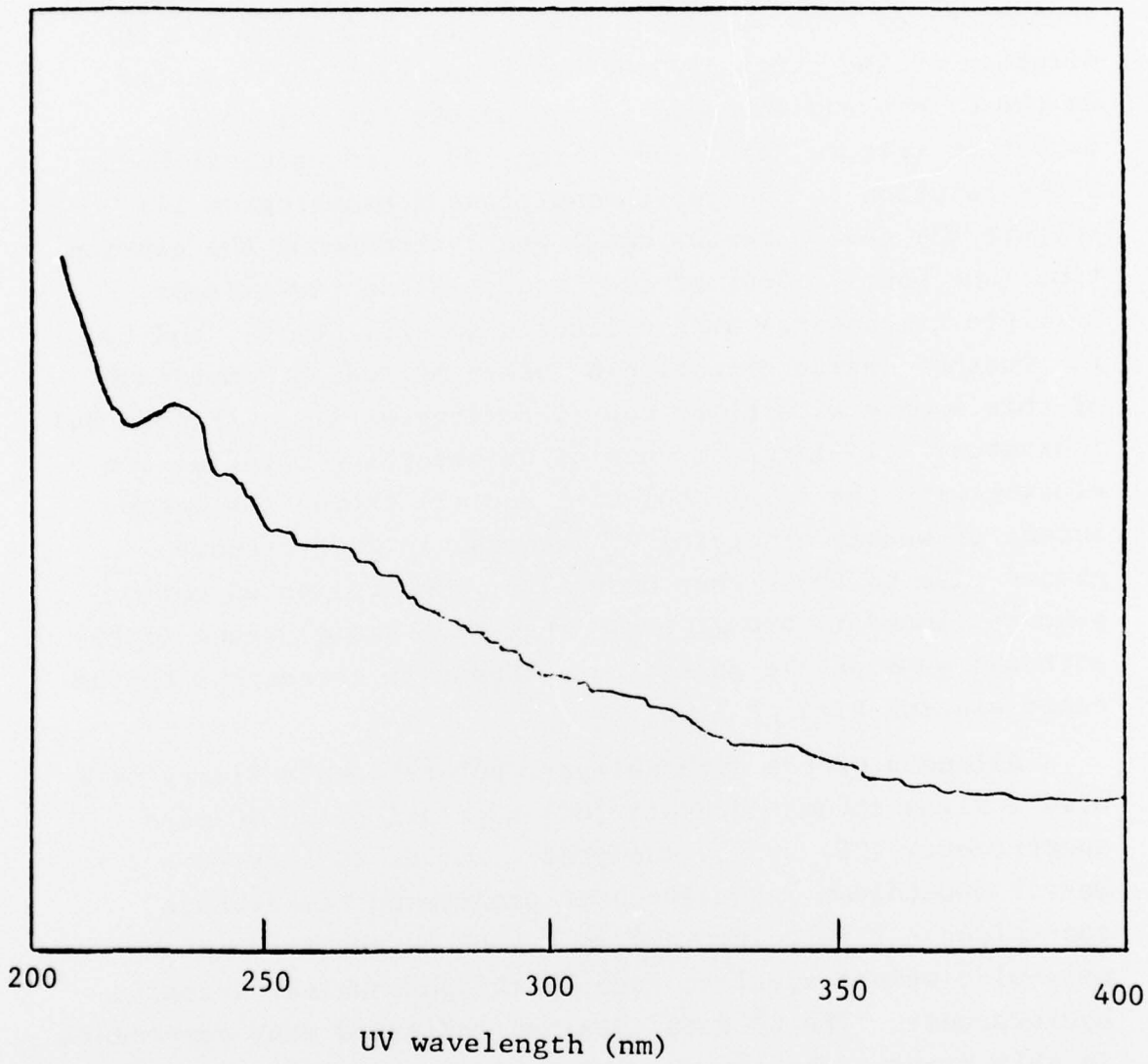

Figure B1

INITIAL UV SCAN OF EXTRACTED CARBON RESIDUE (dilution = 1:500)

phase) solvent gradient assembly and UV detector (245 nm) was used to gain some information regarding the number and types of components present in the sample. For these analyses, the following parameters were used: Temp. = 50°C; Pres. = 450 psi; Gradient - 70:30 to 30:70 at 3% linear increments of MeOH solution. Initially, 100 µl of a 1:10 dilution or the original MeOH stock solution was injected on the column and found to be too dilute for suitable detection (Figure B2). Subjecting 100 µl of original MeOH stock solution to the above conditions (Chromatogram II), (Figure B3) gave numerous small peaks throughout the elution time (one hour). Four of the later eluting peaks (some multiple components) were collected (JT-f5, f6, f7, and f8) for further characterization by other methods. Comparison of this sample with blank run (Chromatogram III), (Figure B4) indicates: (1) large amounts of UV absorbing material are eluting with the sample solvent, and (2) there is a large amount of weakly absorbing UV material in MeOH extract giving rise to the higher base line. The collected components eluted in the general range of benzo(a)pyrene (BaP), although some of the peaks found appear to correspond to the exact elution time of BaP.

Aliquots of the methanol-particulate sample slurry were used for gas chromatographic (GC) separation and GC-mass spectrometry (MS) survey analyses. In the GC survey, a Dexsil 300 column was used under programmed temperature conditions. This column allows a good survey for higher molecular weight species, such as the polynuclear aromatic hydrocarbons. The GC data obtained indicated many components in this range. The concentration levels of the species detected were estimated to be 1-10 x 10^{-6} g/ml of the methanol sample solution. The actual mass of the individual species injected was 0.01-0.1 x 10^{-6} g assuming proportional volumes in the sample. This level was not sufficient to allow mass spectral identification with the present equipment

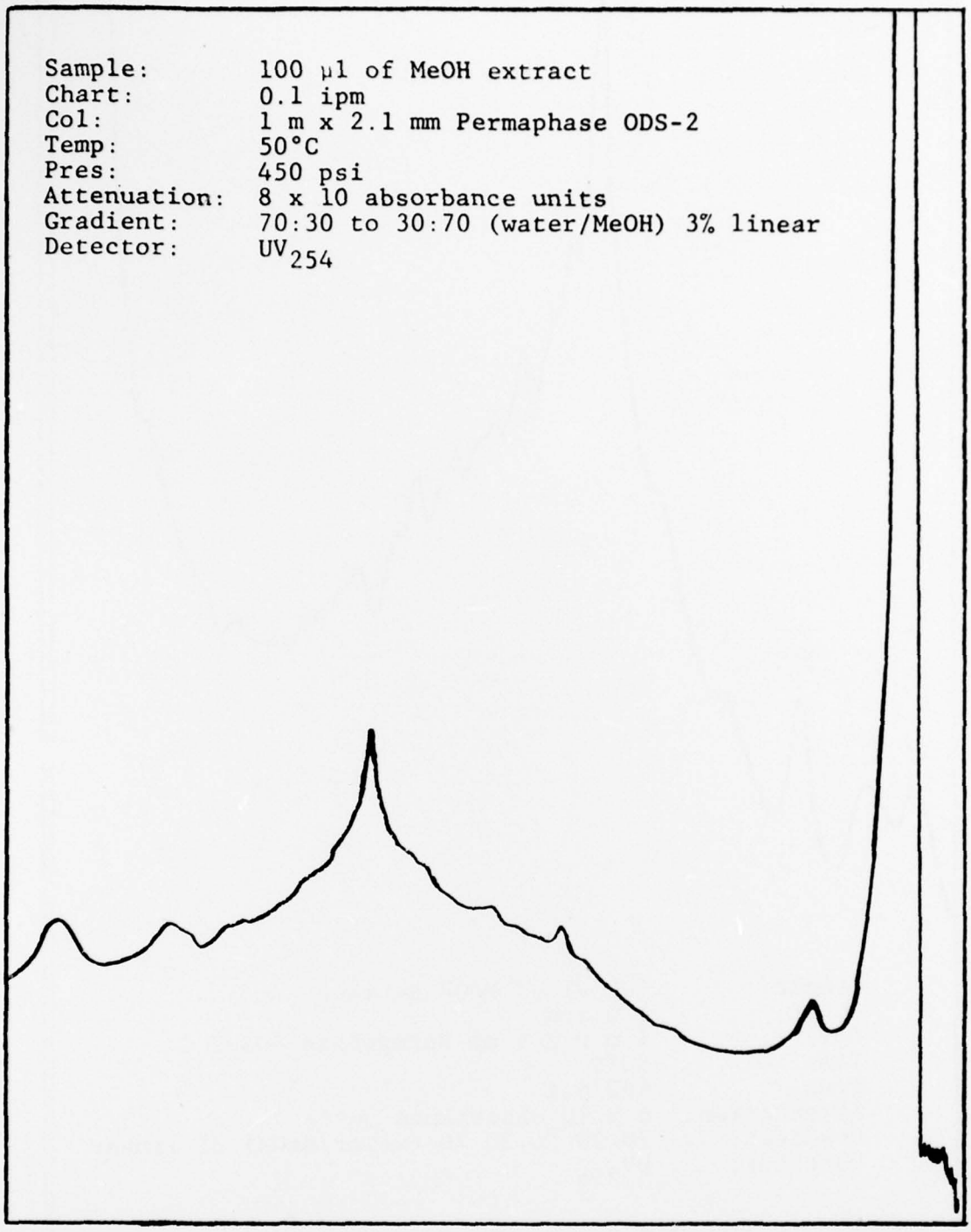

Figure B2

HIGH PRESSURE LIQUID CHROMATOGRAPHY TRACE
OF EXTRACTED CARBON RESIDUE

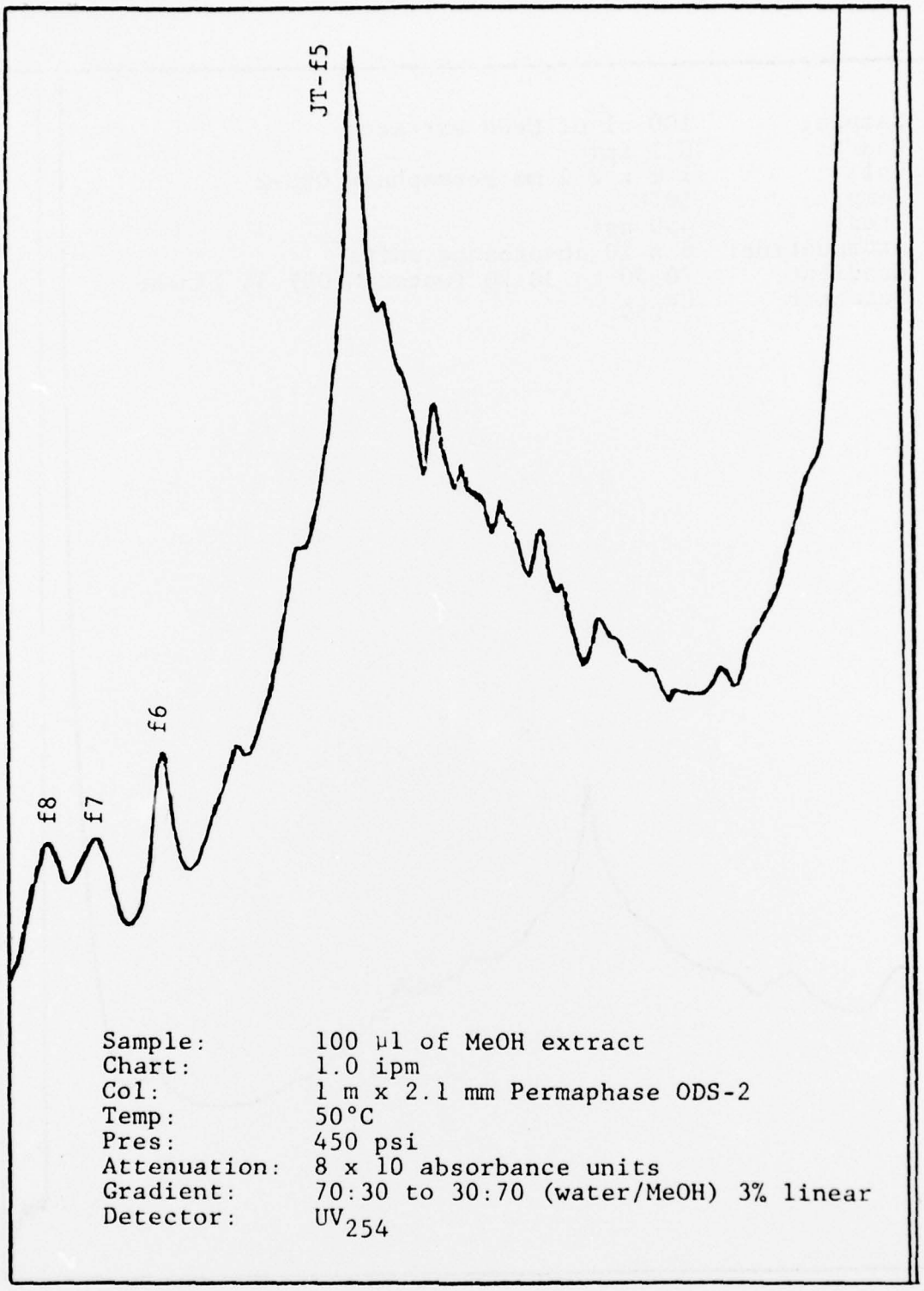

Sample:	100 µl of MeOH extract
Chart:	1.0 ipm
Col:	1 m x 2.1 mm Permaphase ODS-2
Temp:	50°C
Pres:	450 psi
Attenuation:	8 x 10 absorbance units
Gradient:	70:30 to 30:70 (water/MeOH) 3% linear
Detector:	UV_{254}

Figure B3

HIGH PRESSURE LIQUID CHROMATOGRAPHY TRACE OF EXTRACTED CARBON RESIDUE (CONCENTRATED)

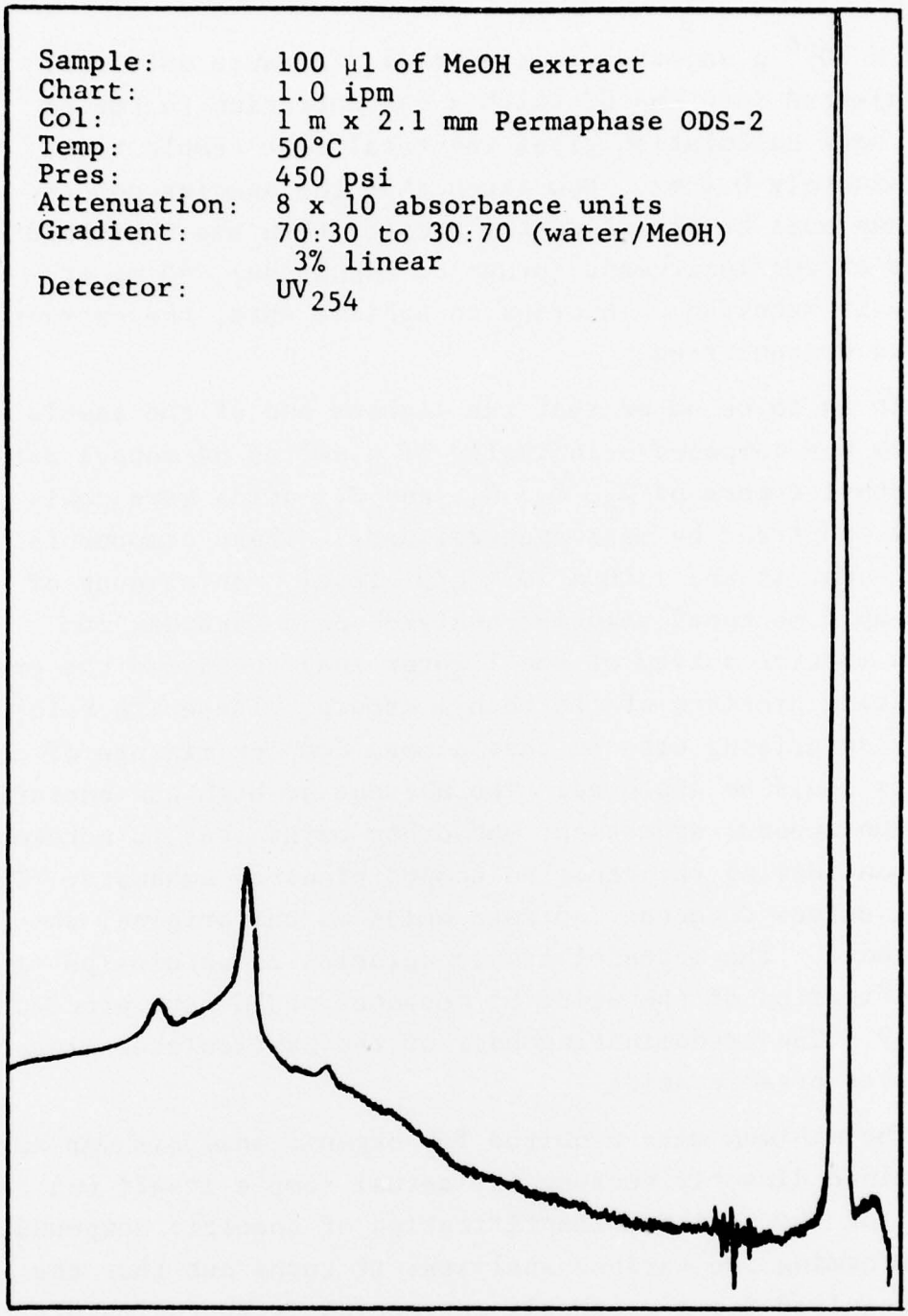

Figure B4

HIGH PRESSURE LIQUID CHROMATOGRAPHY TRACE OF
MeOH (METHANOL) BLANK

(0.1×10^{-6} g injected is required). Because only 5 µl was injected into the GC (with a concentration factor of two), back calculation gives the total soot sample to be approximately 0.4 mg. Now given that the species concentrations must be significantly greater than the threshold values of the instrument (order of magnitude), 40 mg of sample is required. In order to achieve this, the extract must be concentrated.

It is to be noted that the lighter end of the sample mixture was composed principally of a series of methyl esters. The methyl esters of C_6, C_7, C_8, and C_{10} acids were positively confirmed by mass spectral data. These components are present at the 1-10 x 10^{-3} g/ml level. An aliquot of the sample methanol solution analyzed on a Carbowax 20M column (better survey of the lighter end) confirmed the predominating presence of the methyl esters. These are relatively surprising data in that a more complex mixture of components would be expected. The absence of high concentrations of hydrocarbons, aromatics, and other oxygenates is noteworthy when considering the reported compositions of exhausts. The methyl esters detected indicate acids as the original sample components. The methanol sample solution is acidic (pH ∿1-2). Esterification of the acids by methanol would have proceeded readily. The predominating odor of the particulates clearly indicates organic acids.

The minimum mass required for organic analysis was not determined directly because the actual sample itself was too small for the positive identification of specific compounds. In performing the various analyses, it turns out that the mass required for a weighable extraction is approximately the amount needed for a class separation and in turn this is the amount required for a gas chromatographic analysis coupled with mass spectrometry. What happens is that each phase of the analysis has an improvement in sensitivity

proportional to the reduction in mass of the sample. Whereas the sample was only slightly too small for a full analysis, new GC-MA equipment at IITRI will improve the sensitivity by at least an order of magnitude. This translates into a rough estimate that 100 mg will be an adequate sample mass for organic analysis.